Hans-Otto Carmesin

Cosmological and Elementary Particles Explained by Quantum Gravity

Cosmological and Elementary Particles

Explained by Quantum Gravity

This text has also been published in the form of a book and is available in book trading companies or book stores since August 2021.

author: Hans-Otto Carmesin

title: Cosmological and Elementary Particles Explained by Quantum Gravity

ISBN: 978-3-96831-018-3

ISSN: 2629 1525

Please cite this text as follows:

Carmesin, Hans-Otto (August 2021): Cosmological and Elementary Particles Explained by Quantum Gravity. Verlag Dr. Köster, Berlin.

Hans-Otto Carmesin

August 12, 2021

b

Cosmological and Elementary Particles Explained by Quantum Gravity

Berlin: Verlag Dr. Köster

Book Series: Universe: Unified from Microcosm to Macrocosm, Volume 5

Hans-Otto Carmesin

August 12, 2021

Contents

Chapter 1

Basic Concepts

1.1 Introduction

1.1.1 Four great concepts

Physical theories are based on four great fundamental concepts:

Firstly, Leukippos (fifth century BC) and his student Demokritos (460-370 BC) proposed that objects are constituted by smallest indivisible particles, see e. g. Tsoucalas et al. (2013), Oldershaw (1998), Wußing and Brentjes (1987). They proposed an essential argument: These particles constitute the phases gas, fluid and solid including the corresponding phase transitions. Dalton (1808) established the modern concept of the atom. Constituents of atoms are investigated in the current field of elementary particle physics, see e. g. Tanabashi et al. (2018). Boltzmann (1877) developed statistical physics, **SP** including the universal constant k_B, while van der Waals (1873) applied that theory in order to model phase transitions.

Secondly, Brahe (1588) and Kepler (1627) developed the basic observation and analysis of gravity, while Newton (1686) developed the law of gravity including the universal constant G, measured by Cavendish (1798), see also Carmesin et al. (2021).

Thirdly, Planck (1900) discovered the quantization of objects in nature, introduced quantum physics, **QP**, including the universal constant h, **zero-point oscillations, ZPOs**, and the

corresponding **zero-point energy, ZPE** (Planck (1911)).

Fourthly, Einstein (1905) applied the invariance of the velocity of light, the universal constant c, in order to derive the special relativity theory, SRT. Moreover, Einstein (1915) discovered the curvature of spacetime, leading to his proposal of the general relativity theory, **GRT**, including a theory for gravity and SRT.

1.1.2 Interesting problems

Scientific progress is often achieved by identifying and solving problems, see e. g. Popper (1974). Thereby scientific explanations can be achieved and tested Ruben (1990).

Hierarchy problem: In nature there occur objects at very different energy scales. For instance, the neutrinos have rest energies in the meV-scale, the electron, muon, tauon and quarks have rest energies ranging from 511 keV (electron) or 2.15 MeV (up-quark) to 173 GeV (top-quark), see Tanabashi et al. (2018), while the Planck energy is $1.22 \cdot 10^{19}\, GeV$. These different energy-scales cannot be explained by the standard model of elementary particles Peskin (2015). That problem is called hierarchy problem, see e. g. Shaposhnikov and Shkerin (2018).

Mass problem: Aad et al. (2012) and Chatrchyan et al. (2012) discovered the Higgs boson. In the standard model of elementary particles, that particle can basically explain the masses of the W bosons, W^+, W^- and W^0 (also called Z), the quarks, the electron, the muon and the tauon, see e. g. (Peskin, 2015, 9-10). However, the mass of the Higgs boson as well as the masses of the neutrinos are not explained by the standard model.

Fine - tuning problem: The macrocosm is described by the standard model of cosmology, **SMC** using 6 parameters, see e. g.

Collaboration (2020a). The microcosm is described by the standard model of elementary particles, **SMEP**, using 62 parameters, see e. g. (Peskin, 2015, p. 12) or Tanabashi et al. (2018). All these parameters take particular values that should be explained by basic physical theories. These theories include a small number of universal constants, namely G, c, k_B and h. The problem of the determination of the above parameters is an essential part of the fine - tuning problem Landsman (2016).

H_0 tension and σ_8 tension: According to the SMC, the cosmological parameters H_0 and σ_8 should be constant. However, the observed values depend on the probe that is used in a measurement. These problems are called H_0 tension and σ_8 tension.

1.1.3 Unification

In this book we combine the above four basic theories: statistical physics, gravity, quantum physics and relativity. We name that combination quantum gravity. With it we derive the time evolution of the light horizon, including dimensional phase transitions and ranging from the Planck scale to the actual light horizon, see Fig. (1.1). Additionally, we derive the masses of elementary particles, see Fig. (1.1). All results are in precise accordance with observation and have been derived from quantum gravity only. In particular, the only numerical input are the universal constants G, c, k_B and h as well as the **Hubble constant** H_0 as a time reference for the present-day time, the time after the Big Bang. Altogether, we present the first unification of quantum physics, gravity and elementary particle physics based on first principles only.

1.1.4 Aims and organization of the book

In this book we aim to apply quantum gravity in order to explain all cosmological parameters, except the Hubble constant

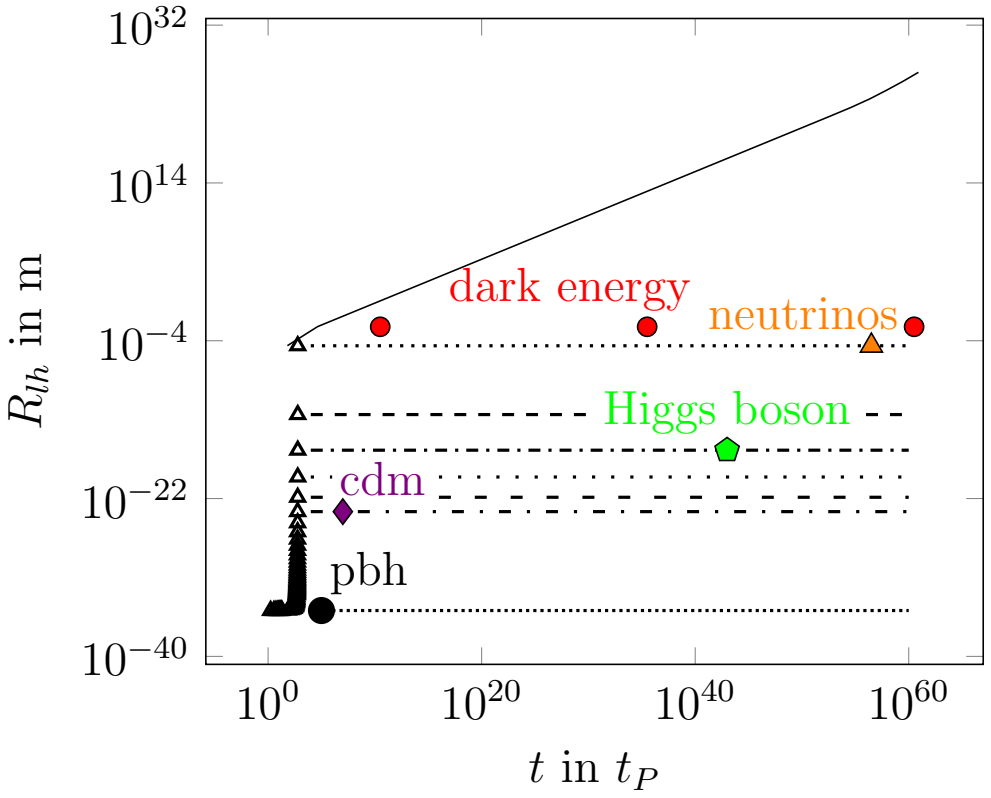

Figure 1.1: Time evolution of the light horizon including dimensional phase transitions (solid line and open Δ). Quanta of spacetime of early phases (other lines). Elementary particles: neutrinos ν (full Δ) Higgs boson (pentagon), quanta of dark energy at $D = 3$ (upper $\circ$), cold dark matter, cdm ($\diamond$) and primordial black holes, pbh (lower $\circ$).

H_0, as H_0 is used as a time reference describing the time after the Big Bang. In order to achieve our aim, we additionally explain the formation of masses on the basis of quantum gravity.

In order to achieve our advanced and innovative aim in a scientific and clear manner, we present our method first:

In chapter 1 we elaborate basic concepts in cosmology, including the standard model of cosmology, the standard model of elementary particles as well as cosmological parameters and the density parameters in particular.

In chapter 2 we combine gravity and quantum physics. With it we derive the Planck scale, and therefrom we derive the incompleteness of GRT.

We solve that incompleteness by analyzing gravitational instabilities and resulting phase transitions in the early universe, see Chapter 3.

Using these transitions, we derive the density parameter of photons Ω_γ in chapter 4.

In order to analyze other quanta in addition to photons, we derive the quanta of spacetime in chapter 5.

Using these quanta of spacetime, we derive the quanta of dark energy including their time evolution in chapter 6.

These quanta of the dark energy constitute the present-day vacuum, including its spectrum of excitation, see chapter 7.

Using that spectrum of excitation, we derive the formation of the neutrinos, including the corresponding density parameter Ω_ν in chapter 8.

Similarly, we apply the spectrum of excitation of the vacuum in order to derive the formation of the Higgs boson in Chap. 9.

Based on chapter 6, we derive the density parameter of dark energy Ω_Λ in chapter 10.

The remaining cosmological parameter, the amplitude of matter fluctuations σ_8, is derived separately in chapter 11.

In Chap. 12 we combine the developed and tested methods, and so we are able to derive all density parameters simulta-

neously. Thus, we derive the cosmological parameters without using them, except H_0 that we use as a time reference.

We provide solutions of the H_0 tension and of the σ_8 tension in chapter 13.

In chapter 14 we present a discussion of our results, including the following essential insight: The precise derivation of the cosmological parameters and masses of elementary particles provides a clear evidence of our theory.

Altogether, we show that the standard model of cosmology, including its cosmological parameters, can be explained and extended by quantum gravity. Furthermore, we show that the formation of mass in the standard model of elementary particles can basically be explained by quantum gravity. In particular, the hierarchy problem is solved by quantum gravity[1].

1.2 Physical constants

In this section we elaborate the concept of physical constants in the context of a laboratory, in which these constants can be measured. For it we introduce the concept of an ideal laboratory. Of course, many sophisticated laboratories have been built, and we do not try to improve any of these, we simply reflect their purpose in principle.

Definition 1 Ideal laboratory

(1) A physical system is an ideal laboratory, if the following conditions are provided:

(1a) Fields that exist outside the system are either screened or averaged to zero in the system.

[1]I derived the present theory progressively. The publication started in 2017 in books, papers and my book series. See e. g. Carmesin (2017b), Carmesin (2018h), Carmesin (2018g), Carmesin (2018f), Carmesin (2018a), Carmesin (2019d), Carmesin (2017b), Carmesin (2019a), Carmesin (2019f), Carmesin (2020b), Carmesin (2020a), Carmesin (2021c), Carmesin (2021a), Carmesin (2021d).

(1b) The system contains a clock that measures the own time t_{own} in the system.

(1c) In particular, a homogeneous universe frame, HUF, see (Carmesin, 2021c, Def. 2), has zero gravitational field.

(2) An example is the homogeneous universe frame, HUF, see (Carmesin, 2021c, DEF. 2 and PROP. 2).

(3) The statistical variance of fields in a HUF has been analyzed in (Carmesin, 2021c, THM. 27 and section 8.3).

(4) Experiments that are performed in an ideal laboratory or in another laboratory provide physical laws and physical quantities as empirical results.

More realistically, we introduce the concept of equivalent laboratories:

Definition 2 Equivalent laboratories

Two laboratories are called equivalent, if one of the following conditions holds:

(1) Either both laboratories provide the same empirical results.

(2) Or both laboratories provide empirical results that can be transformed by the laws of special relativity theory, SRT, or by the laws of general relativity theory, GRT, so that the transformed empirical results are equal.

(3) An example is a freely falling system from which other than gravitational external fields are screened. That system is equivalent to an ideal laboratory.

(4) Another example is a screened system at Earth for which the gravitational field G^* is known, so that gravitational effects can be eliminated by transformations according to GRT.

(5) Another example is a pair of ideal laboratories that exhibit a relative velocity v, so that the relativistic effects can be eliminated by transformations according to the laws of SRT.

Next we introduce the concept of a physical constant:

Definition 3 Physical constant

A physical quantity Q is a physical constant, if the following conditions hold:

(1) Q can be measured in an ideal laboratory.

(2) Q takes the same value at each time t shown by the clock in that ideal laboratory: $\frac{dQ}{dt} = 0$.

(3) A physical constant that is essential for a basic physical theory is called universal constant. Examples are:

(3a) the constant of gravitation G, essential for gravity,

(3b) the velocity of light c, essential for relativity,

(3c) the Boltzmann constant k_B, essential for thermodynamics or statistical physics,

(3d) the Planck constant h, essential for quantum physics and

(3e) the electric field constant ε_0.

We emphasize the following: The above definitions show that the concept of a physical constants is well defined. There is a precise procedure, by which one may test whether a physical quantity is a constant. That property of constancy has been tested very precisely, for many physical constants[2]. And that testing is still going on, always using the best methods. A list of universal physical constants is presented in table (15.1).

[2]In the literature, there are still suggestions that a universal physical constant could vary with time. The present definitions make clear that such a suggestion represents a hypothesis only. Moreover, such a suggested variation with time is proposed in spite of a very clear concept of a physical constant. Additionally, such a suggested variation with time is proposed in spite of very precise empirical evidence of the constancy of the universal constants.

1.3 Essential cosmological parameters

In this section we analyze usual cosmological parameters, and we identify those cosmological parameters that are essential for the cosmological dynamics.

Hinshaw et al. (2013) observed the CMB and evaluated the measurements by using the SMC or ΛCDM model characterized by six-parameters. So they fitted six cosmological parameters to their observations. As such parameters may be transformed, there is some freedom in the choice of the parameters (see also Collaboration (2020a) or Tanabashi et al. (2018)).

The universe exhibits a time-evolution, whereby states and objects that form early are the basis for states and objects forming later. Thus the present-day observations are characterized by the present day time t_0 after the Big Bang. That time t_0 can be derived from the **Hubble constant** H_0, one of the six parameters, see for instance Carmesin (2019d). Accordingly, we use H_0 as a time reference. With it we determine exact values of five additional cosmological parameters: the **density parameters** Ω_Λ, Ω_M, Ω_r and Ω_K as well as the **amplitude of matter fluctuations** σ_8. We determine these exact values by application of the three basic physical theories, quantum physics, general relativity theory, GRT, including SRT, and statistical physics. These physical theories include the corresponding universal constants G, c, k_B and h. Additionally, we use the physics of neutrinos and of the Higgs-particle including the corresponding elementary particles, see e. g. Tanabashi et al. (2018).

Altogether, we need only one cosmological parameter, the time reference H_0, and from H_0 we derive the other cosmological parameters based on quantum gravity only.

Next we analyze these six parameters and several additional interesting cosmological parameters in detail.

1.3.1 Concept of the Hubble constant H_0

In this section, we summarize the concept of the Hubble constant. Hubble (1929) discovered the Hubble law: The distances d of galaxies are proportional to their redshifts z.

Thereby, galaxies should not be too near in order to avoid peculiar motions, and galaxies should not be too far away in order to avoid motions with clear negative or positive acceleration.

The Hubble law is usually explained by the **expansion of space** (see e. g. Friedmann (1922), Lemaitre (1927), Einstein and de Sitter (1932), Amendola (2021)). That expansion is often modeled by a uniform scaling. That scaling is often modeled with a **scale factor** R, whereby R is a function of the time t (see e. g. (Tanabashi et al., 2018, p. 352)). In such a model the ratio of the time derivative $\dot{R}$ divided by the radius R is the expansion rate:

$$H := \frac{\dot{R}}{R} \tag{1.1}$$

That expansion rate is called **Hubble parameter** (see e. g. (Tanabashi et al., 2018, p. 352)).

In general, the Hubble parameter is a function $H(t)$ of the time t or a function $H(z)$ of the redshift z. In particular, the Hubble constant H_0 is the value of the Hubble parameter at the present time t_0 (see e. g. (Tanabashi et al., 2018, p. 128)).

$$H_0 := H(t_0) \tag{1.2}$$

1.3.2 Dynamics via the Hubble parameter $H(t)$

As the $H(t)$ includes the time derivative $\dot{R}$, it can be used in order to express a differential equation, DEQ, for $R(t)$. That DEQ is called Friedmann Lemaître equation, **FLE** (Friedmann (1922) and Lemaitre (1927) or (Amendola, 2021, Eq. 3.1.2)):

$$\boxed{\frac{\dot{R}^2}{R^2}H^2 = \frac{8\pi G \cdot \rho}{3} - K \cdot \frac{c^2}{R^2}} \tag{1.3}$$

Hereby ρ is the density, and the parameter K is the **curvature parameter** (see e. g. (Tanabashi et al., 2018, p. 352)). By comparison, we see that the curvature parameter K corresponds to the following additional density ρ_K (see (Amendola, 2021, p. 22, 23)):

$$\frac{8\pi G \cdot \rho_K}{3} = -K \cdot \frac{c^2}{R^2} \text{ or} \tag{1.4}$$

$$\rho_K := -K \cdot \frac{3c^2}{8\pi G \cdot R^2} \tag{1.5}$$

Physical basis of the DEQ: The FLE has been derived from GRT in a macroscopic framework, see Friedmann (1922) and Lemaitre (1927) or e. g. Straumann (2013), Carmesin (1996). Moreover, the FLE has been derived on the basis of the GRT and of microscopic objects, see (Carmesin, 2021c, THM 24). Thereby, microscopic objects include matter, radiation and the quanta of spacetime (including the dark energy), so a possible pressure of these objects is already included on the microscopic level (in an implicit manner). In particular, an additional 'dark energy equation of state parameter' w, see e. g. (Tanabashi et al., 2018, p. 129), does not occur here, and it is not necessary, as it is already inherent to the present theory, see (Carmesin, 2021c, theorems 21, 22, 29, 30).

Critical density ρ_{cr}: By definition, the critical density is the density ρ at which the curvature parameter K in the above DEQ vanishes, see e. g. (Amendola, 2021, p. 23) or Eq. 1.3:

$$\rho_{cr} := \frac{3H^2}{8\pi G} \tag{1.6}$$

1.3.3 On the observation of the Hubble constant H_0

Each observation of H_0 uses some objects that arrive at Earth. These objects have formed or have been emitted at some time

t_{em} and are observed at the present time t_0. The ratio of the corresponding scale factors is one plus the **redshift**:

$$1 + z := 1 + \frac{\lambda(t_0) - \lambda(t_{em})}{\lambda(t_{em})} = \frac{\lambda(t_0)}{\lambda(t_{em})} = \frac{R(t_0)}{R(t_{em})} \tag{1.7}$$

The redshift z is a quantity that is typically measured. The corresponding scale factor $R(t_{em})$ is usually denoted by R, for short. Accordingly, we introduce a dimensionless scale factor:

$$x_R := \frac{R}{R(t_0)} = \frac{R(t_{em})}{R(t_0)} = \frac{1}{1+z} \tag{1.8}$$

1.3.4 Density ρ in the DEQ corresponding to $H(t)$

In this section we analyze the densities inherent to the FLE.

Basic types of densities: The density ρ in the above FLE is the sum of the following particular densities (see e. g. (Tanabashi et al., 2018, p. 128, 353)): the density of matter ρ_m, the density of relativistic species also called the density of radiation ρ_r and the density of the vacuum ρ_Λ:

$$\rho = \rho_\Lambda + \rho_m + \rho_r \tag{1.9}$$

Each present-day density $\rho_j(t_0)$ is usually normalized by $\rho_{cr}(t_0)$, the corresponding ratio is called **density parameter** Ω_j (see e. g. (Amendola, 2021, p. 23)):

$$\Omega_j := \frac{\rho_j(t_0)}{\rho_{cr}(t_0)} \tag{1.10}$$

For instance, we get $\Omega_M = \frac{\rho_m(t_0)}{\rho_{cr}(t_0)}$, or $\Omega_K := \frac{\rho_K(t_0)}{\rho_{cr}(t_0)}$, see Eq. (1.5).

Redshift inherent to densities: In SRT, the energy E of an object with an own mass or rest mass m_0 and a momentum p is as follows, see e. g. (Moore, 2013, Eq. (3.20)):

$$E = \sqrt{m_0^2 \cdot c^4 + p^2 \cdot c^2} \tag{1.11}$$

In quantum physics, the momentum p is equal to the Planck constant h divided by the wavelength λ of the object, see e. g. Ballentine (1998) or Landau and Lifschitz (1979a) or Carmesin et al. (2020):

$$p = \frac{h}{\lambda} \tag{1.12}$$

As a consequence of the above two Eqs., the energy of a quantum object is as follows:

$$E = \sqrt{m_0^2 \cdot c^4 + \frac{h^2 \cdot c^2}{\lambda^2}} \tag{1.13}$$

In cosmology, objects for which the second summand in the above root is large compared to the first summand are summarized as relativistic species, see e. g. (Hinshaw et al., 2013, section 4.3). These are represented by a density ρ_r, and the energy of such an object is described (within an appropriate approximation) as follows:

$$E_r = \frac{h \cdot c}{\lambda} \tag{1.14}$$

These relativistic species include photons with the density ρ_γ, neutrinos with the density ρ_ν and so-called **extra radiation species** ρ_{ERS}, see e. g. (Hinshaw et al., 2013, section 4.3).

In cosmology, objects are summarized as matter, if the first summand in Eq. (1.11) is large compared to the second, see e. g. (Collaboration, 2020a, table 2). These are represented by a density ρ_m, and the energy of such an object is described (within an appropriate approximation) as follows:

$$E_m = m_0 \cdot c^2 \tag{1.15}$$

These matter species include baryons with the density ρ_b and cold dark matter, **CDM** with the density ρ_c, see e. g. (Collaboration, 2020a, table 2) or (Hinshaw et al., 2013, table 2).

Redshift and densities: As the volume V of a ball with the radius $R(t_{em})$ is proportional to $R(t_{em})^3$, we get:

$$V(t_{em}) = V(t_0) \cdot x_R^3 \tag{1.16}$$

As the density of matter $\rho_m(t_0)$ is proportional to the inverse volume, we get:

$$\rho_m(t_{em}) = \rho_m(t_0) \cdot x_R^{-3} = \rho_{cr}(t_0) \cdot \Omega_M \cdot x_R^{-3} \tag{1.17}$$

The density of radiation has an additional factor $1/x_R$ as a consequence of the redshift. So we get:

$$\rho_r(t_{em}) = \rho_{cr}(t_0) \cdot \Omega_r \cdot x_R^{-4} \tag{1.18}$$

The density of curvature is proportional to $1/R^2$ (see Eq. 1.4). Thus, we get:

$$\rho_K(t_{em}) = \rho_{cr}(t_0) \cdot \Omega_K \cdot x_R^{-2} \tag{1.19}$$

Altogether, we derive:

$$\rho + \rho_K = \rho_{cr}(t_0) \cdot (\Omega_\Lambda + \Omega_K x_R^{-2} + \Omega_M x_R^{-3} + \Omega_r x_R^{-4}) \tag{1.20}$$

With it we derive a version of the FLE that includes ρ_K:

$$H^2(x_R) = \frac{8\pi G \cdot \rho_{cr}(t_0)}{3}(\Omega_\Lambda + \Omega_K x_R^{-2} + \Omega_M x_R^{-3} + \Omega_r x_R^{-4}) \tag{1.21}$$

We apply Eq. (1.6). Hence we derive:

$$H^2(x_R) = H_0^2 \cdot (\Omega_\Lambda + \Omega_K x_R^{-2} + \Omega_M x_R^{-3} + \Omega_r x_R^{-4}) \tag{1.22}$$

We define the dimensionless Hubble parameter $E(x)$ or $E(z)$, see e. g. (Amendola, 2021, p. 26) or (Riess et al., 2018, p. 3):

$$E(x_R) := \frac{H(x_R)}{H_0} \tag{1.23}$$

We apply Eq. (1.22). Thence we derive:

$$\boxed{E(x_R) = \sqrt{\Omega_\Lambda + \Omega_K x_R^{-2} + \Omega_M x_R^{-3} + \Omega_r x_R^{-4}}} \tag{1.24}$$

1.3.5 Age of the universe t_0

In this section we derive the age of the universe t_0. For it we solve Eq. (1.23) for $H(x_R)$:

$$H(x_R) = H_0 \cdot E(x_R) \tag{1.25}$$

In order to obtain the DEQ, we apply the definition of the Hubble parameter $H(x_R) = \frac{dx_R/dt}{x_R}$:

$$\frac{dx_R}{x_R \cdot dt} = H_0 \cdot E(x_R) \tag{1.26}$$

In order to solve that DEQ, we separate the variables. For it we multiply by $dt/E(x_R)$:

$$\frac{dx_R}{x_R \cdot E(x_R)} = H_0 \cdot dt \tag{1.27}$$

Next we apply the integral, and we denote the resulting dimensionless time integral by I_t:

$$I_{x_1,x_2} := \int_{x_1}^{x_2} \frac{dx_R}{x_R \cdot E(x_R)} = H_0 \int_{t_1}^{t_2} dt = H_0 \cdot (t_2 - t_1) \tag{1.28}$$

In particular, we get the age of the universe t_0 by choosing the boundary values $t_2 = t_0$, $t_1 = 0$, $x_1 = 0$ and $x_2 = 1$:

$$I_{0,1} := \int_0^1 \frac{dx_R}{x_R \cdot E(x_R)} = H_0 \cdot t_0 \tag{1.29}$$

We solve for the age of the universe t_0:

$$t_0 = \frac{I_{0,1}}{H_0} \tag{1.30}$$

For instance, for the case of the observed cosmological parameters in table (15.2), we calculate the following value for the age of the universe t_0:

$$t_0 = 13.8 \cdot 10^9 \text{ years} \tag{1.31}$$

1.3.6 Comoving distance r_{co}

In this section we derive the distance between a source that emits a photon at a time t_{em} and Earth at the present time t_0. At an instant of time t and during a time increment dt, that photon propagates the incremental **light travel distance** $c \cdot dt$. That increment $c \cdot dt$ is increased by the factor $R(t_0)/R(t) = 1/x_R(t)$, during the time interval $[t, t_0]$. So the incremental **complete distance** is as follows:

$$dr_{co} = \frac{1}{x_R(t)} c \cdot dt \tag{1.32}$$

We integrate, in order to derive the complete distance:

$$r_{co}(t_{em}) := \int_{source}^{Earth} dr_{co} = \int_{t_{em}}^{t_0} \frac{1}{x_R(t)} c \cdot dt \tag{1.33}$$

That complete distance r_{co} is also called **comoving distance** or **present-day proper distance**, see e. g. (Tanabashi et al., 2018, Eq. (22.5)). We substitute the integration variable t by x_R. For it we use Eq. (1.27). So we derive:

$$r_{co}(x_R) = \frac{c}{H_0} \int_{x_R}^{1} \frac{dx}{x^2 \cdot E(x)} \tag{1.34}$$

In particular, for the case $t_{em} = 0$ or $x_R = 0$, we derive the **light horizon**:

$$\boxed{R_{lh} = \frac{c}{H_0} \int_{0}^{1} \frac{dx}{x^2 \cdot E(x)}} \tag{1.35}$$

For instance, for the case of the observed cosmological parameters in table (15.2), we calculate the following value for the light horizon R_{lh}:

$$R_{lh} = 4.14 \cdot 10^{26}\,\mathrm{m} \tag{1.36}$$

Similarly, we derive the time evolution of the actual light horizon corresponding to a scaled time x_t. For it we derive the

size $R_{lh}(\frac{t}{t_0})$ that the actual light horizon had or has at a time $x_t = \frac{t}{t_0}$:

$$\boxed{R_{lh}(x_t) = \frac{c}{H_0} \int_0^{x_t} \frac{dx}{x^2 \cdot E(x)}} \tag{1.37}$$

1.3.7 Luminosity distance d_L

We consider a source at a redshift z emitting N photons with wavelength λ and energy $dE = \frac{h \cdot c}{\lambda}$ and distributed in a shell at a comoving distance r_{co} and with a thickness λ. So these photons are distributed in the volume $dV = 4\pi r_{co}^2 \cdot \lambda$. Thus, the energy density is as follows:

$$u(z) = \frac{dE}{dV} = \frac{h \cdot c}{4\pi r_{co}^2 \cdot \lambda^2} \tag{1.38}$$

When these photons are absorbed at Earth at the present time t_0, the wavelength is elongated via the redshift by the factor $1 + z$. So the energy density is as follows:

$$u(z = 0) = \frac{h \cdot c}{4\pi r_{co}^2 \cdot \lambda^2 \cdot (1+z)^2} = u(z) \cdot \frac{1}{(1+z)^2} \tag{1.39}$$

If L is the **luminosity** of the above source, then its flux f at a comoving distance r_{co} in a non-expanding space would be equal to $f = \frac{L}{4\pi r_{co}^2}$. As the flux is equal to $u \cdot c$, the flux in the expanding space is proportional to $\frac{1}{(1+z)^2}$, see (Amendola, 2021, Eq. 3.9.1)

$$f = \frac{L}{4\pi r_{co}^2 \cdot (1+z)^2} \tag{1.40}$$

The above product $r_{co} \cdot (1 + z)$ is called **luminosity distance** d_L, see e. g. (Amendola, 2021, Eq. (3.9.2)):

$$d_L := r_{co} \cdot (1 + z) \tag{1.41}$$

In order to relate the comoving distance to observation including the redshift z, we substitute x in the integral in Eq.

(1.34) by $1/(1+z)$. For it we derive $dx = -dz \cdot x^2$. So we get:

$$r_{co}(z) = \frac{c}{H_0} \int_0^z \frac{dz'}{E(z')} \quad \text{with} \tag{1.42}$$

$$E(z) = \sqrt{\Omega_\Lambda + \Omega_K (1+z)^2 + \Omega_M (1+z)^3 + \Omega_r (1+z)^4} \tag{1.43}$$

Accordingly, the luminosity distance as a function of z is as follows, see also (Riess et al., 2018, Eq. (1)):

$$d_L(z) = \frac{c}{H_0} \cdot (1+z) \cdot \int_0^z \frac{dz'}{E(z')} \tag{1.44}$$

The luminosity distance can be measured for each supernova SNIa, and with it the (inverse) Hubble constant H_0 can be obtained, see (Riess et al., 2018, p. 3), whereby the $E(z)$-function is reconstructed. Here we derive that reconstruction by the direct derivation of the density parameters inherent to $E(z)$. So we can solve the above equation for H_0:

$$\boxed{H_0 = \frac{c}{d_L(z)} \cdot (1+z) \cdot \int_0^z \frac{dz'}{E(z')}} \tag{1.45}$$

1.3.8 Microscopically based cosmological dynamics

As the universe is not divided into a microscopic and a macroscopic dynamics, the FLE should be derived from the dynamics of microscopic particles. This has been achieved in THM. (2), THM. (3), Carmesin (2020b) and Carmesin (2021c).

Proposition 1 Microscopically based cosmological dynamics

Each particle generates gravity, a corresponding curvature of space as well as a respective rate of formation of vacuum, and therefrom the FLE has been derived, see Carmesin (2021c):

$$\boxed{H^2 = \frac{8\pi G \cdot (\rho_\Lambda + \rho_k + \rho_m + \rho_r)}{3}} \tag{1.46}$$

1.3.9 Dynamically essential types of densities

In this section we summarize the types of densities that are essential for the microscopically based cosmological dynamics (Eq. 1.46). These are dynamically essential types of densities:

Definition 4 Dynamically essential types of densities

The types of densities that occur in the microscopically based cosmological dynamics (see proposition 1), and that represent different functions of the redshift z, constitute the set of dynamically essential types of densities.

As an immediate consequence, we apply the density parameters:

Corollary 1 *The microscopically based cosmological dynamics is constituted by the FLE in terms of the following DEQ and in terms of the density parameters (see Eq. 1.22):*

$$\boxed{H^2(x_R) = H_0^2 \cdot (\Omega_\Lambda + \Omega_K x_R^{-2} + \Omega_M x_R^{-3} + \Omega_r x_R^{-4})} \qquad (1.47)$$

1.3.10 Dynamically essential cosmological parameters

In this section we identify those cosmological parameters that are essential for the microscopically based cosmological dynamics. These are dynamically essential cosmological parameters.

We identify five dynamically essential cosmological parameters in Eq. (see Eq. 1.47): H_0, Ω_Λ, Ω_K, Ω_M and Ω_r. This set would be complete, if these parameters were constant as a function of time or as a function of z. However, this is not the case. Empirical evidence for that fact is provided by the so-called H_0 tension, see e. g. Riess et al. (2018) or Scolnic et al. (2018) or Riess et al. (2019).

In fact, I developed a basic theory of the time evolution of space[3], and with it I discovered that the vacuum is a polychromatic mixture of **quanta of spacetime, QST**. In particular

[3]See e. g. Carmesin (2017b), Carmesin (2018g), Carmesin (2018f), Carmesin (2018a), Carmesin (2019d), Carmesin (2019b), Carmesin (2020b), Carmesin (2020a), Carmesin (2021c).

these quanta are permanently formed, accumulate and constitute a polychromatic mixture of quanta. That polychromatic mixture implies that the Hubble constant H_0 is a function of z. For it I derived a correction factor as a function of z, and the resulting $H_0(z)$ turns out to be in precise accordance with observation, whereby I do not execute any fit. Moreover, I derived a semiclassical version of the full theory. That semiclassical theory is fully relativistic, and it is semiclassical with respect to quantum physics. The correction factor of the semiclassical theory is in approximate and in relative precise accordance with the correction factor of the full theory. I derived an explicit formula for the semiclassical correction factor, and it is not only a function of z, it is also a function of the amplitude of matter fluctuations σ_8, see (Carmesin, 2021c, theorem 22). Correspondingly, σ_8 is a sixth dynamically essential cosmological parameter. Moreover, the time evolution of the universe, including the H_0 tension, has been described on the basis of the SRT, the GRT, quantum physics and statistical physics, and on the basis of these six cosmological parameters only, see Carmesin (2021c). Thereby a precise accordance with observation has been achieved. Accordingly, we summarize:

Corollary 2 Dynamically essential cosmological parameters

(1) The dynamically essential cosmological parameters are the following six usually used cosmological parameters:

(a) the Hubble parameter H_0,

(b) the density parameters Ω_Λ, Ω_K, Ω_M and Ω_r,

(c) the amplitude of matter fluctuations σ_8.

(2) The dynamically essential cosmological parameters exhibit mutual dependencies:

(a)

$$\Omega_\Lambda + \Omega_K + \Omega_M + \Omega_r = 1, \tag{1.48}$$

(b) the Hubble constant H_0 exhibits a functional dependency on z and σ_8, see (Carmesin, 2021c, theorem 22)

(c) similarly, Ω_Λ exhibits a functional dependency on z and σ_8, see (Carmesin, 2021c, theorem 22).

(d) moreover, σ_8 exhibits a functional dependency on z, see (Carmesin, 2021c, theorem 22).

(3) The average of interacting pairs of objects in the universe shows that $\Omega_K = 0$, see (Carmesin, 2021c, theorem 32 number (6)). This result corresponds to observation, see e. g. Collaboration (2020a) or Hinshaw et al. (2013).

(4) The density parameter Ω_r can equivalently be substituted by the redshift z_{eq} of the radiation-matter equality, see e. g. (Carmesin, 2019d, Eq. 2.17):

$$\Omega_r = \frac{\Omega_M}{z_{eq} + 1} \tag{1.49}$$

1.4 Constituents of Ω_r

The density of radiation consists of three species, see e. g. Hinshaw et al. (2013): the density of photons ρ_γ, the density of neutrinos ρ_ν and the extra radiation species, ρ_{ERS}. So the density of radiation is the following sum:

$$\rho_r = \rho_\gamma + \rho_\nu + \rho_{ERS} \tag{1.50}$$

$$\text{or } \boxed{\Omega_r = \Omega_\gamma + \Omega_\nu + \Omega_{ERS}} \tag{1.51}$$

These constituents have the common property that their energy varies according to the redshift. Moreover, their amount does not increase according to the FLE. These two properties have essential implications on the time development. We summarize:

Corollary 3 Constituents of radiation *(table 15.2)*

(1) The radiation has the following cosmological constituents:

(a) photons with the density parameter Ω_γ*,*

(b) neutrinos with the density parameter Ω_ν*,*

(c) extra radiation species, with the density parameter Ω_{ERS}*.*

(2) So the density parameter of radiation is the following sum: $\Omega_r = \Omega_\gamma + \Omega_\nu + \Omega_{ERS}$

1.5 Standard model of elementary particles

In this section we present a short description of the standard model of elementary particles (Tanabashi et al. (2018), Bethge and Schröder (1991), Kobel et al. (2017)), so that the results obtained below can be related to that model. The model is essentially constituted by three generations, see e. g. Kobel et al. (2017). These are basically understood by the beta decay.

1.5.1 β-decay

In the beta decay, a neutron, n, decays into a proton, p, an electron, e^- and an electronic antineutrino, $\bar{\nu}_e$:

$$n \to p + \bar{\nu}_e + e^- \tag{1.52}$$

On the level of quarks, the beta decay can be modeled by the decay of a down quark, d, into an up quark, u, an electron, e^- and an electronic antineutrino, $\bar{\nu}_e$:

$$d \to u + \bar{\nu}_e + e^- \tag{1.53}$$

1.5.2 Isospin - pairs

In the above reaction Eq. (1.53), we transfer the antineutrino from the products to the educts by changing it to a neutrino:

$$d + \nu_e \to u + e^- \tag{1.54}$$

This is interpreted by a transformation of a down quark into an up quark combined with a transformation of an electronic neutrino into an electron. Correspondingly, the down quark and the up quark are interpreted as two states such as two spin states. Accordingly, a new isospin has been introduced, and the down quark has isospin $I_z = -1/2$, while the up quark has isospin $I_z = 1/2$. So these two quarks form a pair:

$$\begin{pmatrix} u \\ d \end{pmatrix} \tag{1.55}$$

Similarly, and the electronic neutrino has the isospin $I_z = 1/2$, while the electron has the isospin $I_z = -1/2$, see Eq. (1.58). Thus, these two leptons constitute another isospin pair:

$$\begin{pmatrix} \nu_e \\ e^- \end{pmatrix} \tag{1.56}$$

As these two isospin pairs are combined in the beta decay, they are combined to the following quadruple:

$$\begin{pmatrix} \begin{pmatrix} u \\ d \end{pmatrix} \\ \begin{pmatrix} \nu_e \\ e^- \end{pmatrix} \end{pmatrix} \tag{1.57}$$

1.5.3 Isospin - symmetry

The usual spin states are related to rotations, and these are represented by the special (with determinant one) orthogonal group in three dimensions, the $SO(3)$. Similarly, the isospin states are related to transformations, and these are again represented by a group, the special unitary group in two dimensions, $SU(2)$.

1.5.4 Generations

The quadruple in Eq. (1.57) is a first quadruple that had been developed in several steps: Pauli proposed the existence of the

neutrino as a part of the beta decay in 1930.That neutrino has been directly observed since 1953.The quark model has been proposed around 1960.

Later, two similar quadruples have been discovered. Thereby the top quark was discovered in 1993 and completed these three quadruples. The numbers of these three quadruples are called generations, see Eq. (1.59). The particles of the second and third generation in Eq. (1.59) are the charm quark, c, strange quark, s, top quark, t, bottom quark, b, muon, μ, tauon, τ as well as corresponding neutrinos ν_μ and ν_τ.

$$\begin{pmatrix} gen.1 \\ \begin{pmatrix} u \\ d \end{pmatrix} \\ \begin{pmatrix} \nu_e \\ e^- \end{pmatrix} \end{pmatrix} \rightarrow \begin{pmatrix} I_z \\ \begin{pmatrix} \frac{1}{2} \\ -\frac{1}{2} \end{pmatrix} \\ \begin{pmatrix} \frac{1}{2} \\ -\frac{1}{2} \end{pmatrix} \end{pmatrix} \rightarrow \begin{pmatrix} q \\ \begin{pmatrix} \frac{2}{3} \\ -\frac{1}{3} \end{pmatrix} \\ \begin{pmatrix} 0 \\ -1 \end{pmatrix} \end{pmatrix} \tag{1.58}$$

$$\begin{pmatrix} gen.1 \\ \begin{pmatrix} u \\ d \end{pmatrix} \\ \begin{pmatrix} \nu_e \\ e^- \end{pmatrix} \end{pmatrix} \rightarrow \begin{pmatrix} gen.2 \\ \begin{pmatrix} c \\ s \end{pmatrix} \\ \begin{pmatrix} \nu_\mu \\ \mu \end{pmatrix} \end{pmatrix} \rightarrow \begin{pmatrix} gen.3 \\ \begin{pmatrix} t \\ b \end{pmatrix} \\ \begin{pmatrix} \nu_\tau \\ \tau \end{pmatrix} \end{pmatrix} \tag{1.59}$$

In addition to these particles, the standard model contains bosons that transmit interactions:

The weak interaction is transmitted by W bosons, W^+, W^- and W^0 (also called Z-boson, Z represents zero). The electromagnetic interaction is transmitted by virtual photons. The strong interaction is transmitted by gluons. Beyond the standard model is the hypothetical graviton, see Blokhintsev and Galperin (1934), Carmesin (2021c). The masses of most particles of the standard model are based on the Higgs boson, see e. g. (Peskin, 2015, p. 9-10) or Tanabashi et al. (2018).

1.5.5 Two additional symmetries

We remind that the isospin states form pairs and are related to transformations that represent a group, the special unitary group in two dimensions, the $SU(2)$. Similarly, the quarks u, d and s form a triplet and are related to transformations that represent a group, the special unitary group in three dimensions, the $SU(3)$. That group can explain several elementary particles that are formed from the quarks u, d and s.

An additional symmetry is related to the electromagnetic interaction. An effect of that interaction can be modeled by a change of a phase of a complex number. As numbers represent one dimension, the corresponding group is the special unitary group in one dimension, the $SU(1)$. Altogether, symmetries inherent to elementary particle physics are described by using the groups $SU(1)$, $SU(2)$ and $SU(3)$ including their combinations. Possible relations to higher dimensional groups are being investigated since many decades.

1.5.6 Mixing

The system of elementary particles (Eq. 1.59) has been developed according to reactions such as the beta decay and according to symmetries of $SU(1)$, $SU(2)$ and $SU(3)$. However, the neutrinos of the three generations ν_e, ν_μ and ν_τ can periodically transform into each other, that phenomenon is called neutrino oscillation, see e. g. Tanabashi et al. (2018). Correspondingly, these neutrinos ν_e, ν_μ and ν_τ are modeled as linear combinations of underlying neutrinos ν_1, ν_2 and ν_3. That linear combination is called neutrino mixing and it is described by a mixing matrix U, see e. g. (Tanabashi et al., 2018, S. 14).

Similarly, the masses of the six quarks of the three generations (see Eq. 1.59) are derived on the basis of a mixing matrix, called V_{CKM} see e. g. (Tanabashi et al., 2018, S. 12).

1.5.7 Gauge theory

Each symmetry inherent to elementary particle physics can be described by an operator $\hat{S}$. Each such operator $\hat{S}$ can be expressed in terms of a set of infinitesimal generators $\hat{G}_j$ and by corresponding generalized angles α_j as follows:

$$\hat{S} = \exp[\Sigma_{j=1}^{n} \alpha_j \cdot \hat{G}_j] \tag{1.60}$$

Each local change of a such a symmetry can thus be expressed by local changes of these angles:

$$\alpha_j(\vec{x}) \tag{1.61}$$

In each local theory, such a local angle $\alpha_j(\vec{x})$ cannot propagate faster than the velocity of light. Thus, each global theory must be invariant with respect to such local angles $\alpha_j(\vec{x})$. This statement constitutes the principle of gauge invariance, it can be applied to each local theory, and it has been used in order to derive several theories in elementary particle physics. In the present book series, locality is appropriately generalized to higher dimension.

1.5.8 Open question: formation of mass

The formation of the masses of particles presented in Eq. (1.59), except the neutrino masses, are usually based on the mass m_H of the Higgs boson, see (Peskin, 2015, p. 9-10). However, that mass m_H is not predicted by the SMEP, see (Peskin, 2015, p. 12). Moreover, the derivation of many masses of elementary particles requires additional unexplained parameters, e. g. mixing angles. This shows that the formation of mass is hardly explained by the SMEP. Even the hierarchy problem is unsolved, see e. g. (Shaposhnikov and Shkerin, 2018, p. 1) or Tanabashi et al. (2018), so not even the different scales of the masses of elementary particles have been explained.

Chapter 2

Quantum Gravity

In this chapter we summarize essential results of quantum gravity. In particular, we derive the **length limit** and the **density limit** in nature. Thereby we introduce the **Planck scale**, and we apply it to the time evolution of the actual light horizon R_{lh}.

2.1 Shortest observable standard deviation

In this section we derive the shortest and observable standard deviation σ or the **shortest observable uncertainty, SOU** Δx.

2.1.1 Observable objects

In this section we explicate two necessary conditions for an object to be observable in nature:

1. gravitational condition

No object inside the **event horizon** of a black hole can be observed, see Michell (1784b), Schwarzschild (1916), Kerr (1963), Newman and Janis (1965), Mayo and Bekenstein (1996). Here we analyze black holes without charge and without angular momentum, for simplicity. In this case, the **Schwarzschild radius** R_S is the event horizon. Correspondingly, no length inside the event horizon can be observed.

2. quantum condition

Each standard deviation takes at least the value according to the Heisenberg uncertainty principle, see Heisenberg (1927) or e. g. Ballentine (1998). Correspondingly, no object or length with a smaller standard deviation or randomness can be observed in nature. We summarize:

Definition 5 Observable object or quantity

An observable object or quantity fulfills the following two necessary conditions:

(1) The object is outside the event horizons of black holes.

(2) The object or quantity exhibits a sufficient standard deviation alias uncertainty, according to the Heisenberg uncertainty principle.

Next we specify these two conditions in detail. Secondly we combine these two conditions, see e. g. Carmesin (2017b), Carmesin (2018f), Carmesin (2018b), Carmesin (2021a).

2.1.2 Quantum condition

In this section we derive the **quantum state**[1] Ψ with the shortest standard deviation Δx.

Heisenberg uncertainty principle: As a matter of fact, quantum states obey the Heisenberg uncertainty relation, see Heisenberg (1927) or e. g. (Ballentine, 1998, section 8.4).

The cause of that uncertainty is the quantum state, it is NOT the technique of observation. It is similar to throwing the dice: There occurs a large standard deviation of $\sigma = 1.7$ or $\sigma = \sqrt{\frac{1^2+2^2+3^2+4^2+5^2+6^2}{6} - 3.5^2}$, but the cause of that standard

[1] There are also other essential quantum states in the early universe, see e. g. Carmesin (2021c).

deviation is NOT the observation, as you see the dice clearly. The dice themselves cause the standard deviation.

In the case of the standard deviation Δx, the following uncertainty relation including the standard deviation Δp_x of the momentum holds:

$$\boxed{\Delta x \geq \frac{\hbar}{2 \cdot \Delta p_x}} \tag{2.1}$$

2.1.3 Gravitational condition

In this S. we analyze the gravitational condition.

The Schwarzschild radius of a mass m or energy $E = m/c^2$ has the following amount:

$$\boxed{R_S = \frac{2G \cdot m}{c^2} = \frac{2G \cdot E}{c^4}} \tag{2.2}$$

2.1.4 Uncertainty Δx of a quantum state

In this section we analyze the SOU for an arbitrary quantum state.

Δp_x as a function of energy E: As we derive the shortest standard deviation Δx, the standard deviation Δp_x is very large. Thus, the quantum state is relativistic. Thence the relativistic energy - momentum relation holds:

$$E^2/c^2 = p^2 \tag{2.3}$$

In a D dimensional space, the momentum can exhibit D components p_j, with $1 \leq j \leq D$:

$$E^2/c^2 = \Sigma_{j=1}^{D} p_j^2 \tag{2.4}$$

Thereby, each squared component p_j^2 is the sum of the squared averaged value $\bar{p}_j^2$ and the squared standard deviation $(\Delta p_j)^2$:

$$E^2/c^2 = (\Delta p_x)^2 + \bar{p}_x^2 + \Sigma_{j=2}^{D}[\bar{p}_j^2 + (\Delta p_j)^2] \tag{2.5}$$

In the SOU, $(\Delta p_x)^2$ takes the maximal possible value. So the remaining components are nearly zero[2] or zero in the ideal case:

$$\bar{p}_x^2 + \Sigma_{j=2}^{D}[\bar{p}_j^2 + (\Delta p_j)^2] = 0 \tag{2.6}$$

In the following, we name the product $c \cdot \Delta p_x$ equivalent energy corresponding to direction x:

$$E_x = c \cdot \Delta p_x \tag{2.7}$$

We summarize this result:

Proposition 2 Momenta in a quantum state at SOU

In a quantum state Ψ with the shortest observable uncertainty, the energy of that state corresponds to the standard deviation Δp_x only:

$$\boxed{E/c = \Delta p_x = E_x/c} \tag{2.8}$$

All other components of the momentum are zero, or they tend to zero in a possibly existing limit.

In the following, we denote that quantum state as a plane wave type quantum state with momentum p_x.

2.1.5 Lower bound of Δx in terms of E_x

In this section we derive a lower bound of the uncertainty Δx of a quantum state of a SOU, whereby that bound is a function of the equivalent energy E_x.

Naturally, the quantum state obeys the Heisenberg uncertainty relation, Eq. (2.1). We apply PROP. (2) to that equation. So we derive the following lower bound of the uncertainty:

$$\Delta x \geq \frac{\hbar \cdot c}{2 \cdot E_x} \tag{2.9}$$

[2]Correspondingly, the extensions in the dimensions $D \geq 2$ tend to infinity.

2.1.6 Located object in D dimensions

In this section we discover an elementary type of objects located in D dimensional space.

For it we realize that a plane wave type quantum state is located in the x-direction, but it is hardly located in the other directions of space. Such a quantum state is described by a wave function or Hilbert space vector $\Psi_x = \Psi_{r_1}$.

The product state is an elementary combination of D such states, one in each direction:

$$\Psi = \Pi_{j=1}^{j=D} \Psi_{r_j} \tag{2.10}$$

For the case of three dimensions, the momentum of the product state is the following vector:

$$\vec{p} = \begin{pmatrix} p_x \\ p_y \\ p_z \end{pmatrix} = \begin{pmatrix} p_1 \\ p_2 \\ p_3 \end{pmatrix} \tag{2.11}$$

The corresponding absolute value is as follows:

$$p^2 = p_x^2 + p_y^2 + p_z^2 \tag{2.12}$$

Here we consider a frame in which the average of the momentum is zero. Hence we derive:

$$p^2 = (\Delta p_x)^2 + (\Delta p_y)^2 + (\Delta p_z)^2 \tag{2.13}$$

Moreover, we analyze isotropic product states. So we derive:

$$p^2 = 3 \cdot (\Delta p_x)^2 \text{ or } p = \sqrt{3} \cdot \Delta p_x \tag{2.14}$$

As the considered SOUs exhibit relatively large energy, these states are relativistic. Thus, the relativistic energy momentum relation holds, $p = \frac{E}{c}$, in particular $\Delta p_x = \frac{E_x}{c}$. So we derive:

$$E = \sqrt{3} \cdot E_x \tag{2.15}$$

2.1.7 R_S of a located object

In this section we derive the Schwarzschild radius of a located object, see Eq. (2.10).

As a located object has a size and an energy, it can become a black hole. So it can have a Schwarzschild radius, see Eq. (2.2):

$$R_S = \frac{2G \cdot m}{c^2} = \frac{2G \cdot E}{c^4} \tag{2.16}$$

Next we relate that R_S to the uncertainty Δx.

Shell model of the black hole: In this paragraph we derive an elementary well founded theory for the black hole[3]. When energy or matter falls into the black hole by crossing the Schwarzschild radius, then it cannot emit any radiation. So it cannot reduce its energy. Thus, it cannot fall deeper. Hence the energy gathers at a shell with the radius $R \geq R_S$ (see also Carmesin (2021c)).

Uncertainty Δx of the black hole: For the case of the shell model of the black hole, we derive the uncertainty Δx of the location of the energy. For it we derive the average of $\langle x^2 \rangle$:

$$x^2 + y^2 + z^2 = R^2 \tag{2.17}$$

We apply the average:

$$\langle x^2 \rangle + \langle y^2 \rangle + \langle z^2 \rangle = \langle R^2 \rangle = R^2 \tag{2.18}$$

As the black hole is isotropic, the three averages over the coordinates are equal. So we derive:

$$3\langle x^2 \rangle = R^2 \tag{2.19}$$

Without loss of generality, we choose the origin of the coordinate system at the center of the black hole. Thus, we have $\langle x^2 \rangle =$

[3] Akiyama et al. (2019) achieved the first direct observation of a black. Accordingly, there is no detailed and well tested theory of a black hole available at the present-day. In that situation, we derive a basic theory here.

$(\Delta x)^2$. With it we derive:

$$3(\Delta x)^2 = R^2 \text{ or } \Delta x \geq \frac{1}{\sqrt{3}} \cdot R \tag{2.20}$$

Using $R \geq R_S$ we derive:

$$\Delta x \geq \frac{1}{\sqrt{3}} \cdot R_S \tag{2.21}$$

We insert Eq. (2.16). So we derive the uncertainty Δx that a black hole with an energy E has:

$$\Delta x \geq \frac{1}{\sqrt{3}} \cdot \frac{2G \cdot E}{c^4} \tag{2.22}$$

As the uncertainty Δx corresponds to one direction in space only, we express the energy E in terms of E_x, see Eq. (2.15): Thus, we derive:

$$\boxed{\Delta x \geq \frac{2G \cdot E_x}{c^4}} \tag{2.23}$$

We summarize our results:

Proposition 3 Located objects

In D dimensions, D plane wave type quantum state with momenta p_j, $1 \leq j \leq D$ with wave functions of Hilbert state vectors $\Psi_j = \Psi_{r_j}$ can form a product state:

$$\Psi = \Pi_{j=1}^{j=D} \Psi_{r_j} \tag{2.24}$$

In the following, we denote the object described by that product state Ψ a located object. A located object has the following properties, if it is described in a frame at which the momentum of a located object is zero and in a coordinates system that has the origin at the center of a located object:

(1) The momentum is $\sqrt{D}$ multiplied by Δp_x:

$$p = \sqrt{D} \cdot \Delta p_x \tag{2.25}$$

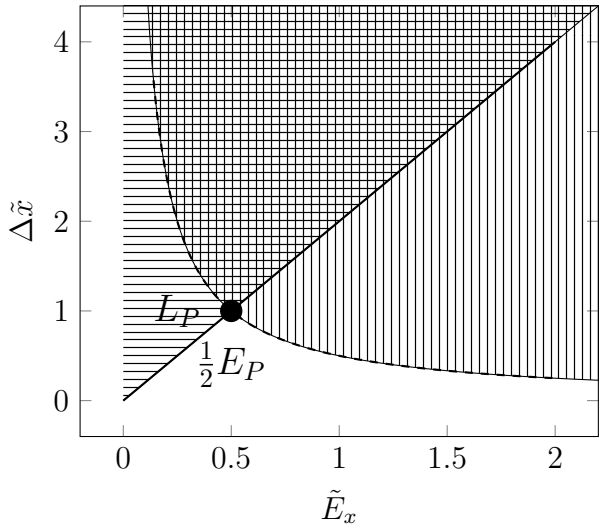

Figure 2.1: Shortest observable uncertainty (dot): Observable states outside the event horizon of a possible black hole (horizontal lines). Sufficient uncertainty according to the Heisenberg uncertainty relation (vertical lines). Observable and sufficient uncertainty (intersection).

(2) The energy is $\sqrt{D}$ multiplied by E_x:

$$E = \sqrt{D} \cdot E_x \tag{2.26}$$

(3) Naturally, the located object can form a black hole, resulting in the following lower bound for the uncertainty:

$$\Delta x \geq \frac{2G \cdot E_x}{c^4} \tag{2.27}$$

(4) Naturally, the located object obeys the Heisenberg uncertainty relation, resulting in the following lower bound for the uncertainty:

$$\Delta x \geq \frac{\hbar \cdot c}{2 \cdot E_x} \tag{2.28}$$

2.1.8 Combination of the two lower bounds

In this section we combine the two lower bounds of a located object, see proposition (3). For it we present these two lower

bounds in a $\Delta c/E$)- diagram. Hereby we apply Planck units, see table (15.3), see Fig. (2.1).

The states with sufficient uncertainty Δx according to the Heisenberg uncertainty relation (proposition (3, part (4)) are marked by vertical lines. Simultaneously, the states with sufficient uncertainty Δx according to gravity, see PROP. (3, part (3)), are marked by horizontal lines.

Hence the states with sufficient uncertainty correspond to the intersection of the above two sets of states, these are marked by crossing lines in Fig. (2.1). Obviously there is a state with the smallest observable uncertainty. It is marked by the dot.

We derive the coordinates of that point as follows: Firstly, we set equal the terms in Eqs. (2.27) and (2.9)

$$\frac{2G \cdot E_x}{c^4} = \frac{\hbar \cdot c}{2 \cdot E_x} \tag{2.29}$$

We solve for E_x:

$$E_x^2 = \frac{1}{4} \cdot \frac{\hbar \cdot c^5}{G} \tag{2.30}$$

We identify the second fraction with the square of the Planck energy, E_P^2, see table 15.3. Moreover, we take the root. So we derive the energy E_x:

$$E_x = \frac{1}{2} \cdot E_P \tag{2.31}$$

In order to derive the corresponding uncertainty, we insert the above energy into Eq. (2.9). As we analyze the shortest length, we use the equality instead of the inequality. Thence we derive:

$$\Delta x = \frac{\hbar \cdot c}{E_P} \tag{2.32}$$

We identify the above fraction with the Planck length L_P, see table 15.3. So we derive:

$$\Delta x = L_P \tag{2.33}$$

We summarize our result:

Proposition 4 Shortest observable uncertainty, SOU

The shortest observable uncertainty has the following properties:

(1) The shortest observable uncertainty is a length, by definition of the word 'short'.

(2) The SOU is equal to the Planck length:

$$\boxed{\Delta x_{SOU} = L_P = \sqrt{\frac{\hbar \cdot G}{c^3}} = 1.616 \cdot 10^{-35}\,\mathrm{m}} \tag{2.34}$$

(3) The energy E_x corresponding to Δx_{SOU} is equal to one half of the Planck energy:

$$\boxed{E_{x,SOU} = \frac{1}{2} \cdot E_P \;\text{ with }\; E_P = \sqrt{\frac{\hbar \cdot c^5}{G}} = 1.956 \cdot 10^{9}\,\mathrm{J}} \tag{2.35}$$

(3) The **dynamical mass** $m = \frac{E}{c^2}$ *corresponding to $E_{x,SOU}$ is equal to one half of the Planck energy divided by c^2, it is the Planck mass:*

$$\boxed{M_{x,SOU} = \frac{1}{2} \cdot M_P \;\text{ with }\; M_P = \sqrt{\frac{\hbar \cdot c}{G}} = 2.176 \cdot 10^{-8}\,\mathrm{kg}} \tag{2.36}$$

2.1.9 Upper bound for the density

The quantum state with the SOU, provides an upper limit of the density. It is derived in this section.

At an uncertainty $\Delta\tilde{x}$ see dotted line in figure (2.2), the observable and sufficiently uncertain states are represented by the area marked by crossing horizontal and vertical lines in that figure. Among these states at that uncertainty $\Delta\tilde{x}$, the state with the largest density is the state with the largest energy $\tilde{E}_x$ at that dotted line. It is the state at the straight line in that figure. These states are characterized by Eq. (2.27). In particular, the

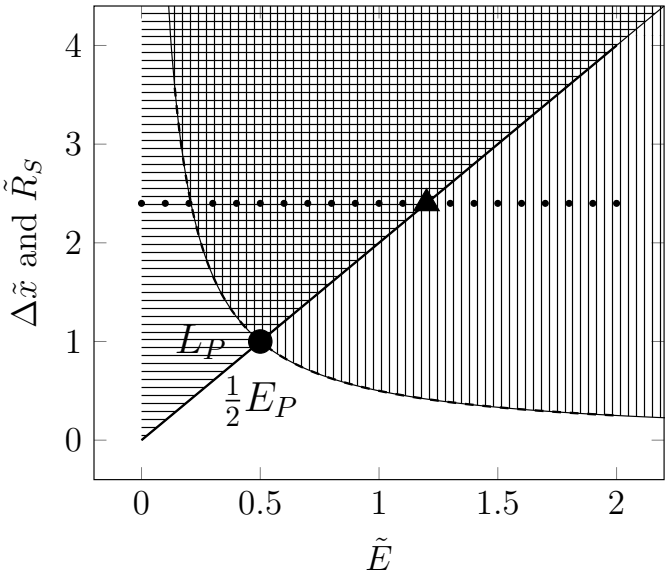

Figure 2.2: An upper bound for the density: Observable states (horizontal lines). Sufficient uncertainty (vertical lines). Observable and sufficient uncertainty (intersection). Dots show states at an uncertainty $\Delta\tilde{x}$, among these states, the observable state with the largest energy is marked by the triangle.

inequality defines the area marked by horizontal lines, whereas the straight line is determined by the corresponding equality:

$$\Delta x = \frac{2G \cdot E_x}{c^4} \tag{2.37}$$

The corresponding density is the energy divided by c^2 and by the volume. By construction, it is an upper bound for the density:

$$\rho \leq \frac{E_x}{c^2 \cdot V} \quad \text{with} \quad V = \frac{4\pi}{3}(\Delta x)^3 \tag{2.38}$$

We solve Eq. (2.37) for E_x, and we insert the resulting term in the above equation for the density. Moreover, we insert the above term for the volume. So we derive:

$$\rho \leq \frac{c^4 \cdot \Delta x}{c^2 \cdot 2G \cdot \frac{4\pi}{3}(\Delta x)^3} \tag{2.39}$$

We simplify the above term. Thus, we derive:

$$\rho \leq \frac{1}{2} \cdot \frac{3}{4\pi} \cdot \frac{c^2}{G \cdot (\Delta x)^2} \tag{2.40}$$

The above term is proportional to $(\Delta x)^{-2}$. Hence the largest upper bound for the density occurs at the smallest possible value of Δx. It is the Planck length, see proposition (4). Hence we derive the following upper bound:

$$\rho \leq \frac{1}{2} \cdot \frac{3}{4\pi} \cdot \frac{c^2}{G \cdot L_P^2} \tag{2.41}$$

We identify the last fraction in the above equation by the Planck density, see table (15.3):

$$\rho \leq \frac{1}{2} \cdot \frac{3}{4\pi} \cdot \rho_P \tag{2.42}$$

Moreover, we identify $\frac{3}{4\pi} \cdot \rho_P$ by the Planck density of a ball, $\bar{\rho}_P$, see table (15.3):

$$\rho \leq \frac{1}{2} \cdot \bar{\rho}_P \tag{2.43}$$

Here we apply the scaled density $\tilde{\rho} = \rho/\bar{\rho}_P$, see table (15.3):

$$\boxed{\tilde{\rho} \leq \frac{1}{2}} \tag{2.44}$$

We summarize our result:

Proposition 5 An upper bound of the density

As derived from gravity and quantum physics, the density has a natural upper limit as follows:

$$\boxed{\rho \leq \frac{1}{2} \cdot \frac{3}{4\pi} \cdot \rho_P = \frac{1}{2} \cdot \bar{\rho}_P} \tag{2.45}$$

2.1.10 On the measurement of a standard deviation

In general, the significance of a measurement of an observable A of a quantum state Ψ is limited by the standard deviation σ, naturally. This standard deviation is alternatively named uncertainty ΔA. In particular, that standard deviation can be measured by executing a large number of measurements at an ensemble of quantum objects that are in the considered state Ψ. So a number N of measurement values A_j can be obtained. Therefrom the empirical standard deviation can be calculated:

$$\Delta_{empirical} = \sigma_{empirical} = \sqrt{\Sigma_j^N A_j^2/N - (\Sigma_j^N A_j/N)^2} \qquad (2.46)$$

In this manner an operational significance of the uncertainty is achieved, see e. g. (Ballentine, 1998, Fig. 8.2 or section 8.4).

2.2 Incompleteness of GRT

In this section we analyze the time evolution of the actual light horizon R_{lh} by using Eq. (1.37). Figure (2.3) shows the result. In the limit time to zero, the light horizon goes to zero, and as a consequence, the density diverges. This property of the model is physically not realistic, and this discrepancy is denoted as the singularity problem, see e. g. Kiefer (2003).

2.2.1 Singularity problem

Next we analyze, whether that singularity problem is physically essential: If the light horizon R_{lh} reaches the Planck length L_P at a physically possible density $\rho < \frac{\rho_P}{2}$, then the singularity problem is not physically essential, since all physical possible lengths are reached at physically possible densities in that case. In the other case, the singularity problem is physically essential as not all physically possible lengths are reached.

Accordingly, we evaluate the densities $\rho(t)$ corresponding to values $R_{lh}(t)$ that the actual light horizon can take. For it we

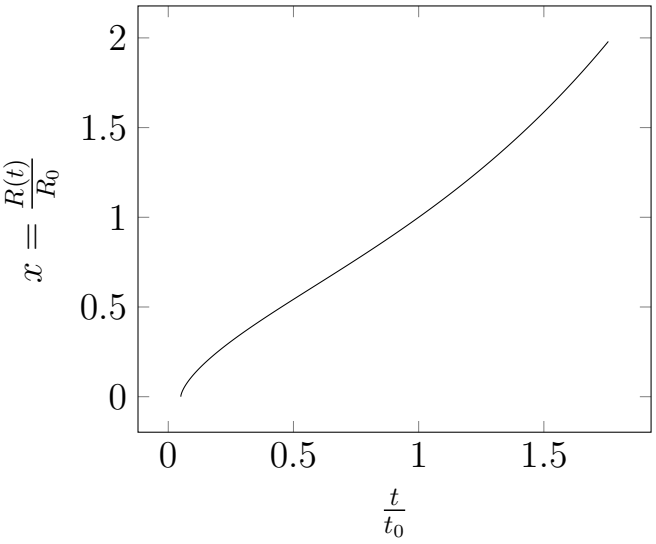

Figure 2.3: Time evolution of the scale factor. The time is presented in units of the age of the universe t_0, while the scale factor is shown in units of R_0. We calculate the graph by application of Eq. (1.28).

show the densities $\rho(t)$ and the corresponding values $R_{lh}(t)$ as a function of the time t, see Fig. (2.4). The figure shows that the maximally possible density $\frac{\rho_P}{2}$ is reached at values $R_{lh}(t)$ that are 30 orders of magnitude larger than the physical limit of the Planck length L_P. So the singularity problem is very essential. Moreover, the GRT is incomplete, as it does not provide the full dynamics of the values values $R_{lh}(t)$ of the light horizon.

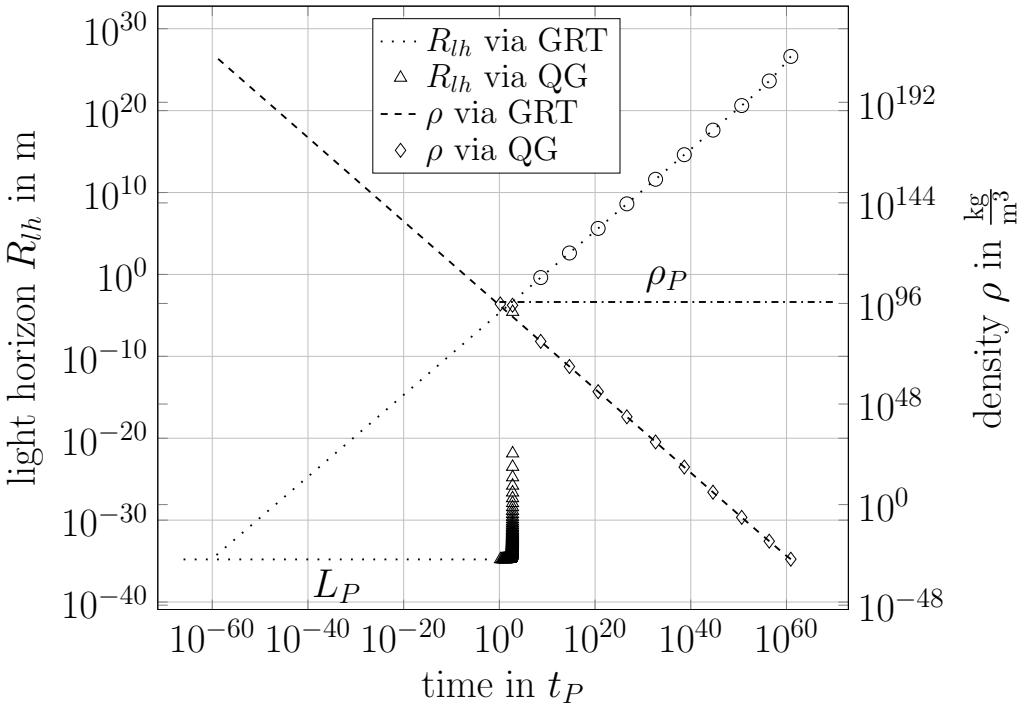

Figure 2.4: Density limit of expansion of space: The time evolution of R_{lh} according to the GRT ($\circ$) ranges from the present-day value $4.14 \cdot 10^{26}$ m backwards to 0.003 mm, as at this point the density ($\diamond$) achieves the Planck density $\rho_P = 5.155 \cdot 10^{96} \frac{\text{kg}}{\text{m}^3}$ (dashdotted), and no higher density is physically possible.
However, the physically possible lengths can be as short as the Planck length L_P (loosely dotted). Hence the time evolution of the GRT is **incomplete**.
In contrast, we derive the **complete time evolution** of $R_{lh}(t)$, ranging from the current value $4.14 \cdot 10^{26}$ m backwards to L_P. For it we apply GRT ($\circ$) combined with dimensional phase transitions ($\triangle$) derived by quantum gravity, see (3). Thereby, the phase transitions cause the **extremely rapid distance enlargement in the early universe**

Chapter 3

Transitions in the early universe

In this section we present dimensional transitions that take place in the early universe. For it we emphasize that physics in dimensions $D > 3$ has been observed in experiments with photons as well as in experiments with electrons, see Lohse et al. (2018), Zilberberg et al. (2018). The results of this chapter have been published since Carmesin (2017b) and are presented recently in Carmesin (2021c).

3.1 Kinetic energy in D dimensions

In this section we make transparent how the kinetic energy of a mass m is naturally defined in D dimensions:

$$E_{kin} = \frac{1}{2m} \Sigma_{j=1}^{j=D} p_j^2 \tag{3.1}$$

3.2 Gravity in $D \geq 3$ dimensions

In this section we show that the gravitational energy is naturally defined in $D \geq 3$ dimensions. For it we remind that GRT can be derived from Gaussian gravity, see (Carmesin, 2021c, theorem 1). And Gaussian gravity can naturally be defined in $D \geq 3$ dimensions, see e. g. Fig. (3.1).

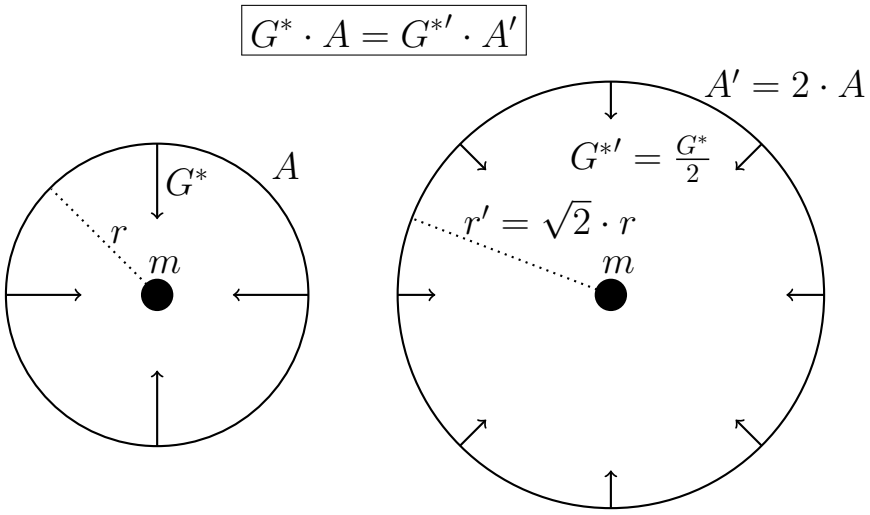

Figure 3.1: Gaussian gravity of a mass m: All balls around m have the same flux $G^*(r) \cdot A(r)$. This means the same product of the gravitational field $G^*(r)$ and area $A(r)$. Consequently, we derive in D dimensions: $G^*(r) \propto \frac{1}{A(r)} \propto \frac{1}{r^{D-1}}$.

3.2.1 Gravity term for $D \geq 3$

According to Gaussian gravitation, the gravitational field $G^*(r)$ at a distance r from a mass is proportional to $1/r^{D-1}$ (Fig. 3.1, and Gauss (1840)):

$$G^* \propto \frac{1}{r^{D-1}} \tag{3.2}$$

The same proportionality applies to the gravitational force F which a mass M exerts on a mass m at the distance r. Moreover, the force is proportional to each of the masses:

$$F \propto \frac{M \cdot m}{r^{D-1}} \tag{3.3}$$

The proportionality factor is a gravitational constant for dimension D, G_D:

$$F = -G_D \cdot \frac{M \cdot m}{r^{D-1}} \tag{3.4}$$

The potential energy or gravitational energy is the integral of the force. By DEF., the energy is zero in the limit r to infinity:

$$E_G = -G_D \cdot \frac{M \cdot m}{(D-2) \cdot r^{D-2}} \tag{3.5}$$

The gravitational constant can be derived (see e.g. Carmesin (2017b), Carmesin (2019d)). The following holds:

$$G_D = G \cdot (D-2) \cdot L_P^{D-3} \tag{3.6}$$

We summarize:

Proposition 6 Gravitation in D dimensions

(1) Two objects at a distance r, with masses or dynamic masses M and m, exert the gravitational force $F = -G_D \cdot \frac{M \cdot m}{r^{D-1}}$ on each other in $D \geq 3$ dimensions with $G_D = G \cdot (D-2) \cdot L_P^{D-3}$.

(2) The corresponding energy is: $E_G = -G_D \cdot \frac{M \cdot m}{(D-2) \cdot r^{D-2}}$

(3) As kinetic and gravitational energy are naturally defined in $D \geq 3$ dimensions, the fact that we live in three dimensions is not the only physically possible case. Instead, it must be explained why three dimensional space is stable in the present-day universe, see e. g. Carmesin (2017b), Carmesin (2018a), Carmesin (2021c).

(4) When the space changes from a dimension $D + s$ to a dimension D, then s directions of translation symmetry are lost. Thus, such a transition is a symmetry breaking phase transition, see Landau and Lifschitz (1979b), we call it **dimensional phase transition**.

3.2.2 Special radii at scaled densities $\tilde{\rho}_D$

In this section we analyze the radius b of a black hole and the radius a_M of radiation with dynamic mass M as a function of the density $\tilde{\rho}_D$.

Radius a_M depending on the scaled density: We derive how the radius a_M depends on the scaled density ρ_D. We use natural units (see table 15.3).

According to the redshift, the dynamic mass is proportional to the inverse wavelength $M_{dyn} \propto \frac{1}{a_M}$. For example, for $a_M = L_P$ is $M_{dyn} = \frac{M_P}{2}$ (Fig. 2.1). Both relations result in:

$$\frac{1}{2\tilde{a}_M} = \tilde{M}_{dyn} \tag{3.7}$$

Here we use the term for the density, where V_D denotes the volume of a hyper ball with radius 1:

$$\rho_D = \frac{M_{dyn}}{V_D \cdot a^D} \tag{3.8}$$

Hereby the volume of a unit ball is as follows:

$$V_D = \frac{\pi^{D/2}}{\Gamma(1+D/2)};\ \Gamma(x+1) = \Gamma(x) \cdot x; \Gamma(1) = 1; \Gamma\left(\frac{1}{2}\right) = \sqrt{\pi} \tag{3.9}$$

We use the Planck density related to a ball $\bar{\rho}_{D,P} = \frac{M_P}{V_D \cdot L_P^D}$ (table 15.3). So we get:

$$\tilde{\rho}_D = \frac{\rho_D}{\bar{\rho}_{D,P}} = \frac{\tilde{M}_{dyn}}{\tilde{a}_M^D} \tag{3.10}$$

In total we get:

$$\frac{1}{2\tilde{a}_M} = \tilde{M}_{dyn} = \tilde{\rho}_D \cdot \tilde{a}_M^D \tag{3.11}$$

Resolved we get:

$$\boxed{\tilde{a}_M = (2\tilde{\rho}_D)^{-1/(D+1)}} \tag{3.12}$$

Schwarzschild radius: We determine the Schwarzschild radius b depending on the density. We proceed like Michell (Michell

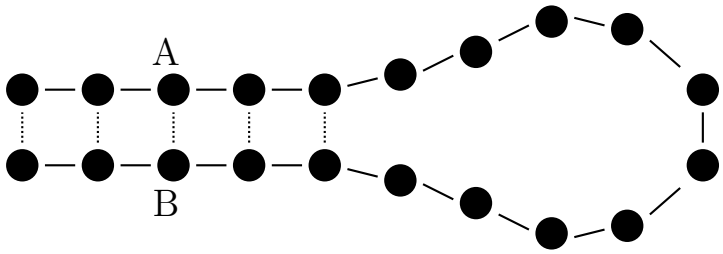

Figure 3.2: At high density near the Planck scale, $\rho \approx \rho_P$, the space exhibits a grainy structure (dots) at the scale of the Planck length, $L \approx L_P$. At such a density, a layer of **shortcuts** (dotted) can form spontaneously. The corresponding critical density is derived in S. (3.3).

(1784a)). We equate the kinetic energy $\frac{1}{2}M \cdot v^2$ with the potential energy and choose the velocity of light c. So we get:

$$\frac{1}{2} \cdot c^2 = \frac{G_D \cdot m}{(D-2) \cdot b^{D-2}} \tag{3.13}$$

We use $G_D = G \cdot (D-2) \cdot L_P^{D-3}$ and we use natural units. So we get (table 15.3):

$$\boxed{\tilde{b} = (2\tilde{\rho}_D)^{-1/2}} \tag{3.14}$$

3.3 Critical density $\rho_{cr.sc.}$ for shortcuts

In this section we derive an example of a dimensional phase transition: At a critical density $\rho_{cr.conn.}$, connections of a length $dL \approx L_P$ and with the volume $dV \approx L_P^3$ form spontaneously, for an illustration of several formed connections see Fig. (3.2). Thereby the dimension is increased and a dimensional phase transition takes place.

Condition for the transition: If the rate of change of the vacuum inside the connection $\dot{\varepsilon}_{inside} = \frac{\delta V}{\delta t \cdot dV}|_{inside}$ is negative, then the shortcut permanently looses vacuum, so it vanishes. If the rate of change of the vacuum inside the connection $\dot{\varepsilon}_{inside}$ would be

larger than zero, then the shortcut would permanently get new vacuum, so that can happen for a short time only. If the rate of change of the vacuum inside the connection $\dot{\varepsilon}_{inside}$ is equal to zero, then the shortcut contains a constant amount of vacuum, correspondingly, the shortcut is stable. This shows that the shortcut becomes stable at the condition $\dot{\varepsilon}_{inside} = 0$. Hence, at the critical density $\rho_{cr.conn.}$, the rate of change of the vacuum inside the connection $\dot{\varepsilon}_{inside} = \frac{\delta V}{\delta t \cdot dV}|_{inside}$ is zero.

Contributions to the rate $\dot{\varepsilon}_{inside}$: Some vacuum flows from the connection to neighboring regions A and B, see Fig. (3.3), at a rate $\dot{\varepsilon}_{out}$. Similarly, some vacuum flows from neighboring regions A and B to the connection at another rate $\dot{\varepsilon}_{in}$. Thirdly, some vacuum forms in the connection at a rate $\dot{\varepsilon}_{formation}$. Next we analyze these rates in detail.

Rate of outward flow: The vacuum dV of the connection can escape at the velocity of light in two directions, see Fig. (3.3). For that escape it requires the time $dt = L_P/c = t_P$, whereby t_P is the Planck time. Thereby a quantum flows in each of the two directions with the probability 50 %. Thus, during the time t_P, the volume dV of the connection leaves that volume. So the rate of outward flow is as follows:

$$\frac{\delta V}{\delta t}|_{out} = -\frac{dV}{t_P} \tag{3.15}$$

We solve for the rate per volume:

$$\dot{\varepsilon}_{out} = \frac{\delta V}{\delta t \cdot dV}|_{out} = -\frac{1}{t_P} \tag{3.16}$$

Rate of inward flow: As the cube of length L_P at a region A has six equal surfaces, one of which is directed to the connection, the sixth part of its rate $\frac{\delta V}{\delta t \cdot dV}|_{from\ A}$ propagates to the connection:

$$\frac{1}{6} \cdot \dot{\varepsilon}|_{from\ A} = -\frac{1}{6 \cdot t_P} \tag{3.17}$$

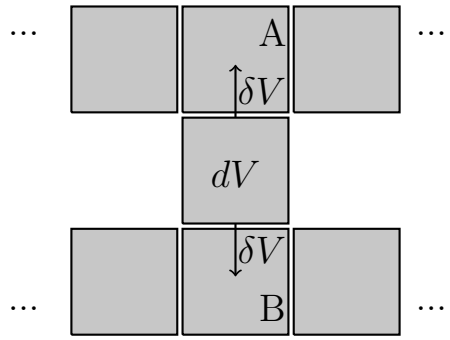

Figure 3.3: Flow of vacuum δV from dV: We assume that the vacuum essentially flows to existing vacuum. In order to get an estimation we analyze cubes with length $L \approx L_P$.

So the rate propagating from A to the connection is positive and has the absolute value of the above term:

$$\dot{\varepsilon}_{in,from\ A} = +\frac{1}{6 \cdot t_P} \tag{3.18}$$

The same rate propagates to the connection coming from B. So we derive:

$$\dot{\varepsilon}_{in} = \frac{2}{6 \cdot t_P} \tag{3.19}$$

Rate of formation of vacuum: Additionally, the density ρ of the connection forms vacuum. The exact rate depends on the symmetry. We model and analyze the rate for the unidirectional formation of vacuum, as it may propagate orthogonal to the surface of the cube. So we get, see Carmesin (2021c):

$$\dot{\varepsilon}_{formation} = \sqrt{8\pi \cdot G \cdot \rho} \tag{3.20}$$

Sum of rates: We add the above three rates. So the total rate is as follows:

$$\dot{\varepsilon}_{inside} = \dot{\varepsilon}_{out} + \dot{\varepsilon}_{in} + \dot{\varepsilon}_{formation} \tag{3.21}$$

We insert the corresponding terms and set the rate to zero:

$$\dot{\varepsilon}_{inside} = \frac{-1}{t_P} + \frac{2}{6 \cdot t_P} + \sqrt{8\pi \cdot G \cdot \rho} = 0 \tag{3.22}$$

We solve for the root in the above Eq.:

$$\sqrt{8\pi \cdot G \cdot \rho} = \frac{2}{3 \cdot t_P} \tag{3.23}$$

We solve for the density:

$$\rho = \frac{1}{18\pi} \cdot \frac{1}{t_P^2 \cdot G} \tag{3.24}$$

The second fraction in the above is equal to the Planck density. So we derive the following for the **critical density of spontaneous connection formation**, $\rho_{cr.conn.}$:

$$\boxed{\rho_{cr.conn.} = \frac{1}{18\pi} \cdot \rho_P = 0.018 \cdot \rho_P} \tag{3.25}$$

In terms of the Planck density for a ball $\bar{\rho}_P = \rho_P \cdot 3/(4\pi)$ (see appendix), we get:

$$\boxed{\rho_{cr.conn.} = \frac{2}{27} \cdot \bar{\rho}_P = 0.074 \cdot \bar{\rho}_P} \tag{3.26}$$

Theorem 1 New vacuum can form new connections.

New connections form spontaneously at densities above the critical density $\tilde{\rho}_{cr.conn.} = \frac{2}{27}$.

At higher dimension, there occurs a sequence of critical densities (Eq. 3.93, Fig. 3.9).

3.4 Dimensional phase transitions in a binary fluid

In the early universe there was a binary fluid consisting of photons and very small black holes, whereby it is possible to define an averaged position of photons in the vicinity of a mass, see Carmesin (2020b). For the case of a real gas, van der Waals (1873) derived a phase transition, a condensation, by analyzing

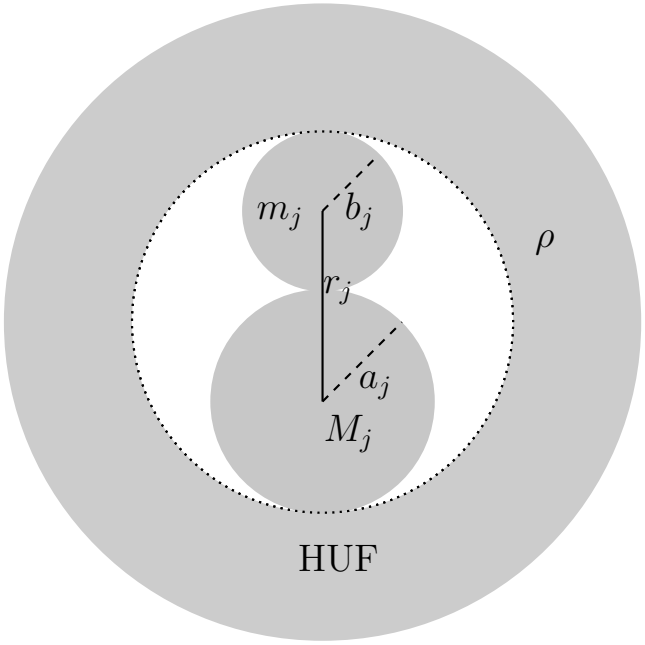

Figure 3.4: Pair j of adjacent objects or particles in a HUF at a density ρ of the universe.

two prototypical particles that represent the gas including the particle - particle - interactions.

Similarly and in this section, we derive the dimensional phase transitions that occurred in the binary fluid of the early universe by analyzing two objects, see Fig. (3.4).

3.4.1 Quantized FLE for pairs

In this section we generalize the FLE by deriving the quantized dynamics for the expectation value $\langle \dot{r}_j \rangle$ of the time derivative of the radius r_j of a pair of objects that is located in a HUF. Moreover, we form the average over pairs. For it we combine the energy term of the Gaussian gravity (see Eq. 3.5).

Applications of the HUF: Here we investigate the distance r_j and the potential of the mass m_j with respect to the mass M_j.

The gravitational energy of the objects m_j and M_j in the

HUF is as follows:

$$E_G = -G_D \cdot \frac{M_j \cdot m_j}{(D-2) \cdot r_j^{D-2}} \tag{3.27}$$

With the term of the kinetic energy $E_{kin,j} = \frac{\sum_{i=1}^{D} p_{j,i}^2}{2m_j}$ we get:

$$\frac{\sum_{i=1}^{D} p_{j,i}^2}{2m_j} - G_D \cdot \frac{M_j \cdot m_j}{(D-2) \cdot r_j^{D-2}} = E_j \tag{3.28}$$

Accordingly, the following applies to quantum objects:

$$\frac{\sum_{i=1}^{D} \hat{p}_{j,i}^2}{2m_j} - \frac{G_D}{D-2} \cdot m_j \cdot M_j \cdot \hat{r}_j^{2-D} = \hat{E}_j \tag{3.29}$$

We derive the expectation value $\langle \hat{E}_j \rangle$ of the energy term (Eq. 3.29) and divide by $m_j \cdot c^2$:

$$\frac{\langle \hat{E}_j \rangle}{m_j \cdot c^2} = \frac{\sum_{i=1}^{D} \left\langle \hat{p}_{j,i}^2 \right\rangle}{2m_j^2 \cdot c^2} - \frac{G_D}{(D-2) \cdot c^2} \cdot \left\langle M_j \cdot \hat{r}_j^{2-D} \right\rangle \tag{3.30}$$

We separate the fluctuations from the expectation value by applying the identity:

$$\left\langle \hat{p}^2 \right\rangle = \langle \hat{p} \rangle^2 + (\Delta p)^2 \tag{3.31}$$

So we get:

$$\frac{\langle \hat{E}_j \rangle}{m_j \cdot c^2} = \frac{\sum_{i=1}^{D} \langle \hat{p}_{j,i} \rangle^2}{2m_j^2 \cdot c^2} + \frac{\sum_{i=1}^{D} (\Delta p_{j,i})^2}{2m_j^2 \cdot c^2} - \frac{G_D \cdot \left\langle M_j \cdot \hat{r}_j^{2-D} \right\rangle}{(D-2) \cdot c^2} \tag{3.32}$$

We use the identity $\langle \hat{p} \rangle / m = \langle \dot{r} \rangle$. So we get:

$$\frac{\langle \hat{E}_j \rangle}{m_j \cdot c^2} = \frac{\sum_{i=1}^{D} \langle \dot{r}_{j,i} \rangle^2}{2 \cdot c^2} + \frac{\sum_{i=1}^{D} (\Delta p_{j,i})^2}{2m_j^2 \cdot c^2} - \frac{G_D \cdot \left\langle M_j \cdot \hat{r}_j^{2-D} \right\rangle}{(D-2) \cdot c^2} \tag{3.33}$$

In the first summand, we add the components:

$$\sum_{i=1}^{D} \langle \dot{r}_{j,i} \rangle^2 = \langle \dot{r}_j \rangle^2 \tag{3.34}$$

We call the remaining term **reduced normalized energy** $E_{D,j}$:

$$\boxed{E_{D,j} = \frac{\sum_{i=1}^{D} (\Delta p_{j,i})^2}{2m_j^2 \cdot c^2} - \frac{G_D}{(D-2) \cdot c^2} \cdot \left\langle M_j \cdot \hat{r}_j^{2-D} \right\rangle} \tag{3.35}$$

So the following holds (Eq. 3.33):

$$\frac{\langle \hat{E}_j \rangle}{m_j \cdot c^2} = \frac{\langle \dot{r}_j \rangle^2}{2 \cdot c^2} + E_{D,j} \tag{3.36}$$

The left hand side of the above Eq. is identified with one half of a quantized **curvature parameter** of a pair, $k_j/2$:

$$\frac{-k_j}{2} = \frac{\langle \hat{E}_j \rangle}{m_j \cdot c^2} = \frac{\langle \dot{r}_j \rangle^2}{2 \cdot c^2} + E_{D,j} \tag{3.37}$$

Here we apply the average over the pairs, and we denote it by rectangular brackets:

$$\frac{-[k_j]}{2} = \frac{[\langle \dot{r}_j \rangle^2]}{2 \cdot c^2} + [E_{D,j}] \tag{3.38}$$

In order to obtain a generalized FLE, we multiply by $2c^2/[\langle r_j \rangle^2]$, and we resolve:

$$\boxed{\frac{[\langle \dot{r}_j \rangle^2]}{[\langle r_j \rangle^2]} = -\frac{2[E_{D,j}] \cdot c^2}{[\langle r_j \rangle^2]} - \frac{[k_j] \cdot c^2}{[\langle r_j \rangle^2]}} \tag{3.39}$$

This DEQ is the quantized FLE for pairs in D dimensions:

Theorem 2 FLE derived from pairs of quantum objects

The FLE can be derived as an average over pairs of quantum objects. The resulting quantized FLE for pairs in D dimensions is as follows:

$$\frac{[\langle \dot{r}_j \rangle^2]}{[\langle r_j \rangle^2]} = -\frac{2[E_{D,j}] \cdot c^2}{[\langle r_j \rangle^2]} - \frac{[k_j] \cdot c^2}{[\langle r_j \rangle^2]} \tag{3.40}$$

3.4.2 Quantized FLE

In this section we derive the quantized FLE. In the quantized FLE for pairs, the fraction $\frac{[\langle \dot{r}_j \rangle^2]}{[\langle r_j \rangle^2]}$ is an averaged Hubble parameter $[H_j]$. The Hubble parameter $[H_j]$ describes a uniform scaling. This is characterized by a scale factor $dk_{t\to t+dt}$:

$$dk_{t\to t+dt} = \frac{a(t) + \dot{a}(t) \cdot dt}{a(t)} = 1 + H(t) \cdot dt \tag{3.41}$$

Thus, a homogeneous scale factor implies a homogeneous Hubble parameter. So the uniform scaling implies that we can replace the averaged Hubble parameter by the global Hubble parameter:

$$\frac{[\langle \dot{r}_j \rangle^2]}{[\langle r_j \rangle^2]} = \frac{\dot{r}^2}{r^2} = H^2 \tag{3.42}$$

We apply this relation to the quantized averaged FLE:

$$\boxed{\frac{\dot{r}^2}{r^2} = -\frac{2[E_{D,j}] \cdot c^2}{[\langle r_j \rangle^2]} - \frac{[k_j] \cdot c^2}{[\langle r_j \rangle^2]}} \tag{3.43}$$

This DEQ is the quantized FLE or extended FLE, EFLE. In this DEQ the term with the averaged curvature parameter $[k_j]$ is relatively small (see Collaboration (2020b), Carmesin (2020b)). So we get:

$$\boxed{\frac{\dot{r}^2}{r^2} = -\frac{2[E_{D,j}] \cdot c^2}{[\langle r_j \rangle^2]}} \tag{3.44}$$

Theorem 3 Quantized or extended FLE

(1) The quantized FLE in D dimensions is as follows:

$$\frac{\dot{r}^2}{r^2} = -\frac{2[E_{D,j}] \cdot c^2}{[\langle r_j \rangle^2]} - \frac{[k_j] \cdot c^2}{[\langle r_j \rangle^2]} \tag{3.45}$$

(2) As the averaged curvature parameter $[k_j]$ is nearly zero, the quantized FLE in D dimensions is nearly as follows:

$$\frac{\dot{r}^2}{r^2} = -\frac{2[E_{D,j}] \cdot c^2}{[\langle r_j \rangle^2]} \tag{3.46}$$

3.4.3 Condensation: Ground state

Lohse et al. (2018) and Zilberberg et al. (2018) showed experimentally that quantum systems can use higher dimensional space. Similarly as in the case of the shortcuts (Sect. 3.3), such a possibility may give rise to a dimensional phase transition, that is driven by the attractive gravitational interaction. Thus, such a dimensional phase transition is a **condensation**. Hence the corresponding states are **low energy states** (Sect. 3.3). Thus, the corresponding states can be modeled by **ground states** in an adequate approximation.

Correspondingly, we analyze the ground state of the mass m_j of a pair j in this section.

Uncertainty relation at dimension D: In this paragraph we derive the uncertainty relation as a function of the dimension D, see Eq. (3.53). In general, the components of the position Δr_i and the momentum Δp_k obey the uncertainty relation:

$$\Delta r_i \cdot \Delta p_k \geq \frac{\hbar}{2} \text{ for } i = k \quad \text{and} \tag{3.47}$$

$$\Delta r_i \cdot \Delta p_k \geq 0 \text{ for } i \neq k \tag{3.48}$$

This can be expressed with the Kronecker symbol $\delta_{ik} = 1$ for $i = k$ and $\delta_{ik} = 0$ for $i \neq k$:

$$\Delta r_i \cdot \Delta p_k \geq \frac{\hbar}{2} \cdot \delta_{ik} \tag{3.49}$$

We square both sides of the relation and sum both sides:

$$\sum_{i=1}^{D} \sum_{k=1}^{D} (\Delta r_i)^2 \cdot (\Delta p_k)^2 \geq \frac{\hbar^2}{4} \cdot \sum_{i=1}^{D} \sum_{k=1}^{D} \delta_{ik} \tag{3.50}$$

Here we identify:

$$\sum_{i=1}^{D} (\Delta r_i)^2 = (\Delta r)^2 \text{ and } \sum_{k=1}^{D} (\Delta p_k)^2 = (\Delta p)^2 \tag{3.51}$$

We apply $\sum_{i=1}^{D}\sum_{k=1}^{D}\delta_{ik}=D$:

$$(\Delta r)^2\cdot(\Delta p)^2\geq\frac{\hbar^2}{4}\cdot D \tag{3.52}$$

We extract the root and show the relation (qed):

$$\boxed{\Delta r\cdot\Delta p\geq\frac{\hbar}{2}\cdot\sqrt{D}} \tag{3.53}$$

Minimal uncertainty at the ground state: In this paragraph we show that the uncertainty takes its minimum at the ground state: We analyze the ground state of the energy operator $\hat{E}_{D,j}$. So the wave function is a Gaussian function at high density (Carmesin (2019d), Carmesin and Carmesin (2020)). Thus, the inequality in the uncertainty relation becomes an equality:

$$\Delta p\cdot\Delta r=\frac{\hbar}{2}\sqrt{D} \tag{3.54}$$

So the uncertainty takes its minimum at the ground state.

Energy as a function of spatial uncertainties: In this paragraph we show that the energy $E_{D,j}$ can be expressed as a function of spatial uncertainties $(\hat{\Delta}r_j)^2=\tilde{r}_j^2-\langle\tilde{r}_j\rangle^2$ or $(\Delta r_j)^2=\langle(\hat{\Delta}r_j)^2\rangle$.

For it we apply Eq. (3.51) to Eq. (3.35):

$$E_{D,j}=\frac{(\Delta p_j)^2}{2m_j^2\cdot c^2}-\frac{G_D}{(D-2)\cdot c^2}\cdot\left\langle M_j\cdot\hat{r}_j^{2-D}\right\rangle \tag{3.55}$$

Furthermore, we apply the uncertainty relation in Eq. (3.54). Moreover, we use natural units and mark the corresponding quantities with a tilde:

$$E_{D,j}=\frac{D}{8\tilde{m}_j^2\cdot(\Delta\tilde{r}_j)^2}-\tilde{M}_j\cdot\left\langle\tilde{r}_j^{2-D}\right\rangle \tag{3.56}$$

Here we apply the identity:

$$\langle\tilde{r}_j^{2-D}\rangle=\left\langle(\tilde{r}_j^2)^{\frac{2-D}{2}}\right\rangle \tag{3.57}$$

Here we introduce the difference of $\tilde{r}_j^2$ and $\langle \tilde{r}_j \rangle^2$:

$$\tilde{r}_j^2 - \langle \tilde{r}_j \rangle^2 = (\hat{\Delta}\tilde{r}_j)^2 \tag{3.58}$$

The expectation value of $(\hat{\Delta}\tilde{r}_j)^2$ is the square of the standard deviation or uncertainty:

$$\langle (\hat{\Delta}\tilde{r}_j)^2 \rangle = (\Delta \tilde{r}_j)^2 \tag{3.59}$$

As the expectation value of $(\hat{\Delta}\tilde{r}_j)^2$ is the square of the uncertainty, $\hat{\Delta}\tilde{r}_j$ is the corresponding **uncertainty operator**. We apply this uncertainty operator to Eq. (3.57):

$$\langle \tilde{r}_j^{2-D} \rangle = \left\langle \left(\langle \tilde{r}_j \rangle^2 + (\hat{\Delta}\tilde{r}_j)^2 \right)^{\frac{2-D}{2}} \right\rangle \tag{3.60}$$

Here we factorize $\langle \tilde{r}_j \rangle^2$:

$$\langle \tilde{r}_j^{2-D} \rangle = \langle \tilde{r}_j \rangle^{2-D} \cdot \left\langle \left(1 + \frac{(\hat{\Delta}\tilde{r}_j)^2}{\langle \tilde{r}_j \rangle^2} \right)^{\frac{2-D}{2}} \right\rangle \tag{3.61}$$

This Eq. combined with Eq. (3.56) represents the energy $E_{D,j}$ as a function of the uncertainty operator.

Energy as sum of classical term and quantum term: In this paragraph we show that the energy $E_{D,j}$ can be expressed as a sum of a classical term and a quantum term, in linear order in the fraction $\frac{(\hat{\Delta}\tilde{r}_j)^2}{\langle \tilde{r}_j \rangle^2}$. For it we expand Eq. (3.61) in linear order:

$$\langle \tilde{r}_j^{2-D} \rangle = \langle \tilde{r}_j \rangle^{2-D} \cdot \left\langle 1 + \frac{2-D}{2} \cdot \frac{(\hat{\Delta}\tilde{r}_j)^2}{\langle \tilde{r}_j \rangle^2} \right\rangle \tag{3.62}$$

Here we evaluate the expectation values:

$$\langle \tilde{r}_j^{2-D} \rangle = \langle \tilde{r}_j \rangle^{2-D} - \frac{D-2}{2} \cdot \frac{(\Delta \tilde{r}_j)^2}{\langle \tilde{r}_j \rangle^D} \tag{3.63}$$

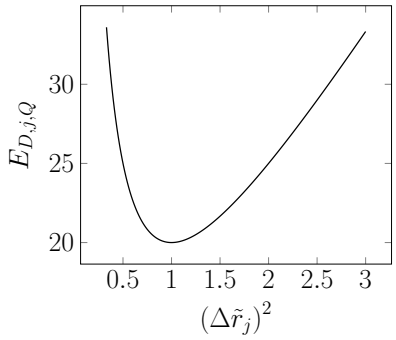

Figure 3.5: Variation of fluctuations (Eq. 3.65): Example: $\frac{D}{8\tilde{m}_j^2} = 10$ and $\frac{(D-2)\tilde{M}_j}{2\langle\tilde{r}_j\rangle^D} = 10$. The quantum term $E_{D,j,Q}$ (Eq. 3.65) is presented as a function of the square of the uncertainty $(\Delta\tilde{r}_j)^2$. The minimum can be determined completely robustly. In the figure: $\Delta\tilde{r}_j \approx 1$ and thus $\Delta\tilde{p}_j \approx \frac{\sqrt{D}}{2}$.

We apply this result to Eq. (3.56). So we get:

$$E_{D,j} = \frac{D}{8\tilde{m}_j^2 \cdot (\Delta\tilde{r}_j)^2} - \frac{\tilde{M}_j}{\langle\tilde{r}_j\rangle^{D-2}} + \frac{(D-2)\cdot(\Delta\tilde{r}_j)^2 \cdot \tilde{M}_j}{2\cdot\langle\tilde{r}_j\rangle^D} \quad (3.64)$$

Terms containing the uncertainty $\Delta\tilde{r}_j$ form the quantum term:

$$\boxed{E_{D,j,Q} = \frac{D}{8\tilde{m}_j^2 \cdot (\Delta\tilde{r}_j)^2} + \frac{(D-2)\cdot(\Delta\tilde{r}_j)^2 \cdot \tilde{M}_j}{2\cdot\langle\tilde{r}_j\rangle^D}} \quad (3.65)$$

The rest is the classical gravity term:

$$\boxed{E_{D,j,cl,G} = -\frac{\tilde{M}_j}{\langle\tilde{r}_j\rangle^{D-2}}} \quad (3.66)$$

Hence we get:

$$\boxed{E_{D,j} = E_{D,j,Q} + E_{D,j,cl,G}} \quad (3.67)$$

3.4.4 Minimization of reduced energy via $\Delta\tilde{r}_j$

In this section we show that the energy, minimized with respect to $\Delta\tilde{r}_j$, is presented by Eq. (3.71).

The energy function $E_{D,j,Q}([\Delta\tilde{r}_j]^2)$ shows a clear minimum (Fig. 3.5). The minimum corresponds to the basic state. We determine the minimum: $(\Delta\tilde{r}_j)^2$ is called x:

$$E_{D,j,Q} = \frac{D}{8\tilde{m}_j^2 \cdot x} + \frac{(D-2) \cdot x \cdot \tilde{M}_j}{2 \cdot \langle \tilde{r}_j \rangle^D} \tag{3.68}$$

We determine the derivative

$$E_{D,j,Q}(x)' = -\frac{D}{8\tilde{m}_j^2 \cdot x^2} + \frac{(D-2) \cdot \tilde{M}_j}{2 \cdot \langle \tilde{r}_j \rangle^D} \tag{3.69}$$

The minimum is at the slope zero (Fig. 3.5). Therefore we use $E_{D,j,Q}(x)' = 0$ in the above equation, resolve to x, use $(\Delta\tilde{r}_j)^2$ for x and get:

$$(\Delta\tilde{r}_j)^4 = \frac{D \cdot \langle \tilde{r}_j \rangle^D}{4(D-2) \cdot \tilde{m}_j^2 \cdot \tilde{M}_j} \tag{3.70}$$

We use this result in $E_{D,j,Q}$ and get:

$$\boxed{E_{D,j,Q} = \frac{\sqrt{D \cdot (D-2) \cdot \tilde{M}_j}}{2\tilde{m} \cdot \langle \tilde{r}_j \rangle^{D/2}}} \tag{3.71}$$

Proposition 7 Reduced normalized energy $E_{D,j}$

The energy $E_{D,j}$ of a pair j is as follows:

(1) The expectation value is as follows:

$$E_{D,j} = \frac{\sum_{i=1}^{D} (\Delta p_{j,i})^2}{2m_j^2 \cdot c^2} - \frac{G_D}{(D-2) \cdot c^2} \cdot \left\langle M_j \cdot \hat{r}_j^{2-D} \right\rangle \tag{3.72}$$

(2) At the ground state, $E_{D,j}$ is as follows:

$$E_{D,j} = E_{D,j,Q} + E_{D,j,cl,G} \tag{3.73}$$

$$E_{D,j,cl,G} = -\frac{\tilde{M}_j}{\langle \tilde{r}_j \rangle^{D-2}} \tag{3.74}$$

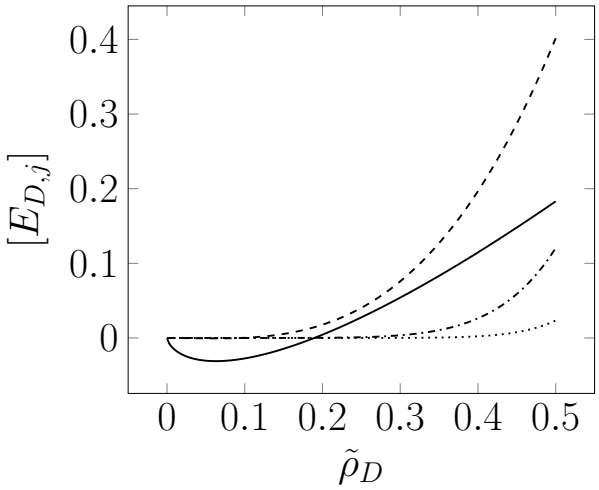

Figure 3.6: Energy $[E_{D,j}]$ for an averaged black hole in the gravitational field of an averaged photon. (Sect. 3.4.5): $[E_{3,j}]$ (solid line), $[E_{6,j}]$ (dashed), $[E_{12,j}]$ (dashdotted), $[E_{18,j}]$ (dotted).

$$E_{D,j,Q} = \frac{\sqrt{D \cdot (D-2) \cdot \tilde{M}_j}}{2\tilde{m} \cdot \langle \tilde{r}_j \rangle^{D/2}} \tag{3.75}$$

3.4.5 Minimization of reduced energy via D

In this section we analyze the energy $[E_{D,j}]$ for the case of a black hole m_j and an averaged photon M_j and as a function of the density.

We apply equation (3.14), and we average:

$$[\tilde{b}_j] = (2\tilde{\rho}_D)^{\frac{-1}{2}} \tag{3.76}$$

Moreover, we use equation (3.12), and we average:

$$[\tilde{a}_j] = (2\tilde{\rho}_D)^{\frac{-1}{D+1}} \tag{3.77}$$

With these relations, we plot the graphs of the energy $[E_{D,j}](\rho_D)$ for the dimensions $D = 3$, $D = 7$, $D = 12$ and $D = 301$ (Fig. 3.6). The figure shows: At low density, the energy is minimal at

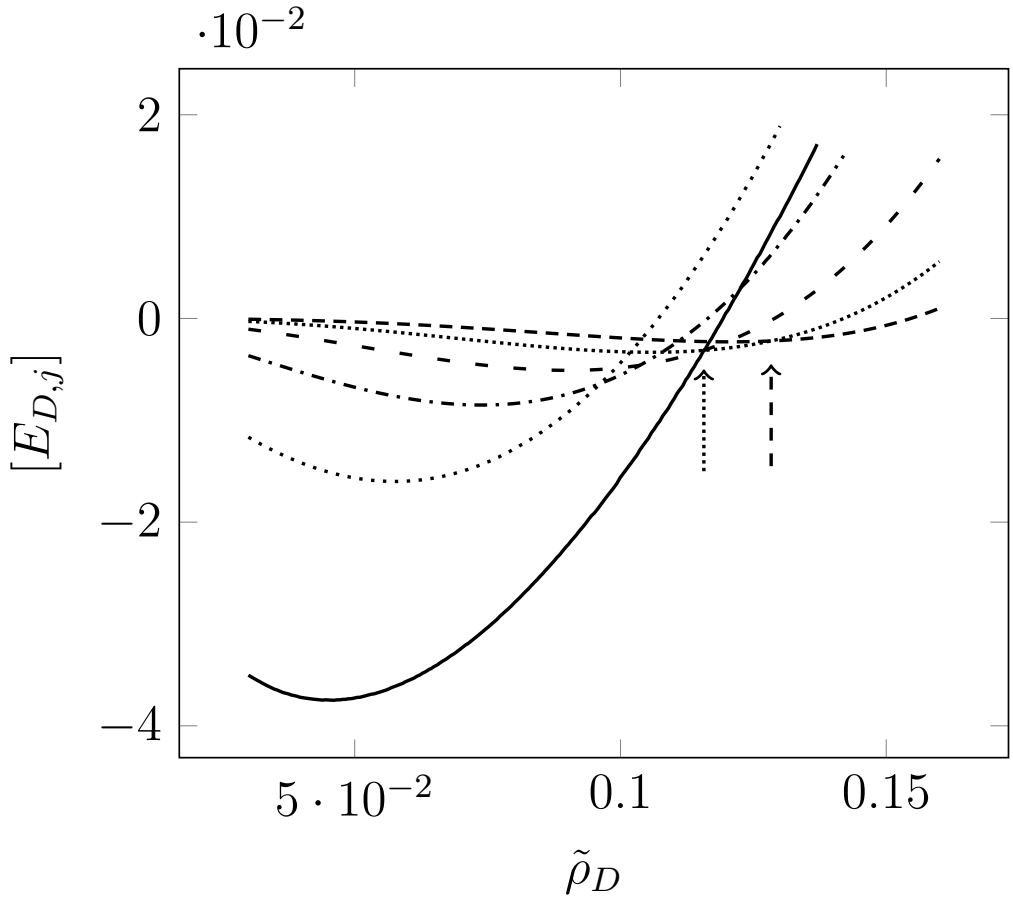

Figure 3.7: Reduced normalized energy $[E_{D,j}]$: $[E_{3,j}]$ (line), $[E_{4,j}]$ (dotted), $[E_{5,j}]$ (dashdotted), $[E_{6,j}]$ (loosely dashed), $[E_{7,j}]$ (dotted closely), $[E_{8,j}]$ (dashed). Dotted arrow marks transition from $D = 7$ to $D = 3$ at critical density $\tilde{\rho}_{D=3,c} = 0.11569$. Dashed arrow marks transition from $D = 8$ to $D = 7$ at critical density $\tilde{\rho}_{D=7,c} = 0.12835$.

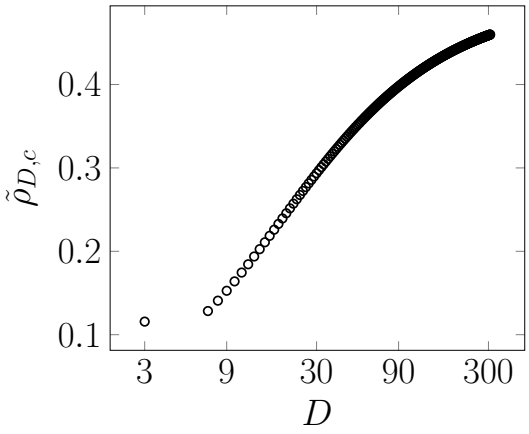

Figure 3.8: Critical densities $\tilde{\rho}_{D,c}$ as a function of dimension D. The dimensional transitions to $D = 3$ start at $D = 7$. So the following dimensions D are established: $D \in \{3, 7, 8, 9, ...\}$

.

the dimension $D = 3$, however, at high density, minimal energy occurs at high dimension $D >> 3$.

The sequence of these transitions is evaluated for the case of the adequate approximation $\tilde{r}_j \approx \tilde{b}_j$ so that the quantum part of the reduced energy takes the following form (Eq. 3.75):

$$E_{D,j,Q} = \frac{\sqrt{D \cdot (D-2) \cdot \tilde{M}_j}}{2\tilde{m} \cdot \langle \tilde{b}_j \rangle^{D/2}} \tag{3.78}$$

For this case, the reduced energies as a function of the scaled density are shown in Fig. (3.7). That figure illustrates that there is an energetically optimal dimension at each density. Accordingly, the critical densities $\tilde{\rho}_{D,c}$ can be determined at which the dimensional transition takes place from a dimension $D + s$ to the dimension D. These critical densities $\tilde{\rho}_{D,c}$ are shown as a function of the dimension D in Fig. (3.8).

Only dimensions $D \geq 3$ occur, as the vacuum is represented by corresponding gravitational waves. These can exist in dimensions $D \geq 3$ only, as they have one direction of propagation and at least two transverse directions according to their quadrupo-

lar structure or according to the fact that the elongations in Fig (5.3) cannot become negative. For D towards infinity, the critical densities $\tilde{\rho}_{D,c}$ tend to $1/2$, see Fig. (3.8). However, only $D < 302$ is within the actual light horizon, see below.

3.5 Connections: sequence of $\tilde{\rho}_{D,cr,conn.}$

In the previous section, we derived a sequence of dimensional phase transitions for the case of the binary fluid that existed in the early universe, see Carmesin (2020b). Additionally, we show that these transitions do also take place in two very different systems:

In this section (3.5), we show that the dimensional phase transitions also take place in a relativistic system with high density, hereby the system forms connections similar to wormholes, according to GRT.

In the next section (3.6), we show that the dimensional phase transitions take place at high density in a Bose gas as well.

Altogether, these three very different systems provide strong evidence for the fact that the dimensional phase transitions took place at high density in the early universe.

In this section in particular, we derive the critical densities $\tilde{\rho}_{D,cr,conn.}$ for the spontaneous formation of shortcuts at dimensions D ranging from $D = 3$ to $D = 301$. For it we apply the dimensional extension of the FLE, the **EFLE** and THM. (3).

EFLE: We apply the EFLE for the case of negligible curvature parameter k (Eq. 3.44):

$$\frac{\dot{r}^2}{r^2} = -\frac{2[E_{D,j}] \cdot c^2}{[\langle r_j \rangle^2]} \tag{3.79}$$

Hereby we identify the averages over pairs $[\langle r_j \rangle^2]$ and $[E_{D,j}]$ by the corresponding ideal values of cosmology:

$$\frac{\dot{r}^2}{r^2} = -\frac{2E_D \cdot c^2}{r^2} \tag{3.80}$$

We multiply by r^2, and we apply natural units:

$$\dot{\tilde{r}}^2 = -2E_D \tag{3.81}$$

The reduced normalized energy contains a quantum correction that is numerically not essential here. Accordingly we use the classical part (Eq. 3.66):

$$E_{D,j,cl,G} = -\frac{\tilde{M}_j}{\langle \tilde{r}_j \rangle^{D-2}} \tag{3.82}$$

Again we use the average over the pairs:

$$E_{D,cl,G} = -\frac{\tilde{M}}{\tilde{r}^{D-2}} \tag{3.83}$$

Here we apply $\tilde{M} = \frac{1}{\tilde{a}}$ (Sect. 3.2.2). As an approximation, we use $\tilde{a} \approx \tilde{b}$ and $\tilde{b} = (2\tilde{\rho}_D)^{-1/2}$ (Sect. 3.2.2):

$$E_{D,cl,G} = -\frac{1}{2} \cdot (2\tilde{\rho}_D)^{\frac{D-1}{2}} \tag{3.84}$$

We insert this Eq. into Eq. (3.81):

$$\dot{\tilde{r}}^2 = (2\tilde{\rho}_D)^{\frac{D-1}{2}} \tag{3.85}$$

We apply the root:

$$\dot{\tilde{r}} = (2\tilde{\rho}_D)^{\frac{D-1}{4}} \tag{3.86}$$

We use the chain rule in order to derive the rate of isotropic formation of vacuum:

$$\dot{\tilde{V}} = D \cdot (2\tilde{\rho}_D)^{\frac{D-1}{4}} \tag{3.87}$$

We derive the corresponding rate for the unidirectional formation of vacuum. For it we divide by $\sqrt{D}$:

$$\dot{\tilde{V}}_{uni} = \sqrt{D} \cdot (2\tilde{\rho}_D)^{\frac{D-1}{4}} \tag{3.88}$$

Derivation of $\tilde{\rho}_{D,cr,conn.}$: The outward flow in Eq. (3.15) is expressed in terms of natural units:

$$\dot{\tilde{\varepsilon}}_{out} = -1 \tag{3.89}$$

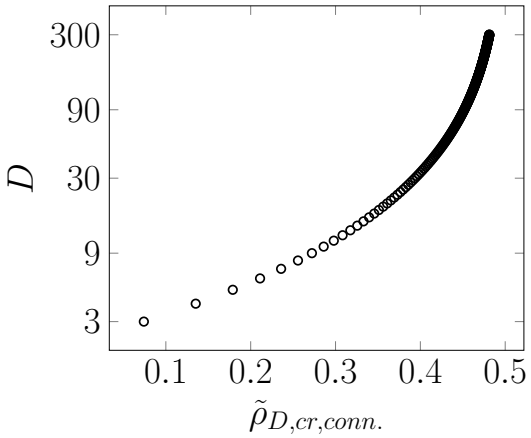

Figure 3.9: Dimension D as a function of the critical densities $\tilde{\rho}_{D,cr,conn.}$.

.

Similarly, the inward flow in Eq. (3.19) is represented in terms of natural units:

$$\dot{\tilde{\varepsilon}}_{in} = \frac{1}{D} \tag{3.90}$$

The rate of vacuum formation $\dot{\tilde{\varepsilon}}_{formation}$ is equal to the rate for the unidirectional formation of vacuum in Eq. (3.88) divided by $d\tilde{V}$. For the present case of a cube with length L_P, the volume is $d\tilde{V} = 1$. So we get:

$$\dot{\tilde{\varepsilon}}_{formation} = \sqrt{D} \cdot (2\tilde{\rho}_D)^{\frac{D-1}{4}} \tag{3.91}$$

At the critical density, the sum of these three rates is zero (see Eq. 3.21):

$$\dot{\tilde{\varepsilon}}_{inside} = \dot{\tilde{\varepsilon}}_{out} + \dot{\tilde{\varepsilon}}_{in} + \dot{\tilde{\varepsilon}}_{formation} = -1 + \frac{1}{D} + \sqrt{D} \cdot (2\tilde{\rho}_D)^{\frac{D-1}{4}} = 0 \tag{3.92}$$

We solve for the density:

$$\boxed{\tilde{\rho}_D = \tilde{\rho}_{D,cr,conn.} = \frac{1}{2} \cdot \left(\frac{D-1}{D^{3/2}} \right)^{\frac{4}{D-1}}} \tag{3.93}$$

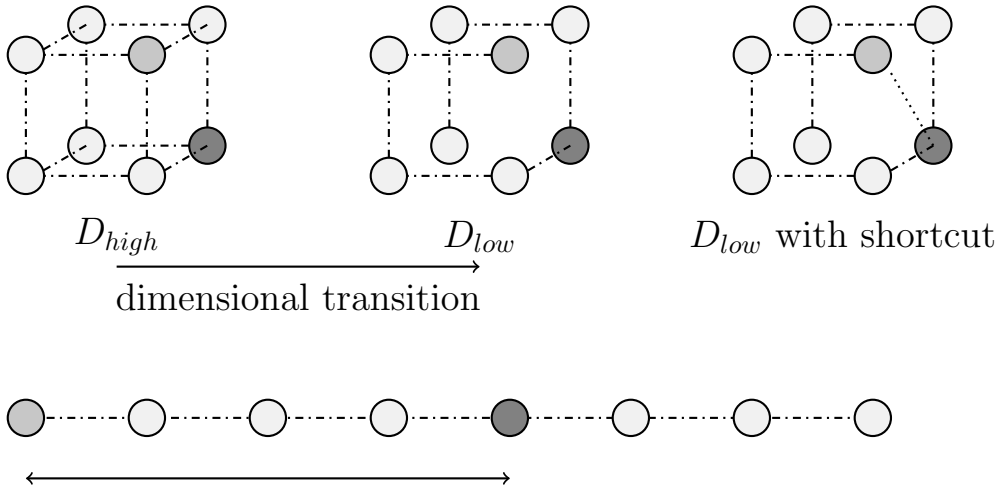

Figure 3.10: Points (circles) and dimensional connections (dash-dotted): Dimensional transition from D_{high} (left cube) to D_{low} (middle cube and lower linear representation). At D_{low}, a shortcut (dotted) is formed (right cube).

We present the stable dimensions D as a function of the critical densities $\tilde{\rho}_{D,cr,conn.}$, at which shortcuts form spontaneously at D (Fig. 3.9): $\tilde{\rho}_{D,cr,conn.} = \frac{1}{2} \cdot \left(\frac{D-1}{D^{3/2}}\right)^{\frac{4}{D-1}}$

3.6 Dimensional transitions in a Bose gas

If the dimension D of space is increased by one, see for instance Fig. (3.9), then motions along the additional direction of space become possible. These additional motions are described by an additional translation symmetry. Such a change of the macroscopic symmetries of a physical state constitutes a phase transition, see e. g. Landau and Lifschitz (1979b). So the change of a dimension constitutes a dimensional phase transition. We emphasize here that physics in higher dimension has already been observed in experiments based on photons as well as in experiments based on electrons, see e. g. Lohse et al. (2018), Zilberberg et al. (2018).

The phase transitions that occur at high density near $\frac{\rho_P}{2}$ can be modeled in very different systems. For instance, these phase

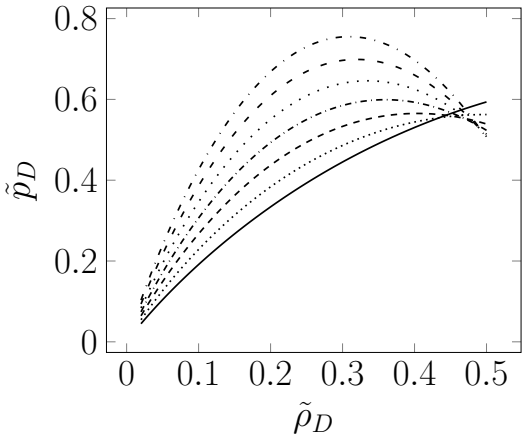

Figure 3.11: Bose gas: pressure $\tilde{p}_D(\tilde{\rho}_D)$ for various dimensions D: $D = 3$ (solid line), $D = 4$ (dotted), $D = 5$ (dashed), $D = 6$ (dashdotted). $D = 7$ (loosely dotted), $D = 8$ (loosely dashed), $D = 9$ (loosely dashdotted). Dimensional phase transitions occur at the critical densities $\tilde{\rho}_{D=3,c} \approx 0.435$, $\tilde{\rho}_{D=4,c} \approx 0.45$, $\tilde{\rho}_{D=5,c} \approx 0.465$, $\tilde{\rho}_{D=6,c} \approx 0.48$, $\tilde{\rho}_{D=7,c} \approx 0.487$, $\tilde{\rho}_{D=8,c} \approx 0.493$, $\tilde{\rho}_{D=9,c} \approx 0.497$.

transitions have been modeled in a Bose gas, see (Carmesin, 2021c, section 8.4), Sawitzki and Carmesin (2021). That model shows that the phase transition is a condensation, whereby the phase with the lowest pressure is taken, and so high dimensional phases form at high density, see Fig. (3.11).

3.7 Dimensional horizon $D_{horizon}$

In the time evolution of the universe, the density was high initially, and it decreased as a function of the time. So the dimension D was high originally near or at the Planck scale. Then the density decreased according to the EFLE, and whenever a critical density was reached, dimensional phase transition reduced the **dimension of space**. So D decreased until $D = 3$ was achieved. That process is called **dimensional unfolding** or **cosmic unfolding**, see e. g. Carmesin (2021c), Carmesin (2017b).

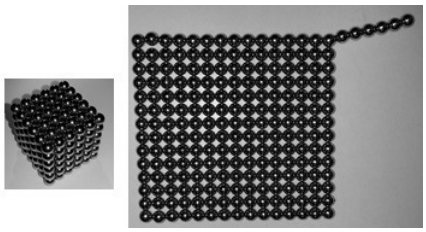

Figure 3.12: 216 magnetic balls model local objects or observable regions at high density and illustrate the relation between the distance and the dimension D: If the dimension increases from two (right) to three (left), then the largest distance decreases. More generally and conversely, a decrease of the dimension D implies an increase of the largest distance.

During the process of dimensional unfolding, the dimension D decreased, and thereby the distances were enlarged, see Fig. (3.12). At a transition from a dimension $D+s$ to a dimension D, the distances enlarge by a so-called **dimensional distance enlargement factor** $Z_{D+s\to D}$, see e. g. (Carmesin, 2021c, 8.2.9). The space that is enclosed in the actual light horizon achieved a largest dimension, the so-called **dimensional horizon**, $D_{horizon}$ or shortly D_{hori}, see e. g. (Carmesin, 2021c, 8.2.10). Thereby the following relation holds:

$$Z_{D_{hori}\to D=3} = 2^{(D_{hori}-3)/3} \tag{3.94}$$

In order to determine the dimensional horizon, we use the complete scale factor $k_{D_{hori}\to t_0}$ ranging from the dimensional horizon until today, and we apply the complete enlargement factor $q_{D_{hori}\to t_0}$ ranging from the dimensional horizon until today, and we form the fraction:

$$Z_{D_{hori}\to D=3} = \frac{q_{D_{hori}\to t_0}}{k_{D_{hori}\to t_0}} \tag{3.95}$$

The exact value of the dimensional horizon depends on the details of the dimensional phase transitions, and these depend on the details of the fluid in the early universe. However, all realistic cases show that the actual value of the dimensional horizon

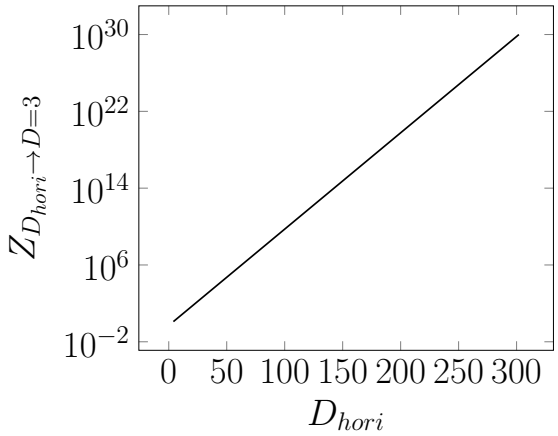

Figure 3.13: Dimensional distance enlargement factor $Z_{D_{hori}\to D=3}$ as a function of the dimensional horizon D_{hori}.

is as follows, see e. g. (Carmesin, 2021c, 8.2.10):

$$D_{hori} \in [301, 302] \tag{3.96}$$

The dimensional distance enlargement factor is shown as a function of the dimension in Fig. (3.13).

For the case of the Bose gas, the critical density at the dimensional horizon is practically equal to the maximal possible value 0.5:

$$\boxed{\tilde{\rho}_{D_{hori},c} \approx 0.5} \tag{3.97}$$

For the more realistic case of the binary fluid in the early universe, the dimensional horizon is as follows, see (Carmesin, 2021c, 8.2.10):

$$\boxed{D_{hori} = 301.23} \tag{3.98}$$

3.8 Coexistence of phases

In general, different phases of a substance can coexist, see e. g. Landau and Lifschitz (1979b). For instance, in the case of water, at a lake there can be liquid water in the lake, while some fraction of the water of the lake can swim in the form of solid ice at the surface of the like, and simultaneously, another

fraction of the water at the lake is present in the form of vapor above the surface of the lake. Altogether, all phases of water can exist simultaneously in nature.

An analogous situation can in principle and in general occur for the case of quanta of space time during cosmic unfolding: When a dimension D is reached at a dimensional phase transition, then there may remain some quanta of spacetime in higher dimensions $D + s \geq D$. That possibility can be realized at especially low restrictions, as the classical rate gravity waves, RGWs, corresponding to the quanta of spacetime exhibit zero energy in a homogeneous universe frame, HUF. We summarize our findings:

Proposition 8 Coexistence of phases

(1) In general, different phases of an object can coexist in nature.

(2) If part (1) is applied to the quanta of spacetime, then the following holds: Then phases of the quanta of spacetime that occur during the process of cosmic unfolding can coexist. In particular, when a dimensional phase transition to a dimension D takes place during the cosmic unfolding, then the quanta of spacetime QST_D in that dimension D become stable, whereby the quanta of spacetime of higher dimension QST_{D+s} can still exist in general and possibly in metastable states:

$$\boxed{QST_D \ \text{ can coexist with } QST_{D+s}} \tag{3.99}$$

(3) When a dimension D is reached during cosmic unfolding, then the QST at $D + s > D$ are outside the D-dimensional space.

$$\boxed{QST_{D+s} \ \text{ are outside } D-\text{dimensional}-\text{space}} \tag{3.100}$$

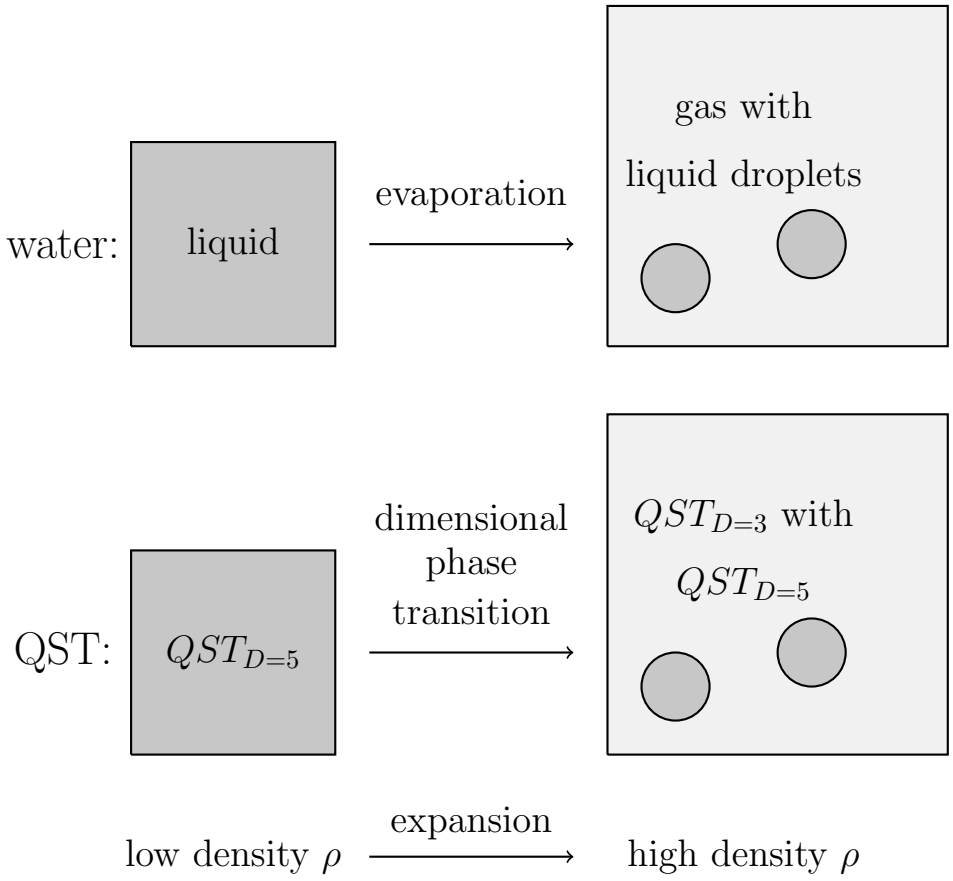

Figure 3.14: Coexistence of phases: Water: liquid and gas can coexist. Quanta of spacetime: $QST_{D=3}$ and $QST_{D=5}$ can coexist, for instance.

3.9 Expansion and Enlargement via FLE in D dimensions

Using the EFLE, we can derive the full time evolution of the space included in the present-day light horizon, see for instance Carmesin (2017b), Carmesin (2019d), Carmesin (2021c). The result is presented in Fig. (1.1). With it the horizon problem has been solved, see e. g. Carmesin (2018h), Schöneberg and Carmesin (2021). The solution shown in Fig. (1.1) includes the time evolution of the dimension.

Using that solution, the time evolution of the energy has been derived, see e. g. Carmesin (2020b). As a result, we find that the energy started from zero-point energies, ZPE, of zero-point oscillations, ZPO. This corresponds to the fact that the energy at the Planck scale is equal to $E_P/2$, see Fig. (2.1), corresponding to $E = \frac{1}{2} \cdot \hbar \cdot \omega_P$, whereby ω_P is the Planck circular frequency.

3.10 Transition of a ZPO

In this section we analyze possible transitions from one ZPO to another ZPO.

Example: As an example, we consider the molecule n-butane. It occurs in one of two **conformations**, *trans* and *cis* or *gauche* (Figs. 3.15, 3.16 or Falvo et al. (2018), Balabin (2009), Rodrigo and Freitas (2009)).

Hereby the conformation *trans* has a lower energy than the conformation *cis* or *gauche*, see e. g. Balabin (2009).

In each of these conformations, the molecule can exhibit a ZPO, e. g. in the form of a vibration. So there can exist a low ZPE, ZPE_{low}, in the conformation *trans* as well as a low ZPE, ZPE_{high}, in the conformation *cis* or *gauche*.

Moreover, the molecule can exhibit transitions among these

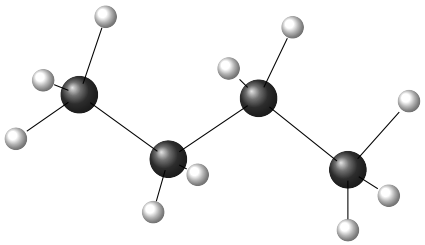

Figure 3.15: n-butane, C_4H_{10}, in the $trans$-conformation, see Balabin (2009), Rodrigo and Freitas (2009).

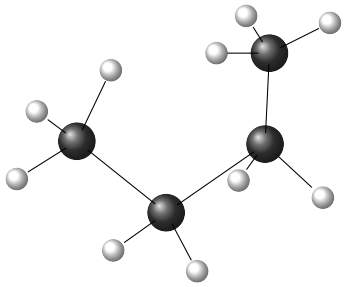

Figure 3.16: n-butane, C_4H_{10}, in the cis or $gauche$-conformation, see Falvo et al. (2018), Balabin (2009), Rodrigo and Freitas (2009).

conformations, see e. g. Ramirez and Laso (2001). So the molecule can in principle exhibit a transition from the ZPO with the low energy ZPE_{low} to the ZPO with the high energy ZPE_{high}. That transition constitutes an excitation from a low ZPE, ZPE_{low} to a high ZPE, ZPE_{high}.

Excitation among ZPOs: The above example shows that a transition from a ZPO with low energy ZPE_{low} to a ZPO with a high energy, ZPE_{high} is possible in nature.

Chapter 4

Derivation of Ω_γ

In this chapter we derive the value of the density parameter Ω_γ of the **primordial photons**. As outlined in the introduction, in this chapter we determine Ω_γ by using Ω_ν, whereas in chapter (12) we determine all density parameters simultaneously.

4.1 Time reference: Hubble time

The universe evolves since the Big Bang. So the present state depends on the time t_0 ranging from the Big Bang until today. An indicator for that time is the Hubble time:

$$t_{Hubble} = 1/H_0 \tag{4.1}$$

It is an indicator for the present time t_0. So we use it without derivation. Thereby H_0 is not a parameter that should be determined by theory. In contrast, H_0 is a parameter that defines the time after the Big Bang. At this time all observed values $x_{observed}(t_0)$ have been measured, and hence corresponding values $x_{theoretical}(t_0)$ should be derived.

Moreover, observed values of H_0 depend on the redshift z_{probe} at which the radiation of the probe was emitted.

$$H_0 = H_0(z_{probe}) \tag{4.2}$$

Here we use that value of H_0 that is observed by using probes emitted at the redshift $z_{CMB} \approx 1090$ of the CMB. Here we use

the time reference value measured by Collaboration (2020a):

$$\boxed{\text{time reference} = H_0(z_{CMB}) = 67.36(54)\,\frac{\text{km}}{\text{s}\cdot\text{Mpc}}} \tag{4.3}$$

$$\boxed{\text{with}\ \ z_{CMB} = 1089.92(25)} \tag{4.4}$$

4.2 Is heterogeneity essential for Ω_r?

In this section we analyze dynamical consequences that the heterogeneity in the universe has upon relativistic species and the corresponding density parameters Ω_γ, Ω_ν and Ω_{ERS}.

Observation: More than 95 % of the present-day photon energy is part of the CMB, see Penzias and Wilson (1965), Bennett et al. (2013), Collaboration (2014), Collaboration (2020a). The CMB is very homogeneous. It is characterized by an overdensity

$$\delta(\vec{r}) := \frac{\rho(\vec{r}) - \rho_h}{\rho_h} << 1 \tag{4.5}$$

of 0.0044 %, see e. g. (Carmesin, 2021c, p. 165), Collaboration (2020a):

$$\delta(CMB) = \delta(z = 1090) = 4.4 \cdot 10^{-5} \tag{4.6}$$

In contrast, the present-day overdensity is more than 18000 times larger, see e. g. (Carmesin, 2021c, p. 165).

Dynamic separation: These observational findings show that the heterogeneity in the universe essentially formed after the CMB had been emitted. Moreover, that overdensity did hardly influence the CMB or most of the photon energy in the universe. So the dynamics of the density of the photons is essentially separated from the dynamics of the overdensity in the universe.

Furthermore, most of the present-day neutrinos have been emitted thermally at approximately the same time at which

the CMB was emitted, see e. g. Tanabashi et al. (2018). Correspondingly, the dynamics of the density of the neutrinos is essentially separated from the dynamics of the overdensity in the universe.

As the photons and the neutrinos form the radiation in the universe described by Ω_r, the dynamics of the density of the radiation is essentially separated from the dynamics of the overdensity in the universe.

Theoretic argument for that dynamic separation: At the redshift $z \approx 3400$, the densities of radiation and matter have been equal, see e. g. Tanabashi et al. (2018) or Collaboration (2020a). Hence the era of the dominance of the radiation was long before the time of the emission of the CMB, whereas the era of large heterogeneity started long after the time of the emission of the CMB. Thus, these two eras are dynamically separated in a very good approximation. We summarize our result:

Proposition 9 Separation of the dynamics of radiation and heterogeneity

(1) The era of radiation was long before the emission of the CMB at $z = 1090$.

(2) The era of large heterogeneity started long after the emission of the CMB at $z = 1090$.

(3) As a consequence, the dynamics of the density of radiation is separated from the heterogeneity in the universe in a very good approximation.

(4) Thence the precise values of Ω_γ *and* Ω_r *can be derived independently of the time evolution of the heterogeneity or overdensity in the universe.*

(5) In particular, the precise values of Ω_γ *and* Ω_r *can be derived for the case of a homogeneous universe.*

(6) Hence the precise value of Ω_γ and Ω_r can be derived for the case of the density parameter $\Omega_\Lambda = 2/3$, see (Carmesin, 2021c, theorem 21 number (3)):

$$\boxed{\Omega_\Lambda = 2/3 \ \text{ for modeling } \ \Omega_r} \tag{4.7}$$

On the basis of this PROP., we develop a concept:

4.3 Concept of the calculation of Ω_γ

In this S. we develop a concept for the calculation of Ω_γ.

In a first subsection, we present quantities that can be derived explicitly. In a second subsection, we prepare the implicit derivation of Ω_γ by using a fixed point of a corresponding **test function** $\Omega_{\gamma,test}(\Omega_{\gamma,hypo})$. In a third subsection, we determine the fixed point.

4.3.1 Explicitly determined quantities

First we derive the present-day value ρ_{Λ,t_0} of density of the vacuum from $\Omega_\Lambda = 2/3$, whereby we determine ρ_{cr,t_0} from H_0:

$$\boxed{\rho_{\Lambda,t_0} = \Omega_\Lambda \cdot \rho_{cr,t_0} \ \text{ with } \ \rho_{cr,t_0} = \frac{3H_0^2}{8\pi \cdot G}} \tag{4.8}$$

Secondly, we determine the corresponding value of that density $\rho_{\Lambda,Dhori}$ for the case of the Big Bang or the dimensional horizon D_{hori}. It is equal to the corresponding density $\rho_{\gamma,Dhori}$, since the densities ρ_γ and ρ_Λ are maximal at the Planck scale, and since that scale is achieved here (see section 4.5.1):

$$\boxed{\rho_{\Lambda,Dhori} = \tilde{\rho}_{\gamma,Dhori} \cdot \bar{\rho}_P} \tag{4.9}$$

Thirdly, we derive the dimensional distance enlargement factor $Z_{Dhori,D3}$ from these two densities, see (Carmesin, 2021c, Eq. 8.138):

$$\boxed{Z_{Dhori,D3} = \left(\frac{\rho_{\Lambda,Dhori}}{300\rho_{\Lambda,t_0}}\right)^{1/4}} \tag{4.10}$$

4.3.2 Implicit determination with a function

In order to determine Ω_γ, we apply the following idea:

Complete determination: If we would know Ω_γ, then we could determine all density parameters as follows: We know $\Omega_K = 0$, $\Omega_\Lambda = 2/3$. Additionally, we know $\Omega_{ERS} = 0.114 \cdot 10^{-5}$ (see section (4.3.7)) Furthermore, we know $\Omega_\nu = 3.7802 \cdot 10^{-5}$ (see section (4.3.6)). Thus, we can determine Ω_M as follows:

$$\boxed{\Omega_M = 1 - \Omega_\Lambda - \Omega_\gamma - \Omega_\nu - \Omega_{ERS} - \Omega_K} \tag{4.11}$$

Note that we need Ω_M in order to determine the light horizon R_{lh}, see Eqs. (1.35) and (1.24).

Test function: In order to use that idea, we introduce a **test function** $\Omega_{\gamma,test}(\Omega_{\gamma,hypo})$ that determines a test value $\Omega_{\gamma,test}$ from a hypothetical value $\Omega_{\gamma,hypo}$. Thereby the test functions applies the laws of physics, and so it tests the hypothetical value.

If the test value $\Omega_{\gamma,test}$ is equal to the hypothetical value $\Omega_{\gamma,hypo}$, then that value $\Omega_{\gamma,hypo}$ is confirmed and obeys the laws of physics. In that case the test function has a **fixed point**:

$$\boxed{\Omega_{\gamma,test} = \Omega_{\gamma,test}(\Omega_{\gamma,hypo})} \tag{4.12}$$

Evaluation of the test function: **Firstly**, we use the hypothetical value $\Omega_{\gamma,hypo}$, then all density parameters are known, and we can derive the **light horizon**, see Eq. (1.35).

Secondly, based on the factor $Z_{Dhori,D3}$ and the light horizon R_{lh}, we derive the scale factor, see (Carmesin, 2021c, Eq. 8.72) or see Eq. (3.95):

$$\boxed{k_{Dhori,t_0} = \frac{\tilde{R}_{lh}}{Z_{Dhori,D3}}} \tag{4.13}$$

Thirdly, we derive the value of the density of the photons at the Big Bang by using the Planck scale, see section (4.5.1) or see Eq. (3.97):

$$\boxed{\tilde{\rho}_{\gamma,Dhori} = 1/2} \tag{4.14}$$

Fourthly, we derive the present-day value ρ_{γ,t_0} of the density of the photons by using $\rho_{\gamma,Dhori}$ and the scale factor, see (Carmesin, 2021c, Eq. 8.74):

$$\boxed{\tilde{\rho}_{\gamma,t_0} = \tilde{\rho}_{\gamma,Dhori} \cdot k^{-4}_{Dhori,t_0}} \tag{4.15}$$

Fifthly, we derive the new value of the density parameter $\Omega_{\gamma,test}$:

$$\boxed{\Omega_{\gamma,test} = \tilde{\rho}_{\gamma,t_0}/\tilde{\rho}_{cr,t_0}} \tag{4.16}$$

With it we derive the new value of Ω_r, see corollary (3):

$$\boxed{\Omega_r = \Omega_\gamma + \Omega_\nu + \Omega_{ERS}} \tag{4.17}$$

4.3.3 Fixed point of $\Omega_{\gamma,test}(\Omega_{\gamma,hypo})$

Using the test function, we solve the fixed point equation:

$$\boxed{\Omega_{\gamma,test}(\Omega_{\gamma,hypo}) = \Omega_{\gamma,hypo}} \tag{4.18}$$

Its solution is a fixed point and obeys the laws of physics:

$$\Omega_{\gamma,test}(\Omega_{\gamma,hypo}) = \Omega_{\gamma,hypo} = \Omega_{\gamma,fixed\ point} \tag{4.19}$$

In the following subsections we present details concerning the above calculations.

4.3.4 Density of curvature parameter

The density parameter of the curvature is zero, see (Carmesin, 2021c, theorem 32 number (6)):

$$\boxed{\Omega_K = 0} \tag{4.20}$$

4.3.5 Used result of the Planck scale

Sometimes we use the Planck units or natural units. These are listed in table (15.3). For instance, the Planck density ρ_P is expressed in terms of the Planck mass M_P and the Planck length L_P:

$$\rho_P = \frac{M_P}{L_P^3} \tag{4.21}$$

Moreover, we use the symmetry of a ball:

$$\bar{\rho}_P = \frac{M_P}{L_P^3 \cdot 4\pi/3} \tag{4.22}$$

We mark quantities in Planck units by a tilde.

4.3.6 Used result of neutrino physics

The density of the primordially formed neutrinos is as follows, see e. g. (Hinshaw et al., 2013, p. 12) or (Tanabashi et al., 2018, Eq. 25.1):

$$\rho_\nu = \frac{7}{8} \cdot \left(\frac{4}{11}\right)^{4/3} \cdot N_{eff} \cdot \rho_\gamma \tag{4.23}$$

Hereby, the density ρ_γ of photons is the same as the density ρ_{CMB} of the CMB, in a very good approximation. Moreover, the effective number of neutrino species is as follows, see (Tanabashi et al., 2018, Tab. 2.1):

$$N_{eff} = 3.13 \pm 0.32 \quad \text{or} \quad \Delta_{obs} N_{eff} = \frac{\Delta N_{eff}}{N_{eff}} = \frac{0.32}{3.13} = 9.7\% \tag{4.24}$$

That **error of measurement** $\Delta_{obs} N_{eff}$ causes an additional error of measurement in Ω_ν:

$$\Delta_{obs,add} \Omega_\nu = 9.7\% \tag{4.25}$$

Moreover, that error of measurement $\Delta_{obs} N_{eff}$ describes an error in the distribution of relativistic species among Ω_γ and Ω_ν,

whereby $\Omega_\gamma + \Omega_\nu = \Omega_r$. Thus $\Delta_{obs} N_{eff}$ causes an additional error of measurement in Ω_γ that is in proportion to Ω_γ and Ω_ν as follows:

$$\Delta_{obs,add}\Omega_\gamma = 9.7\% \cdot \frac{\Omega_r - \Omega_\nu}{\Omega_r} \tag{4.26}$$

As we apply this result only for comparisons with observation, we use the observations in Tab. (15.2):

$$\Delta_{obs,add}\Omega_\gamma = 9.7\% \cdot \frac{9.265 - 3.874}{9.265} = 5.6\% \tag{4.27}$$

Furthermore, we apply ρ_{CMB} in Eq. (4.23). So we derive:

$$\rho_\nu = \frac{7}{8} \cdot \left(\frac{4}{11}\right)^{4/3} \cdot N_{eff} \cdot \rho_{CMB} \tag{4.28}$$

The present **fixed point algorithm** for $\Omega_{\gamma,test}(\Omega_{\gamma,hypo})$ requires a value for ρ_ν or Ω_ν. In chapter (12), we run this algorithm for $\Omega_{\gamma,test}(\Omega_{\gamma,hypo})$ by using the value $\Omega_{\nu,theo}$ that we derive in chapter (8). In the present chapter, we run the algorithm for $\Omega_{\gamma,test}(\Omega_{\gamma,hypo})$ with a value $\Omega_{\nu,lit.}$ based on a method suggested in the literature, see e. g. (Hinshaw et al., 2013, p. 12) or (Tanabashi et al., 2018, Eq. 25.1), whereby the value $\Omega_{\nu,lit.}$ is determined according to Eq. (4.28). In both cases we achieve very precise results, and in chapter (12) we additionally prove that we can derive all cosmological constants by using the universal constants and H_0 as the only numerical input.

Accordingly, in this chapter, we determine $\Omega_{\nu,lit.}$ by using the temperature of the CMB, see e. g. (Collaboration, 2020a, S. 3.1),

$$T_{CMB} = 2.7255(\pm 0.0006)\,\mathrm{K} \tag{4.29}$$

and by application of the Planck distribution, see (Carmesin, 2020b, Eq. 4.68):

$$\rho_{CMB} = \frac{8\pi^5 \cdot (k_B \cdot T_{CMB})^4}{15(h \cdot c)^3 \cdot c^2} = \Omega_{CMB} \cdot \rho_{cr,t_0} \tag{4.30}$$

$$\Omega_{\nu,lit.} = \frac{7}{8} \cdot \left(\frac{4}{11}\right)^{4/3} \cdot N_{eff} \cdot \Omega_{CMB} \tag{4.31}$$

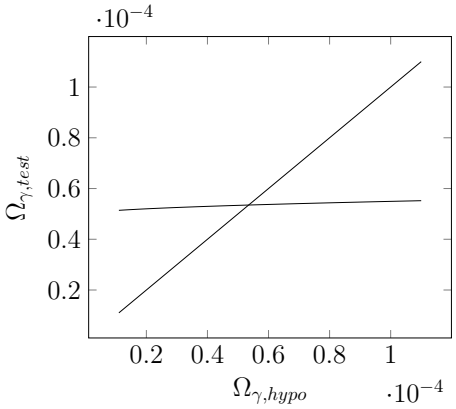

Figure 4.1: Fixed point Ω_γ (Eq. 4.18). The intersection with the diagonal is the fixed point: $\Omega_\gamma = 5.349 \cdot 10^{-5}$. As a consequence we get $\Omega_r = 9.223 \cdot 10^{-5}$, deviating from the observed value by 0.45 % only, see Collaboration (2020a). We obtained these values without executing any fit.

4.3.7 Used result *ERS*

In this S. we summarize the amount of extra radiation species, ERS, see Overbye (2018) or Cooray (2016):

$$\rho_{ERS} = q_{ERS} \cdot \rho_{CMB} \quad \text{with} \quad q_{ERS} = 0.0214 \tag{4.32}$$

The corresponding density parameter is very small:

$$\Omega_{ERS} = 1.166 \cdot 10^{-6} \tag{4.33}$$

Moreover, the extra radiation species are customarily included in the density of neutrinos, see (Hinshaw et al., 2013, S. 4.3). Thus the extra radiation species do not occur explicitly in our fixed point algorithm.

4.4 Fixed point $\Omega_{\gamma,fixed\,point}$

In this section we present the calculation of the fixed point, we compare our theoretical results with observation, and we critically discuss our method.

Primordial photons: The density parameter of the primordial photons at the fixed point is as follows:

$$\boxed{\Omega_{\gamma,\, fixed\, point} = 5.349 \cdot 10^{-5} = \Omega_{\gamma,theo}} \tag{4.34}$$

4.5 Comparison with observation: Ω_γ

We compare this result with the observed temperature of the CMB as follows: Before the emission of the CMB, the primordial photons scatter, and so they are thermalized. For that ideal case, we derive the corresponding temperature according to the Planck law, see e. g. Carmesin (2020b):

$$\rho_\gamma = \frac{8\pi^5 \cdot (k_B \cdot T_\gamma)^4}{15(h \cdot c)^3 \cdot c^2} \tag{4.35}$$

With it we derive $\Omega_{\gamma,obs}$ corresponding to T_{CMB}, see Eq. (4.35):

$$\Omega_{\gamma,obs} = \frac{\rho_{\gamma,obs}}{\rho_{cr,t_0}} = \frac{1}{\rho_{cr,t_0}} \cdot \frac{8\pi^5 \cdot (k_B \cdot T_{CMB})^4}{15(h \cdot c)^3 \cdot c^2} = 5.335 \cdot 10^{-5} \tag{4.36}$$

The relative difference between that observed value and the theoretical value in Eq. (4.34) is as follows:

$$\boxed{\Delta_{theo-obs}\Omega_\gamma = \frac{\Omega_{\gamma,theo} - \Omega_{\gamma,obs}}{\Omega_{\gamma,obs}} = \pm 0.26\%} \tag{4.37}$$

The corresponding error of measurement is caused by the error of T amounting to 0.08% (four times the error of T of 0.02%, according to T^4 in Eq. (4.36)) and the additional error of 5.6%, see Eq. (4.27).

$$\Delta_{obs}\Omega_\gamma = 0.08\% + 5.6\% = 5.68\% \tag{4.38}$$

So the observed differences between theory and observation are smaller than the errors of observation. Hence our theory is in precise accordance with observation. The same holds for Ω_r:

$$\Delta_{theo-obs}\Omega_r = \frac{\Omega_{r,theo} - \Omega_{r,obs}}{\Omega_{r,obs}} = 0.45\% < 3.1\% = \Delta_{obs}\Omega_r \tag{4.39}$$

Theorem 4 Explanation of Ω_γ

(1) The density parameter $\Omega_{\gamma,theo}$ is precisely derived on the basis of the time evolution of the light horizon ranging from the Planck scale to the present-day light horizon and ranging from the Big Bang until today. The result is as follows:

$$\boxed{\Omega_{\gamma,theo} = 5.349 \cdot 10^{-5}} \tag{4.40}$$

(2) The sum of $\Omega_{\gamma,theo} = 5.349 \cdot 10^{-5}$ and $\Omega_\nu = 3.874 \cdot 10^{-5}$ provides $\Omega_r = 9.223 \cdot 10^{-5}$. Both results $\Omega_{\gamma,theo}$ and $\Omega_{r,theo}$ are in precise accordance with observation, as the differences between theory and observation are smaller than the corresponding errors of measurement.

4.5.1 Time evolution of the photons ρ_γ

In this section we analyze the origin and time evolution of the density of the photons ρ_γ.

Many photons originate from the Big Bang. The space that is within the present-day light horizon R_{lh} was within the dimensional horizon D_{hori} at that time. At that dimensional horizon, there has been a binary fluid, consisting of photons and primordial black holes, see Carmesin (2020b). The energy of these black holes transformed to photons via Hawking radiation later. Here we describe the sum of both components by photons only. This is adequate, as the law of conservation of energy holds.

These photons are described by using the Bose gas model, see e. g. (Carmesin, 2021c, chapter 8). Their density at the dimensional horizon was as follows:

$$\tilde{\rho}_{\gamma,Dhori} = 0.5 \tag{4.41}$$

That density is reduced by redshift to its present-day value:

$$\tilde{\rho}_{\gamma,t_0} \tag{4.42}$$

The corresponding scale factor is denoted as follows:

$$k_{Dhori,t_0} \tag{4.43}$$

So the present-day density is derived as follows:

$$\tilde{\rho}_{\gamma,t_0} = \tilde{\rho}_{\gamma,Dhori} \cdot k^{-4}_{Dhori,t_0} \tag{4.44}$$

With it we derive the density parameter:

$$\boxed{\Omega_\gamma = \tilde{\rho}_{\gamma,t_0}/\tilde{\rho}_{cr,t_0}} \tag{4.45}$$

The above photons are scattered and thermalized before the emission of the CMB at the redshift z_{CMB}. These thermalized photons constitute the CMB. So the density $\tilde{\rho}_{\gamma,t_0}$ of the above photons that originate from the dimensional horizon should be equal to the density of the photons observed today, described by the density $\tilde{\rho}_{CMB}$. This equality is indeed confirmed:

Proposition 10 Photon - photon equality

(1) The density parameter $\Omega_{\gamma,theo}$ of the **primordial photons** *originating from the dimensional horizon is as follows:*

$$\Omega_{\gamma,theo} = 5.349 \cdot 10^{-5} \tag{4.46}$$

(2) The density parameter $\Omega_{\gamma,obs}$ of the observed **present-day photons** *is equal to the difference of the density parameter $\Omega_{r,obs} = 9.265 \cdot 10^{-5}$ of all radiation species minus the density parameter $\Omega_{\nu,obs} = 3.874 \cdot 10^{-5}$ of neutrinos:*

$$\boxed{\Omega_{\gamma,obs} = \Omega_{r,obs} - \Omega_{\nu,obs} = 5.291 \cdot 10^{-5} = \Omega_{\gamma,theo} \pm 1.7\%} \tag{4.47}$$

(3) As the difference amounts to 1.7 % only, while the error of measurement is equal to 5.68 %, the amount of the **present-day photons** *is equal to the amount of* **primordial photons**, *within the errors of measurement.*

Chapter 5

Quanta of Spacetime

In this chapter we summarize essential results about the **quanta of spacetime, QST**, see Carmesin (2021c). Moreover, we analyze the QST systematically.

5.1 On tensors in spacetime

In this section we provide useful mathematical facts about tensors that are applied to spacetime.

5.1.1 Deformations

In this section we describe deformations by tensors. For it we describe deformations of an infinitesimal cube with a constant cross sections dA_y orthogonal to the y-direction and with a height dy, see Fig. (5.1).

Non diagonal deformation: First we describe a shift of each cross section dA_y: At each height δy, the cross section is shifted according to a factor $\varepsilon_{x,y}$ by $\delta x = \varepsilon_{x,y} \cdot \delta y$, see Fig. (5.1). Hereby the factor $\varepsilon_{x,y}$ is an element of the deformation tensor, see e. g. (Sommerfeld, 1978, p. 3). The volume is invariant in a non diagonal deformation.

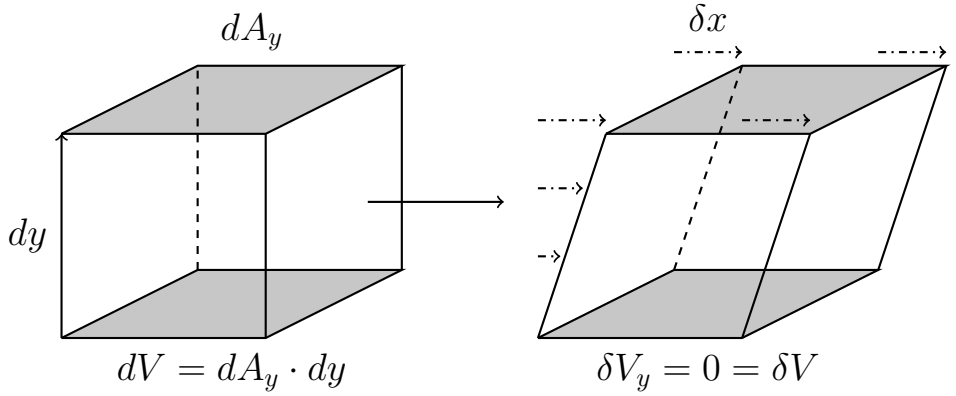

Figure 5.1: Deformation: A cube with a cross section dA_y. At each height δy, the cross section is shifted according to a factor $\varepsilon_{x,y}$ by $\delta x = \varepsilon_{x,y} \cdot \delta y$.

Diagonal deformation or elongation: Next we describe a shift of the cross section dA_y in the direction orthogonal to dA_y: At each height δy, the cross section is shifted according to a factor $\varepsilon_{y,y}$ by $\delta y = \varepsilon_{y,y} \cdot \delta y$, see Fig. (5.2). Hereby the factor $\varepsilon_{y,y}$ is a diagonal element of the deformation tensor, see e. g. (Sommerfeld, 1978, p. 3). In a diagonal deformation, the volume changes as follows:

$$\delta V_y = dA_y \cdot \delta y \tag{5.1}$$

Linear deformation: The above two deformations are linear. We obtain a general linear deformation from the above two particular cases by allowing all coordinate directions. Thus, a general linear deformation is described by the following tensor:

$$\hat{\varepsilon}_{i,j} = \frac{\partial r_i}{\partial r_j} \tag{5.2}$$

So the following shift of a cross section dA_j is achieved:

$$\delta r_i = \hat{\varepsilon}_{i,j} \cdot \delta r_j = \frac{\partial r_i}{\partial r_j} \cdot \delta r_j \tag{5.3}$$

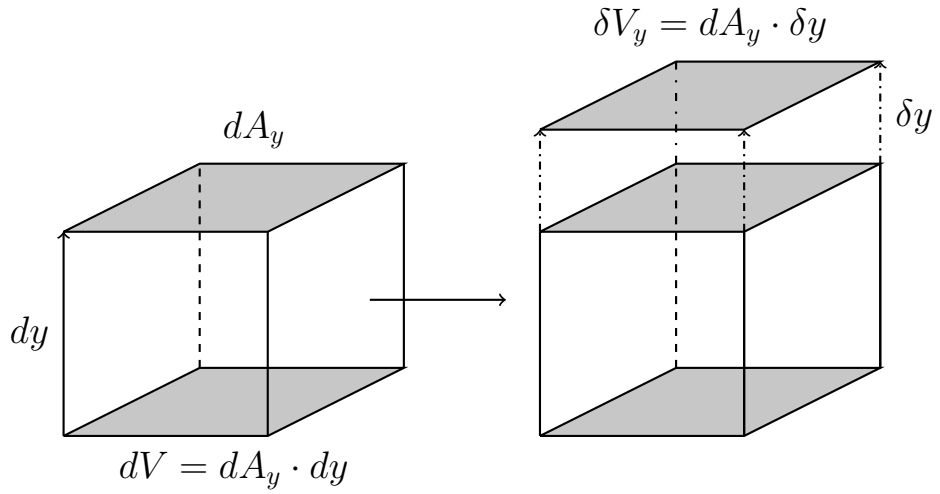

Figure 5.2: Elongation: A cube with a cross section dA_y is elongated by an increment δy.

5.1.2 Linear change of the volume

Similar to Eq. (5.1), the increase of volume is as follows:

$$\delta V_j = dA_j \cdot \delta r_j \tag{5.4}$$

We divide by the volume of the infinitesimal cube, $dV = dA_j \cdot dr_j$. So we derive the following relative change of volume:

$$\frac{\delta V_j}{dV} = \frac{\delta r_j}{dr_j} \tag{5.5}$$

Thus, a linear deformation with the tensor $\hat{\varepsilon}_{i,j}$ causes the following change of the volume:

$$\boxed{\frac{\delta V}{dV} = \Sigma_{j=1}^{j=D} \frac{\delta V_j}{dV} = \Sigma_{j=1}^{j=D} \frac{\delta r_j}{dr_j} = \text{Trace}(\hat{\varepsilon}_{ij})} \tag{5.6}$$

Consequently, the rate of formed volume is analogous to the time derivative of the deformation tensor as follows:

$$\boxed{\frac{\delta V}{dV \cdot \delta t} = \dot{\hat{\varepsilon}} = \text{Trace}(\dot{\hat{\varepsilon}}_{ij})} \tag{5.7}$$

We name the above tensor $\dot{\hat{\varepsilon}}_{ij}$ as the **generalized rate tensor**.

5.2 On fields of spacetime

In this section we summarize basic properties of waves of spacetime, see (Carmesin, 2021c, chapters 1, 2, 5). In the homogeneous universe frame, HUF, the rate gravity scalar RGS is a Lorentz invariant, and it describes a relation between the field $\vec{G}^*$ and the rate $\dot{\hat{\varepsilon}}$ as follows:

$$RGS = \dot{\varepsilon}^2 - G^{*2}/c^2 = \dot{\varepsilon}^2 - \Sigma_{j=1}^{j=D} G_j^{*2} \tag{5.8}$$

This equation has been derived for the particular case of three dimensional space. That equation is obviously generalized to the case of D dimensional space by expressing the square of the field G^{*2} in terms of its Cartesian components, $\Sigma_{j=1}^{j=D} G_j^{*2}$. Hereby all components are added for all dimensions of space, naturally.

Moreover, that scalar is zero, see (Carmesin, 2021c, THM. 7):

$$\boxed{RGS = \dot{\varepsilon}^2 - G^{*2}/c^2 = \dot{\varepsilon}^2 - \Sigma_{j=1}^{j=D} G_j^{*2} = 0} \tag{5.9}$$

This Eq. describes an isotropic system. More generally, the rate $\dot{\varepsilon}$ and the field G^{*2} can represent traces of tensors, see (Carmesin, 2021c, Eq. 5.1). An especially interesting case is an unidirectional system, see (Carmesin, 2021c, Eq. 5.4):

$$\boxed{\dot{\varepsilon}_j^2 - G_j^{*2}/c^2 = 0} \tag{5.10}$$

As this Eq. describes one direction only, this equation can directly be generalized to D dimensions by linear superposition.

5.3 Propagation of waves of spacetime

In this section we determine the propagation of waves in spacetime for waves with tensors in spatial dimensions $D \geq 3$.

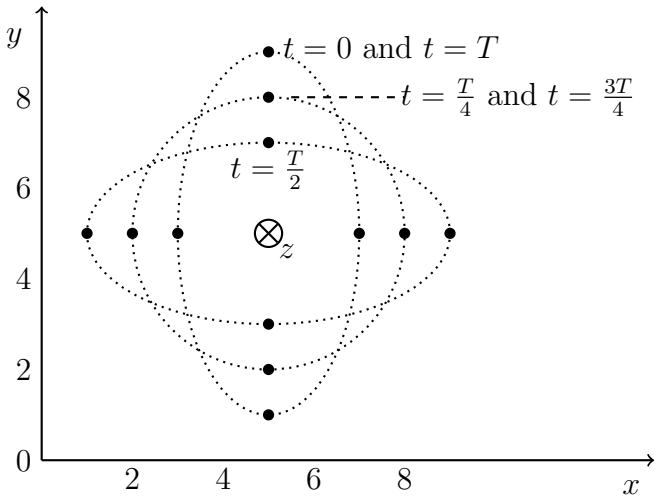

Figure 5.3: Single mode with periodic time T of a gravitational wave propagating to the z direction: Locations in space are indicated by small dots visually combined by dotted lines.

In three dimensional space, the tensor equation is as follows, see Eq. (5.10) or (Carmesin, 2021c, chapter 5):

$$\boxed{\dot{\hat{\varepsilon}}_j^2 - \frac{G_j^{*2}}{c^2} = 0} \tag{5.11}$$

$$\text{with} \quad G_j^* = -\frac{\partial}{\partial j}\phi = -\partial_j \phi \quad \text{we derive the wave Eq.} \tag{5.12}$$

$$\boxed{\dot{\varepsilon}_j^2 - \frac{(\partial_j \phi)^2}{c^2} = 0} \tag{5.13}$$

The solutions of the above DEQ are called **rate gravity waves, RGW**, see Carmesin (2021c).

5.4 An example: gravitational waves

Abbott (2016) discovered the gravitational wave that has been predicted by Einstein (1916) hundred years earlier.

5.4.1 Geometric description

A gravitational wave that propagates in a direction z elongates the space in an orthogonal direction, for instance x, and simultaneously contracts the space the other orthogonal direction, it is y in the example. That elongation and contraction take place periodically. An illustration of that dynamics is shown in Fig. (5.3). In order to derive an algebraic description of gravitational waves, we analyze tensors next.

5.4.2 Elementary deformations

A deformation in a direction Δx and by an amount Δx is described by a tensor as follows:

$$\varepsilon_{i,j} = \begin{pmatrix} 1 & 0 & 0 \\ 0 & 0 & 0 \\ 0 & 0 & 0 \end{pmatrix} \tag{5.14}$$

Similarly, a deformation in a direction Δy and by an amount Δy is described by the following tensor:

$$\varepsilon_{i,j} = \begin{pmatrix} 0 & 0 & 0 \\ 0 & 1 & 0 \\ 0 & 0 & 0 \end{pmatrix} \tag{5.15}$$

In the same manner, a deformation in a direction Δx with an amount proportional to Δy is illustrated in Fig. (5.4), and it is described by the tensor below:

$$\varepsilon_{i,j} = \begin{pmatrix} 0 & 1 & 0 \\ 0 & 0 & 0 \\ 0 & 0 & 0 \end{pmatrix} \tag{5.16}$$

We summarize and generalize these examples in the following definition:

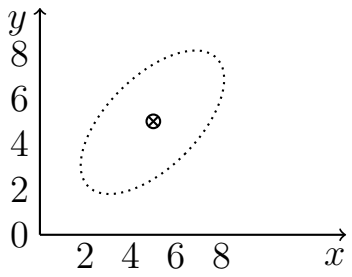

Figure 5.4: Single mode with periodic time T of a gravitational wave propagating to the z direction: Locations in space are indicated by small dots visually combined by dotted lines.

Definition 6 Elementary deformations

(1) A deformation in a direction Δr_i with an amount proportional to Δr_j (see Fig. 5.4), is described by the tensor with a 1 in row i and column j and with zeros at all other indices of the tensor:

$$\varepsilon_{i,j} = \delta_{i,j} \tag{5.17}$$

(2) These deformations cannot be expressed as a linear combination of tensors with more zeros. Correspondingly, these deformations are **elementary deformations**.

(3) As the definition of elementary deformations does not contain a restriction of the dimension D, elementary deformations are defined in each dimension $D \geq 1$.

(4) A **normalized elementary deformation** *is an elementary deformation, the tensor of which has nonzero elements with value 1 only.*

(5) A normalized elementary deformation parallel to the direction of propagation is a longitudinal polarization, and we mark it by an index LONG.

5.4.3 Linear combinations of deformations

Elementary deformations are described by tensors. Tensors can be combined linearly. As a consequence, a linear combination of tensors of elementary deformations describes a linear combination of deformations. We summarize and generalize that description in the following definition:

Definition 7 Combined deformation

If two deformations A and B are described by two tensors $\varepsilon_{A,i,j}$ and $\varepsilon_{B,i,j}$ in a dimension D, then a linear combination of these tensors describes a combined deformation $\varepsilon_{C,i,j}$:

$$a \cdot \varepsilon_{A,i,j} + b \cdot \varepsilon_{B,i,j} = \varepsilon_{C,i,j} \tag{5.18}$$

The gravitational wave in Fig. (5.3) is constituted by a deformation described by the tensor $\delta_{x,x}$ and by a deformation described by the tensor $-\delta_{y,y}$, whereby the elongations and contractions take place locally only. So that gravitational wave is characterized by the following combination of two elementary deformations:

$$\varepsilon_{i,j} = \begin{pmatrix} 1 & 0 & 0 \\ 0 & -1 & 0 \\ 0 & 0 & 0 \end{pmatrix} \tag{5.19}$$

If a gravitational wave propagates in the z direction, then there are two orthogonal dimensions. Accordingly, there are two modes: The mode illustrated in Fig. (5.3) and the mode illustrated in Fig. (5.5). That mode can be obtained from the first mode by a rotation around the z-direction by 45°. That mode is described by the tensor in Eq. (5.20).

$$\varepsilon_{i,j} = \begin{pmatrix} 0 & 1 & 0 \\ -1 & 0 & 0 \\ 0 & 0 & 0 \end{pmatrix} \tag{5.20}$$

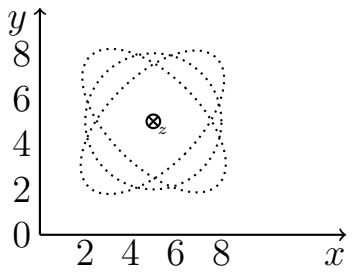

Figure 5.5: Single mode with periodic time T of a gravitational wave propagating to the z direction: Locations in space are indicated by small dots visually combined by dotted lines.

5.4.4 Elementary zero-trace deformations

In this section we characterize the **elementary zero-trace deformations**. For instance, each gravitational wave is constituted by an elementary anti symmetric zero-trace deformation, see e. g. Eqs. (5.19) or (5.20).

Definition 8 Elementary zero-trace anti symmetric deformations

(1) A **elementary zero-trace anti symmetric deformation** *is characterized by a tensor with the following conditions:*

(1a) The tensor is anti symmetric.

(1b) The trace of the tensor is zero.

(1c) The tensor has as many zero tensor elements as possible.

(2) A **normalized elementary zero-trace anti symmetric deformation** *is an elementary zero-trace anti symmetric deformation, the tensor of which has nonzero elements with absolute value 1 only.*

Proposition 11 Normalized elementary zero-trace anti symmetric deformations

(1) The tensor of a normalized elementary zero-trace anti symmetric deformation has two nonzero elements 1 *and* -1.

(1a) Either these two elements are in the diagonal, see e. g. Eq. (5.19): $\varepsilon_{i,i} = 1$ *and* $\varepsilon_{j,j} = -1$

(1b) Or these two elements are not in the diagonal, see e. g. Eq. (5.20). $\varepsilon_{i,j} = 1$ *and* $\varepsilon_{j,i} = -1$

(2) The definition is applicable to each spatial dimension $D \geq 2$.

5.4.5 Unidirectional gravitational waves

In this section we analyze the polarization modes of unidirectional gravitational waves in D dimensions. An unidirectional quadrupole is characterized by a single direction vector $\vec{s}$, see e. g. (Carmesin, 2021c, Eq. 2.19). In D dimensions, a gravitational wave has one wave vector $\vec{k}$ representing the direction of propagation plus $D-1$ linear independent orthogonal direction vectors representing $D-1$ polarization modes: We summarize:

Proposition 12 Unidirectional gravitational waves

In a space with D *dimensions, an unidirectional gravitational wave has* $D-1$ *polarization modes.*

Chapter 6

Time Evolution of Dark Energy

In this chapter we model the dark energy. So we model the QST that form space[1].

6.1 Polarization modes of these QST

We analyze the modes of polarization of these QST of dark energy. Each quantum of dark energy should be **indivisible**, as there is no combination of states observed in the dark energy or in space. So each quantum of dark energy should be represented by a **quantized gravitational wave**. As shown in chapters (3) and (5), it is basically formed during cosmic unfolding.

Moreover, space basically exhibits directions without any more complicated geometric structure. Correspondingly, the quantized gravitational waves of space are represented by unidirectional gravitational waves, see proposition (12).

In addition, the modes exhibit unidirectional quadrupolar symmetry, see (Carmesin, 2021c, chapter 2). So each mode is represented by one wave vector $\vec{k}$ of propagation and by one out of $D-1$ direction vectors in the plane orthogonal to $\vec{k}$. Thus, the number N of polarization modes is equal to $D-1$:

$$N_{QST,dark\ energy} = D - 1 \tag{6.1}$$

[1] I developed such models e. g. in Carmesin (2018g), Carmesin (2018f), Carmesin (2019d), Carmesin (2019c), Carmesin (2019f), Carmesin (2021c), Carmesin (2021a).

6.2 Time evolution of these QST

In this S. we derive the energy of a QST of dark energy, and therefrom we derive the volume and the density of dark energy.

Energy: The energy of these QST is derived from the energy at the dimensional horizon:

$$E_{D_{hori}} \approx \frac{1}{2} \cdot E_P \tag{6.2}$$

During cosmic unfolding, this energy decreases according to the redshift by the dimensional distance enlargement factor:

$$Z_{D_{hori} \to 3} = 2^{(D_{hori}-3)/3} \tag{6.3}$$

With $D_{hori} = 301.35$ we derive:

$$Z_{D_{hori} \to 3} = 8.66 \cdot 10^{29} \tag{6.4}$$

During cosmic unfolding, the number of polarization modes decreases from $N = 301-1$ to $N = 3-1$. So the energy decreases according to the vanishing polarization modes by the additional factor 300/2. So we derive:

$$\boxed{E_\Lambda(D=3) = E_{D_{hori}} \cdot \frac{1}{Z_{D_{hori} \to 3} \cdot 150}} \tag{6.5}$$

We insert $E_{D_{hori}} = 1/2$ and use Eq. (6.4). So we derive the energy of a present-day QST of dark energy:

$$\boxed{E_\Lambda(D=3) = 1.5 \cdot 10^{-23}\,\mathrm{J} = 5.4 \cdot 10^{-5}\,\mathrm{eV}} \tag{6.6}$$

Volume: At the dimensional horizon, the three dimensional volume of a QST is characterized by the radius L_P. During cosmic unfolding, the wavelength of the QST increases by the factor $Z_{D_{hori} \to 3}$. Thus, the volume at three dimensions is as follows:

$$V(D=3) = V_{D=3} \cdot (L_P \cdot Z_{D_{hori} \to 3})^3 \;\text{ with }\; V_{D=3} = \frac{4\pi}{3} \tag{6.7}$$

Density: Hence the energy density of a QST is the ratio of the above energy and volume:

$$\frac{E_\Lambda}{V} = \frac{E_\Lambda(D=3)}{V(D=3)} = \frac{E_{D_{hori}}}{V_{D=3} \cdot 150 \cdot L_P^3 \cdot Z_{D_{hori}\to 3}^4} \tag{6.8}$$

The corresponding density is as follows:

$$\boxed{\rho_{\Lambda,theo} = \frac{E_\Lambda}{V \cdot c^2} \approx \frac{E_P/2}{V_{D=3} 150 c^2 L_P^3 Z_{D_{hori}\to 3}^4} = 7.29 \cdot 10^{-27} \, \frac{\text{kg}}{\text{m}^3}} \tag{6.9}$$

For comparison, the observed density of dark energy is as follows, see table (15.2):

$$\rho_{\Lambda,obs} = 8.66 \cdot 10^{-27} \, \frac{\text{kg}}{\text{m}^3} \cdot 0.6847 = 5.93 \cdot 10^{-27} \, \frac{\text{kg}}{\text{m}^3} \tag{6.10}$$

6.3 Comparison with observation: ρ_Λ

The relative difference is:

$$\Delta_{theo-obs}\rho_\Lambda = \frac{\rho_{\Lambda,theo} - \rho_{\Lambda,obs}}{\rho_{\Lambda,obs}} = \pm 23\% \tag{6.11}$$

Discussion: This result is already quite precise, as the density varies by a factor of 10^{122} during cosmic unfolding.

Furthermore, we used one energy or one wavelength only. That is, we applied a monochromatic analysis. But the dimensional horizon varies slightly as a function of time. Thus, the energy and the corresponding wavelength vary as a function of time as well. Hence a polychromatic vacuum occurs.

Indeed, the difference between theory and observation is below one percent, when we consider the full polychromatic vacuum, see below.

Theorem 5 Present-day formation of dark energy

The dark energy that forms at the present-day t_0 has the following properties:

(1) The energy of a quantum of spacetime of that dark energy depends on the present-day dimensional horizon $D_{hori}(t_0)$ as follows:

$$\boxed{E_\Lambda(D=3,t_0) = \frac{2 \cdot E_{D_{hori}(t_0)}}{Z_{D_{hori}(t_0)\to 3} \cdot (D_{hori}(t_0)-1)}} \tag{6.12}$$

$$\text{with} \quad Z_{D_{hori}(t_0)\to 3} = 2^{(D_{hori}(t_0)-3)/3} \tag{6.13}$$

(2) The density of that dark energy that forms today depends on the present-day dimensional horizon $D_{hori}(t_0)$ as follows:

$$\boxed{\rho_\Lambda(t_{form}=t_0) = \frac{2E_{D_{hori}(t_0)}}{V_{D=3} \cdot (D_{hori}(t_0)-1) \cdot c^2 \cdot L_P^3 \cdot Z^4_{D_{hori}(t_0)\to 3}}} \tag{6.14}$$

(3) The corresponding values are as follows:

$$\boxed{E_\Lambda(D=3,t_0) = 1.5 \cdot 10^{-23}\,\text{J} = 5.4 \cdot 10^{-5}\,\text{eV}} \tag{6.15}$$

$$\boxed{\text{and} \quad \rho_\Lambda(t_{form}=t_0) = 7.29 \cdot 10^{-27}\,\frac{\text{kg}}{\text{m}^3}} \tag{6.16}$$

(4) The quanta of the dark energy travel at the velocity of light, as there is no physical space at rest in any frame, see e. g. Michelson and Morley (1887) or Einstein (1905).

(5) At the present time t_0, the same dark energy forms in the whole universe, according to translation invariance of space.

Chapter 7

Excitation of the Vacuum

In this C. we analyze vacuum and its spectrum of excitation.

7.1 Components of the present-day vacuum

In this S. we summarize the QST forming present-day vacuum.

The main component of present-day vacuum is the stable phase, the three dimensional vacuum, see chapter 6. Additionally, there are coexisting phases, see proposition (8). These coexisting phases are the earlier phases that can in principle coexist with the $3D$ vacuum, since there can always remain QST from earlier times.

Corresponding energies: The corresponding zero-point energies $ZPE_{\Lambda,D}$ are derived as follows: The energy of these QST is derived from the energy at the dimensional horizon:

$$E_{D_{hori}} \approx \frac{1}{2} \cdot E_P \tag{7.1}$$

During cosmic unfolding, this energy decreases according to the redshift by the dimensional distance enlargement factor:

$$Z_{D_{hori} \to D} = 2^{(D_{hori} - D)/D} \tag{7.2}$$

During cosmic unfolding, the number of polarization modes decreases from $N = 301 - 1$ to $N = D - 1$. So the energy decreases

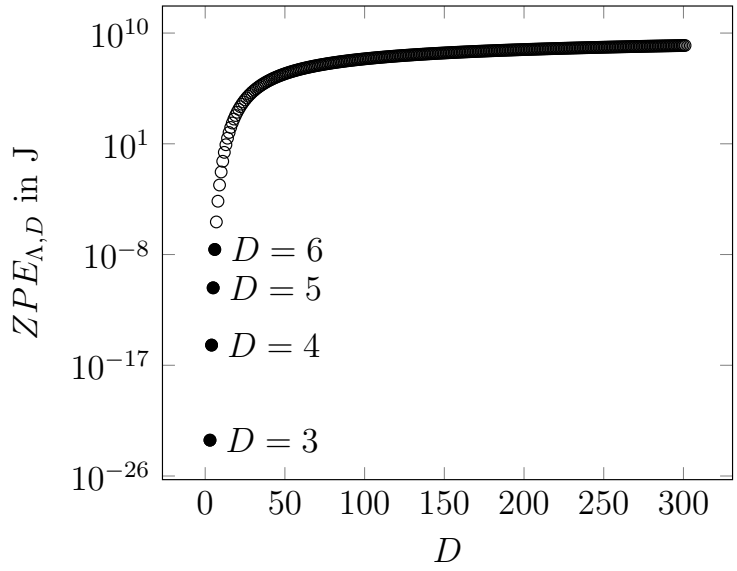

Figure 7.1: Zero-point energy $ZPE_{\Lambda,D}$ of the dark energy as a function of the dimension of the space D, see proposition (13).

according to the vanishing polarization modes by the additional factor $300/(D-1)$. So we derive:

$$ZPE_{\Lambda,D} = E_{D_{hori}} \cdot \frac{D-1}{Z_{D_{hori} \to D} \cdot 300} \tag{7.3}$$

These zero-point energies $ZPE_{\Lambda,D}$ are shown as a function of the dimension of space D in Fig. (7.1). We summarize:

Proposition 13 Present-day vacuum

The present-day vacuum consists of the following gravitational wave QST:

(1) The main component is constituted by the stable three dimensional gravitational waves, based on two modes of polarization, $ZPO_{gw,D=3}$ or $ZPO_{\Lambda,D=3}$.

(2) The coexisting component is constituted by the unstable or metastable gravitational waves at dimensions $D \geq 4$, each based on $D-1$ modes of polarization, $ZPO_{\Lambda,D\geq 4}$.

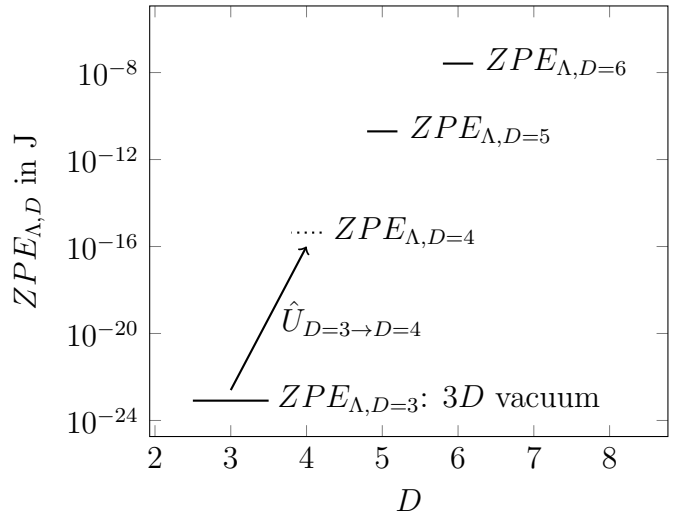

Figure 7.2: Excitation of a QST $ZPE_{\Lambda,D=3}$ of the present-day $3D$ vacuum by a transition $\hat{U}_{D=3\to D=4}$ to a QST $ZPE_{\Lambda,D=4}$. That transition $\hat{U}_{D=3\to D=4}$ is a cosmic folding.

(3) The coexisting component at $D = 4$ is especially unstable, see Fig. (3.7).

(4) The corresponding zero-point energies $ZPE_{\Lambda,D}$ are as follows, see e. g. Fig. (7.2):

$$ZPE_{\Lambda,D} = E_{D_{hori}} \cdot \frac{D-1}{Z_{D_{hori}\to D} \cdot 300} \tag{7.4}$$

7.2 Basic solution of the hierarchy problem

The zero-point oscillations $ZPO_{\Lambda,D\geq 3}$ of the dark energy represent the components of the present-day vacuum. The excitation modes of that present-day vacuum basically represent the elementary particles, see Tanabashi et al. (2018).

In our theory, the zero-point oscillations $ZPO_{\Lambda,D\geq 3}$ have very different energies $ZPE_{\Lambda,D\geq 3}$ ranging from the zero-point energy of the three dimensional vacuum to the Planck energy (see proposition 13 and Fig. 7.1). So within our theory, the

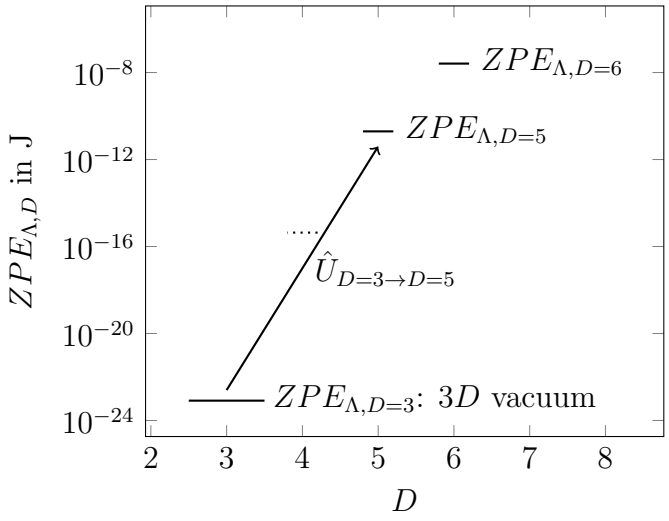

Figure 7.3: Excitation of a QST $ZPE_{\Lambda,D=3}$ of the present-day $3D$ vacuum by a transition $\hat{U}_{D=3\to D=5}$ to a QST $ZPE_{\Lambda,D=5}$. That transition $\hat{U}_{D=3\to D=5}$ is a cosmic folding.

elementary particles have very different energies ranging from the zero-point energy of the three dimensional vacuum to the Planck energy. Hence our theory basically solves the hierarchy problem. We summarize that result:

Theorem 6 Basic solution of the hierarchy problem

(1) In the process of **cosmic unfolding**, *the components of the vacuum form, namely the zero-point oscillations* $ZPO_{\Lambda,D_{hori}\geq D\geq 3}$ *ranging from the dimensional horizon* D_{hori} *to the present-day dimension* $D = 3$, *see e. g. Fig. (7.2).*

(2) In the process of cosmic unfolding, the corresponding zero-point energies $ZPE_{\Lambda,D_{hori}\geq D\geq 3}$ **range** *from the Planck scale to the energy of a QST of the present-day dark energy:*

$$ZPE_{\Lambda,D} = E_{D_{hori}} \cdot \frac{D-1}{Z_{D_{hori}\to D} \cdot 300} \tag{7.5}$$

$$\text{with } E_{D_{hori}} \approx \frac{E_P}{2} \tag{7.6}$$

(3) The energy of an elementary particle basically is the energy of an excitation (or combined excitation) of a QST of the vacuum, see e. g. Tanabashi et al. (2018). The excitation modes of the vacuum are as follows:

(3a) An excitation of a QST of the vacuum can be a transition, that is a cosmic folding (or an inverse cosmic unfolding) with a transition operator $\hat{U}_{D\to D+s}$, from a zero-point oscillation $ZPO_{\Lambda,D}$ to another zero-point oscillation $ZPO_{\Lambda,D+s}$, see section (3.10) and see e. g. Figs. (7.2) and (7.3):

$$ZPO_{\Lambda,D+s} = \hat{U}_{D\to D+s} \cdot ZPO_{\Lambda,D} \tag{7.7}$$

(3b) An excitation of a QST can be a transition $\hat{U}_{q_1\to q_2}$ from one zero-point oscillation $ZPO_{q_1,D}$ with a polarization q_1 to another zero-point oscillation $ZPO_{q_2,D}$ with a polarization q_2, see section (3.10) and see e. g. Fig. (7.4). Thus, the energy is as follows:

$$ZPE_{q_2,D} = E(\hat{U}_{q_1\to q_2} \cdot ZPO_{q_1,D}) \tag{7.8}$$

(3c) An excitation can correspond to a ladder operator (a_κ^+). That excitation transforms a zero-point oscillation $ZPO_{q,D}$ with eigenvalue $n = 0$ of the number operator to a quantum of spacetime $QST_{q,D,n=1}$ with the eigenvalue $n = 1$ of the number operator, see (Carmesin, 2021c, theorem 19) and see Fig. (7.5). Correspondingly, the energy is as follows:

$$E_{q,D,n=1} = ZPE_{q,D} \cdot (2n+1) = ZPE_{q,D} \cdot 3 \tag{7.9}$$

In general, (a_κ^+) transforms a quantum of spacetime $QST_{q,D,n}$ with eigenvalue n of the number operator to a quantum of spacetime $QST_{q,D,n+1}$ with the eigenvalue $n+1$ of the number operator. Thereby the energy is as follows:

$$E_{q,D,n} = ZPE_{q,D} \cdot (2n+1) \tag{7.10}$$

(3d) Additionally, two or more quanta of spacetime $QST_{q,D,n}$ can react and set free an energy of interaction E_{int} (including a

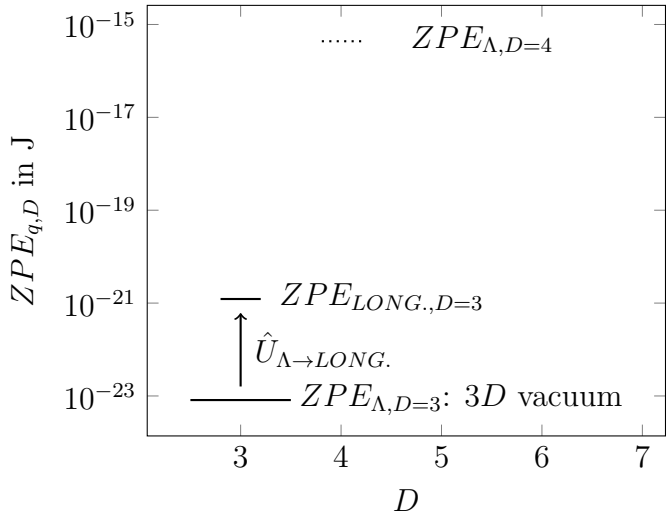

Figure 7.4: Excitation of a QST $ZPE_{\Lambda,D=3}$ of the present-day $3D$ vacuum by a transition $\hat{U}_{\Lambda\to LONG.}$ to a QST $ZPE_{LONG.,D=3}$. That transition $\hat{U}_{\Lambda\to LONG.}$ is a change of polarization.

possible binding energy):

$$\Sigma_{j=1}^{j=j_{max}} QST_{q_j,D,n_j} = QST_{q,D,combined} + E_{int} \tag{7.11}$$

That energy of interaction can contribute to the energy of an elementary particle. Examples for energies of interacting elementary particles can be found in Tanabashi et al. (2018).

(3e) Especially interesting are the most simple combinations that can establish a three dimensional object: Three longitudinal QST can exhibit superposition, so they can extend in three linear independent directions, and thus they can bind to an object. We mark such QST by an index LONG.

(4) As a cosmic folding $\hat{U}_{D\to D+s}$ can correspond to a relatively huge excitation energy (see proposition 13 and Fig. 7.1), the range of energies of the process of cosmic unfolding is basically equal to the range of energies of the elementary particles corresponding to the hierarchy problem.

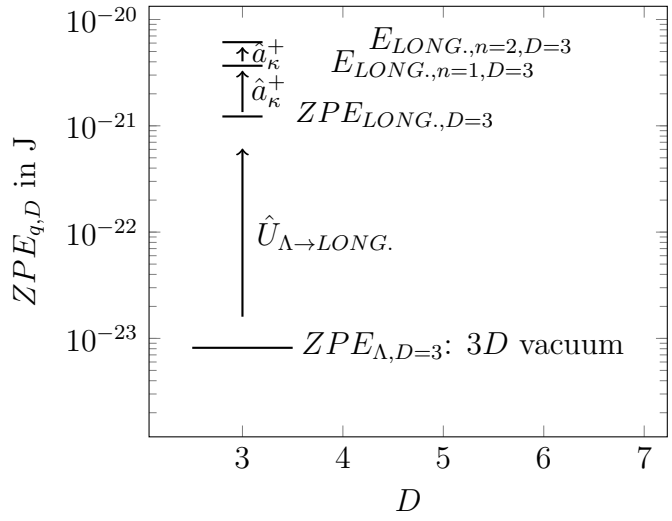

Figure 7.5: Excitation of a ZPO with $ZPE_{LONG.,D=3}$ by the ladder operator $\hat{a}_\kappa^+$ to the QST with $E_{LONG.,n=1,D=3}$. Further excitation of that QST with $E_{LONG.,n=1,D=3}$ by the same ladder operator $\hat{a}_\kappa^+$ to the QST with $E_{LONG.,n=2,D=3}$. The ladder operator causes an increase of the eigenvalue E_n of the energy by the summand $\hbar \cdot \omega$.

7.3 Spectrum of excitation of the vacuum

The spectrum of excitation modes of the vacuum is described shortly in theorem (6). In this part we present a detailed analysis of that spectrum of excitation modes that can arise from the present-day vacuum.

7.3.1 Cosmic folding of ZPOs

The present-day $D = 3$ vacuum is presented by QST of gravitational waves, $ZPO_{\Lambda,D=3}$. These QST formed by transitions $U_{D\to D=3}$ from a zero-point oscillation $ZPO_{\Lambda,D}$ to a zero-point oscillation $ZPO_{\Lambda,D=3}$ during the process of cosmic unfolding:

$$ZPO_{\Lambda,D=3} = \hat{U}_{D\to D=3} \cdot ZPO_{\Lambda,D} \tag{7.12}$$

That transitions $U_{D\to D=3}$ can be inverted:

$$ZPO_{\Lambda,D} = \hat{U}_{D=3\to D} \cdot ZPO_{\Lambda,D=3} \tag{7.13}$$

That cosmic folding increases the energy of the zero-point oscillation $ZPO_{\Lambda,D=3}$, see Eq. 7.5,

$$ZPE_{\Lambda,D=3} = E_{D_{hori}} \cdot \frac{2}{Z_{D_{hori}\to D=3} \cdot 300} \tag{7.14}$$

to:

$$ZPE_{\Lambda,D} = E_{D_{hori}} \cdot \frac{D-1}{Z_{D_{hori}\to D} \cdot 300} \tag{7.15}$$

Hence that cosmic folding is an excitation in the form of a transition from one ZPO to another ZPO see section (3.10). We summarize our result:

Proposition 14 Cosmic folding of a ZPO

(1) At each dimension $D \geq 3$, there can occur a transition from one ZPO to another ZPO in the form of a cosmic folding $U_{D\to D+s}$:

$$ZPO_{\Lambda,D+s} = \hat{U}_{D\to D+s} \cdot ZPO_{\Lambda,D} \tag{7.16}$$

(2) In particular, a zero-point oscillation $ZPO_{\Lambda,D=3}$ of the three dimensional vacuum can be excited by a cosmic folding to a zero-point oscillation $ZPO_{\Lambda,D}$ of the $D > 3$ dimensional vacuum:

$$ZPO_{\Lambda,D} = \hat{U}_{D=3\to D} \cdot ZPO_{\Lambda,D=3} \tag{7.17}$$

(3) In nature, such a zero-point oscillation $ZPO_{\Lambda,D}$ can coexist with the zero-point oscillations $ZPO_{\Lambda,D=3}$ of the three dimensional vacuum, see proposition (8).

7.3.2 On composed excitations

If an excitation of an object is composed of several single excitation modes with different excitation energies, then those excitation modes with a relatively large excitation energy take place in a relatively small time, usually, according to the Heisenberg uncertainty principle and according to Fermi's golden rule.

In the cases analyzed here, the transitions of dimensions have relatively high excitation energy. Accordingly, the ZPOs of various dimensions form relatively rapid.

Similarly, the transitions of polarization modes have relatively medium excitation energy. Accordingly, the ZPOs of various polarization modes form in a medium time interval.

Both ZPOs, those of dimension and those of polarization, determine the kind of the object, its state of dimensional folding and its polarization.

Finally, the excitation modes corresponding to ladder operators typically exhibit relatively low excitation energy, and correspondingly their formation requires a relatively long time interval. These modes do not change the kind of the object, but the energy $E_n = \hbar\omega(n+1/2)$ of the object. Of course, this may change the wave function and related properties of the object.

7.3.3 Transitions of ZPOs

The present-day vacuum is presented by QST of gravitational waves, $ZPO_{gw,D\geq 3}$. Their modes of polarization are presented by tensors ε_q, see section (5.4.5). Moreover, these QST of gravitational waves represent ZPOs, see chapter (6).

In general, there can occur QST with other polarization, see chapter (5). Moreover, transitions from one ZPO to another ZPO can take place in nature, see section (3.10). So in each dimension $D \geq 3$, there can happen transitions from a QST of gravitational waves already present in the vacuum, see proposition 13, to a QST with another mode of polarization. Since the QST of gravitational waves have a relatively low energy in each dimension, as a result of the process of cosmic unfolding, such a transitions is an excitation, typically. We summarize our result:

Proposition 15 Transitions among ZPOs at $D \geq 3$

At each dimension $D \geq 3$, there can occur a transition $U_{q_1 \to q_2}$ from a QST with one mode of polarization, $ZPO_{q_1,D}$ to a QST with another mode of polarization, $ZPO_{q_2,D}$:

$$ZPO_{q_2,D} = \hat{U}_{q_1 \to q_2} \cdot ZPO_{q_1,D} \tag{7.18}$$

7.3.4 Excitation by ladder operators

In this section we summarize the excitation modes of a ZPO of a QST that can be generated by a ladder operator $\hat{a}_\kappa^+$.

In general, a QST $ZPO_{q,\kappa,D}$ has its specific circular frequency ω_κ, see (Carmesin, 2021c, theorem 19) as well as a mode q of polarization. A respective ZPO corresponds to the eigenvalue $n = 0$ of the number operator, see (Carmesin, 2021c, theorem 19). Its energy is the ZPE with:

$$ZPE_{q,\kappa,D} = \frac{1}{2} \cdot \hbar\omega_\kappa \tag{7.19}$$

An excitation by a ladder operator increases the energy of a QST by $\Delta E_\kappa = \hbar\omega_\kappa$. Thus, such a QST $(\hat{a}_\kappa^+)^n \cdot ZPO_{q,\kappa,D}$ has an eigenvalue n of the number operator and the following energy:

$$E_{q,\kappa,D}(n) = \left(n + \frac{1}{2}\right) \cdot \hbar\omega_\kappa \tag{7.20}$$

7.3.5 Combined excitation

In this section we combine the above processes of excitation:

Proposition 16 Excitation of a $ZPO_{q,D}$

(1) At each dimension $D \geq 3$, a $ZPO_{q,D}$ with a polarization q can be excited by a cosmic folding, $U_{D \to D+s}$, by transition $U_{q \to q_2}$ and by ladder operators $\hat{a}_\kappa^+$, so that the following state occurs:

$$(\hat{a}_\kappa^+)^n \cdot \hat{U}_{q \to q_2} \cdot \hat{U}_{D \to D+s} \cdot ZPO_{q,D} \tag{7.21}$$

(2) In particular, in the present-day vacuum, a zero-point oscillation $ZPO_{\Lambda,D=3}$ of the three dimensional vacuum can be excited by a cosmic folding, $U_{D=3\to D}$, by transition $U_{\Lambda\to q_2}$ and by a ladder operator $\hat{a}_\kappa^+$, so that the following state occurs:

$$(\hat{a}_\kappa^+)^n \cdot \hat{U}_{\Lambda\to q_2} \cdot \hat{U}_{D=3\to D} \cdot ZPO_{\Lambda,D=3} \tag{7.22}$$

7.4 Formation of mass

In this section we analyze conditions for the formation of a nonzero rest mass or own mass m_{own}.

Necessary energy: Naturally, there must be energy that can transform into a mass m_{own}.

Velocity below c: According to SRT (e. g. Moore (2013)), an object with an energy E and a velocity v has the following rest mass or own mass:

$$m_{own} = \frac{E}{c^2} \cdot \sqrt{1 - \frac{v^2}{c^2}} \tag{7.23}$$

Thus, an object propagating at the velocity of light c has zero own mass m_{own}. Hence an object must propagate at a velocity smaller c in order to form a nonzero own mass m_{own}.

Velocity at and below c: If an object should transform from energy with zero own mass $m_{own} = 0$ to nonzero own mass $m_{own} > 0$, then it must be able to exhibit the velocity c and a velocity $v < c$. Next we show that the quanta of spacetime have this property.

Velocity of propagation of QST: The dynamics of a quantum of spacetime, QST, is characterized by the rate gravity scalar, see (Carmesin, 2021c, theorem 7):

$$RGS = \dot{\varepsilon}^2 - \frac{G^{*2}}{c^2} = 0 \text{ with } \dot{\varepsilon} = \frac{\delta V}{dV \cdot \delta t} \tag{7.24}$$

Hereby the gravitational field is expressed by the potential:

$$RGS = \dot{\varepsilon}^2 - \frac{\Sigma_j^D (\partial_{x_j} \Phi)^2}{c^2} = 0 \text{ with } G_j^* = -\partial_{x_j} \Phi \tag{7.25}$$

In the especially simple case of unidirectional propagation, the DEQ is as follows:

$$0 = \dot{\varepsilon}^2 - \frac{(\partial_x \Phi)^2}{c^2} \tag{7.26}$$

A typical solution is a plane wave:

$$\varepsilon = \hat{\varepsilon} \cdot \exp(i\omega \cdot t - i \cdot k \cdot x) \tag{7.27}$$

$$\Phi = \hat{\Phi} \cdot \exp(i\omega \cdot t - i \cdot k \cdot x) \tag{7.28}$$

So the DEQ of the QST exhibits a velocity of propagation v_{prop} corresponding to its wavelength λ and periodic time T or according to its circular frequency ω and its wave number k as follows, see (Carmesin, 2021c, Eq. 5.16):

$$v_{prop} = \frac{\lambda}{T} = \frac{\omega}{k} = \frac{\hat{\Phi}}{\hat{\varepsilon}} \frac{1}{c} \tag{7.29}$$

Hereby, the amplitude of the potential $\hat{\Phi}$ has the dimension of a square of a velocity, and its absolute value determines the velocity of propagation v_{prop}. Thereby the potential $\hat{\Phi}$ can change at each transition or excitation or combination with other QST. In this manner the velocity of propagation v_{prop} of the QST can change from $v = c$ to $v < c$, and so the formation of mass can be described by the above DEQ and their solutions.

Proposition 17 Formation of mass by QST

(1) The dynamics of the QST is characterized by the DEQ, a wave Eq.:

$$RGS = \dot{\varepsilon}^2 - \frac{\Sigma_j^D (\partial_{x_j} \Phi)^2}{c^2} = 0 \text{ with } G_j^* = -\partial_{x_j} \Phi \tag{7.30}$$

(2) The above DEQ provides solutions with various velocities, including $v_{prop} = c$ and $v_{prop} < c$.

(3) The solutions of the above DEQ with $v_{prop} < c$ represent objects with a nonzero rest mass or own mass as follows:

$$m_{own} = \frac{E}{c^2} \cdot \sqrt{1 - \frac{v^2}{c^2}} \tag{7.31}$$

7.5 Superposition of QST

Two QST with the same velocity $\vec{v}_{prop}$ that is smaller than the velocity of light c travel together. Moreover, they interact via gravity, and so they exhibit a nonzero **binding energy** $E_{binding} \neq 0$. Hence they are bound without forming a black hole. In particular, their mass can be smaller than the Planck mass. Of course, two or more QST with the same velocity $\vec{v}_{prop} < c$ can propagate together, exhibit a nonzero binding energy and thus constitute an object. Hereby, each of these QST usually is an excitation of the vacuum, and so the superposition is an excitation of the vacuum.

Proposition 18 Binding of QST

Two or more QST with a nonzero own mass (see proposition 17) can combine by linear superposition. Thereby they can exhibit a binding energy, and hereby they can form a new object.

7.6 Formation of objects in $D \geq 3$ dimensions

An object can extend in $D \geq 3$ dimensions by various mechanisms. Two of these mechanisms are as follows:

(1) The object exhibits a polarization that extends in $D-1$ dimensions orthogonal to the direction of propagation. So an extension in D directions is achieved.

For instance, a gravitational wave in D dimensions exhibits one direction of propagation plus a $D-1$ dimensional polarization orthogonal to the propagation (see Figs. 5.3 or 5.5 and Eqs. 5.20 or 5.19). This is an example for case (1).

(2) The object is a linear superposition of D longitudinal QST and with different elementary modes of polarization, so that these modes extend in $D \geq 3$ dimensions altogether, see definition (6). When these QST combine, then they take a common velocity $\vec{v}_{prop} < c$, whereby a longitudinal oscillation remains simultaneously (see section 7.5). Hereby, each of these QST usually is an excitation of the vacuum, and so the object is an excitation of the vacuum. Such a formed object is especially simple, as it is based on elementary modes of polarization, and such objects with minimal energy are analyzed below.

Proposition 19 QST extending in D dimensions

QST can extend in $D \geq 3$ dimensions by one of the following mechanisms:

(1) A QST can extend in $D \geq 3$ dimensions by extending into the direction of propagation via its propagation and by extending into the orthogonal directions via a $D-1$ dimensional polarization.

(2) A QST can extend in $D \geq 3$ dimensions by binding sufficiently many QST with lower dimension, see proposition (18).

7.7 Formation of a fermion at $D = 3$

A fermion in $D = 3$ dimensions can form as a superposition of D longitudinal QST with the same velocity $\vec{v}_{prop} < c$ (see sections 7.5 and 7.6) and with different elementary modes of polarization, so that these modes extend in $D = 3$ dimensions altogether.

These D quanta can in principle rotate and form the same state, distinguished by a phase of the rotation only. These

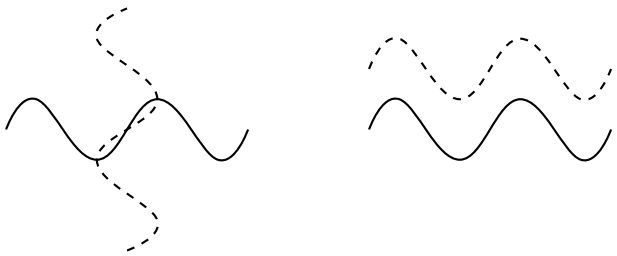

Figure 7.6: As the two quanta at the left have the same wavelength, they can easily form a Bose condensate and loose a dimension thereby, see at the right. Quanta with different wavelength or energy E_n cannot form a Bose condensate, and so an object formed by two quanta with different energy extends in two dimensional directions in a more stable manner.

quanta must be different, according to the Pauli exclusion principle, see e. g. Ballentine (1998). Thus, these D quanta must have different eigenvalues n of the number operator. Hereby, each of these QST usually is an excitation of the vacuum, and so the fermion is an excitation of the vacuum.

Proposition 20 QST forming a fermion

QST can form a fermion in $D = 3$ dimensions by the following mechanism:

(1) The QST can extend in $D = 3$ dimensions by binding sufficiently many QST with lower dimension, see proposition (18).

(2) Thereby the QST that bind should have different eigenvalues n of the number operator, according to the Pauli principle.

(3) Hereby the QST that bind can be excitation modes of the vacuum, see proposition (7.3.5).

7.8 Formation of a boson at $D = 3$

A boson in $D = 3$ dimensions can form as a superposition of D QST with the same velocity $\vec{v}_{prop} < c$ (see sections 7.5 and 7.6)

and with different elementary modes of polarization, so that these modes extend in $D = 3$ dimensions altogether.

These D quanta can in principle form a Bose condensate, see e. g. Klaers et al. (2010). In order to have a stable object extending in three dimensions, a Bose condensate should be avoided. This can be achieved by different QST. Accordingly, these D longitudinal QST should have different eigenvalues n of the number operator. Hereby, each of these QST usually is an excitation of the vacuum, and so the boson is an excitation of the vacuum.

Proposition 21 QST forming a relatively stable boson

QST can form a relatively stable boson in $D = 3$ dimensions by the following mechanism:

(1) The QST can extend in $D = 3$ dimensions by binding sufficiently many QST with lower dimension, see proposition (18).

(2) Thereby the QST that bind should have different eigenvalues n of the number operator, so that a destabilization of the boson by a Bose condensation is avoided.

(3) Hereby the QST that bind can be excitation modes of the vacuum, see proposition (7.3.5).

Chapter 8

Formation of Neutrinos and Ω_ν

In this section we analyze the formation of neutrinos by the **excitation of the vacuum** with the following properties:

(1) The excitation modes are simple longitudinal modes.

(2) The excitation modes extend in three dimensions by combining three modes.

(3) The excitation modes possibly include an operator $\hat{U}_{D=3\to D}$.

(4) Otherwise the excitation modes are at minimal energy.

8.1 Derivation of neutrinos from QST

In this part we construct the formation of neutrinos by QST that are obtained as excitation modes of the vacuum with minimal possible energy or mass.

8.1.1 Dimension of QST of neutrinos

First we determine the operator $\hat{U}_{D=3\to D}$. For it we apply the basic solution of the hierarchy problem, see theorem (6) and Fig. (7.1).

Typical masses of neutrinos are $m_1 = 0.0086\,\frac{eV}{c^2} = 1.5 \cdot 10^{-38}\,\text{kg}$ and $m_3 = 0.0506\,\frac{eV}{c^2} = 9 \cdot 10^{-38}\,\text{kg}$, see (Tanabashi et al., 2018, Eq. 14.13). The corresponding energies are $E_1 = 0.0086\,eV = 1.4 \cdot 10^{-21}\,\text{J}$ and $E_3 = 0.0506eV = 8.1 \cdot 10^{-21}\,\text{J}$.

These correspond to the dimension three of the energies of the ZPO of the vacuum, see theorem (6) and Fig. (7.1). Thus, the basic zero-point energy is as follows, see Eq. (7.15):

$$ZPE_{\Lambda,D=3} = E_{D_{hori}} \cdot \frac{3-1}{Z_{D_{hori}\to D} \cdot 300} = \frac{E_P}{2} \cdot \frac{2}{2^{(301-3)/3} \cdot 300} \quad (8.1)$$

$$\text{or} \quad ZPE_{\Lambda,D=3} = 8.1651 \cdot 10^{-24}\,\text{J} = 5.0968 \cdot 10^{-5}\,\text{eV} \quad (8.2)$$

Hereby we applied the following dimensional horizon:

$$D_{hori} = 301 \quad (8.3)$$

8.1.2 Polarization of the QST of neutrinos

The neutrinos are formed by three quanta of spacetime, QST, each with 1D-polarization, see proposition (20). So the factor $\frac{3-1}{300}$ that reduced the $ZPE_{\Lambda,D=3}$, see Eq. (8.1), is eliminated:

$$ZPE_{\nu,D=3} = ZPE_{\Lambda,D=3} \cdot \frac{300}{3-1} = 1.2248 \cdot 10^{-21}\,\text{J} = 0.0076452\,\text{eV} \quad (8.4)$$

8.1.3 Eigenvalues n of the number operator

In the present-day three dimensional space, the zero-point energy of the three dimensional space can exist. So the lowest possible eigenvalue is zero, $n = 0$. The corresponding energy of the QST is the above ZPE:

$$E_{\nu,D=3,n=0} = ZPE_{\nu,D=3} = 1.2248 \cdot 10^{-21}\,\text{J} \quad (8.5)$$

Hence the other two lowest possible eigenvalues are one and two, $n = 1$ and $n = 2$. The corresponding energies of the QST are as follows:

$$E_{\nu,D=3,n} = ZPE_{\nu,D=3} \cdot (2n+1) \;\text{ in particular,} \quad (8.6)$$

$$E_{\nu,D=3,n=1} = ZPE_{\nu,D=3} \cdot 3 = 3.6743 \cdot 10^{-21}\,\text{J} = 0.022936\,\text{eV} \quad (8.7)$$

$$E_{\nu,D=3,n=2} = ZPE_{\nu,D=3} \cdot 5 = 6.1238 \cdot 10^{-21}\,\text{J} = 0.038226\,\text{eV} \quad (8.8)$$

8.2 Derivation of Ω_ν

In this section we derive the density parameter of the neutrinos, Ω_ν. As we do not model the mixing here, we choose a very simple mixing: In principle, the eigenvalues $n = 0$, $n = 1$ and $n = 2$ can mix in various proportions. In principle, these can be in such a manner that one neutrino consists mostly of QST with $n = 0$, another neutrino consists mainly of QST with $n = 1$, while the third neutrino is predominantly constituted by QST with $n = 2$. In an idealized manner, we model three neutrinos:

$\nu_{n=0}$ formed by three QST with the eigenvalue $n = 0$,

$\nu_{n=1}$ formed by three QST with the eigenvalue $n = 1$ and

$\nu_{n=2}$ formed by three QST with the eigenvalue $n = 2$.

Accordingly, we derive the corresponding density parameters $\Omega_{\nu,n=0}$, $\Omega_{\nu,n=1}$ and $\Omega_{\nu,n=2}$ for the above neutrinos.

8.2.1 Derivation of $\Omega_{\nu,n=0}$

Thermal formation of RGWs: The neutrinos are formed from RGWs with $1D$ polarization. Accordingly, we derive the temperature at which these RGWs formed thermally, $T_{RGW,n=0,form}$. When these RGWs formed, then the neutrinos formed as well, so we obtain the same temperature for the formation of the neutrinos, $T_{RGW,n=0,form} = T_{\nu,n=0,form}$. As the RGW has one direction of polarization only, there is one degree of freedom only, and so the thermal energy $E_{\nu,n=0}$ or $E_{D=3,n=0}$ is as follows:

$$E_{\nu,n=0} = \frac{1}{2} \cdot k_B \cdot T_{\nu,n=0,form} \tag{8.9}$$

We solve for the temperature:

$$T_{\nu,n=0,form} = \frac{2E_{\nu,n=0}}{k_B} = 532.25\,\mathrm{K} \tag{8.10}$$

Comparison with CMB: For comparison, we derive the temperature at which the photons of the CMB formed thermally, $T_{CMB,form}$. It is equal to the current temperature of the CMB, $T_{CMB,t_0} = 2.7255\,\mathrm{K}$, multiplied by the factor $z_{CMB} + 1 = 1091$:

$$T_{CMB,form} = (z_{CMB} + 1) \cdot T_{CMB,t_0} = 2973.5\,\mathrm{K} \tag{8.11}$$

According to the Stefan-Boltzmann law, the ratio of the densities is proportional to the ratio of the temperatures to the power four:

$$\frac{\rho_{\nu,n=0,form}}{\rho_{CMB,form}} = \left(\frac{T_{\nu,n=0,form}}{T_{CMB,form}}\right)^4 \tag{8.12}$$

As a consequence of the definition of the density parameters, the ratio of the densities is equal to the ratio of the density parameters. So we derive:

$$\frac{\Omega_{\nu,n=0}}{\Omega_{CMB}} = \left(\frac{T_{\nu,n=0,form}}{T_{CMB,form}}\right)^4 \tag{8.13}$$

Consequently, the density parameter is as follows:

$$\Omega_{\nu,n=0} = \Omega_{CMB} \cdot \left(\frac{T_{\nu,n=0,form}}{T_{CMB,form}}\right)^4 \tag{8.14}$$

Density parameter: We apply the above Eq. and use the density parameter of the CMB:

$$\Omega_{CMB} = 5.4501 \cdot 10^{-5} \qquad \text{so we get :} \tag{8.15}$$

$$\Omega_{\nu,n=0} = 5.5949 \cdot 10^{-8} \tag{8.16}$$

8.2.2 Derivation of $\Omega_{\nu,n=1}$, $\Omega_{\nu,n=1}$ and Ω_ν

Similarly as above we derive $\Omega_{\nu,n=1}$:

$$\Omega_{\nu,n=1} = 4.5319 \cdot 10^{-6} \tag{8.17}$$

In the same manner as above we derive $\Omega_{\nu,n=2}$:

$$\Omega_{\nu,n=2} = 3.4968 \cdot 10^{-5} \tag{8.18}$$

The density parameter of the three types of neutrinos is the sum of the above parameters:

$$\Omega_\nu = \Sigma_{n=0}^{n=2}\Omega_{\nu,n} = 3.9556 \cdot 10^{-5} = \Omega_{\nu,theo} \tag{8.19}$$

8.3 Comparison with observation: Ω_ν

The density of the extra radiation species ρ_{ERS} is customarily included in the observed density parameter $\rho_{\nu,obs}$, see (Hinshaw et al., 2013, S. 4.3). For that purpose, an effective number N_{eff} of neutrino species is introduced, whereby the observed value is as follows, see (Tanabashi et al., 2018, Tab. 2.1):

$$N_{eff} = 3.13 \pm 0.32(\pm 9.7\%) \tag{8.20}$$

With it the following relation holds (see (Hinshaw et al., 2013, Eq. 14) or (Tanabashi et al., 2018, 25.1)):

$$\rho_{r,obs} = \rho_{\gamma,obs} + \rho_{\gamma,obs} \cdot \frac{7}{8} \cdot \left(\frac{4}{11}\right)^{4/3} \cdot N_{eff} = \rho_{\gamma,obs} + \rho_{\nu,obs} \tag{8.21}$$

Hereby, the observed density of photons $\rho_{\gamma,obs}$ is described by the density of the CMB ρ_{CMB}, in a very good approximation. In order to derive $\Omega_{\nu,obs}$, we divide the above Eq. (8.21) by the critical density ρ_{cr,t_0}, and we solve for $\Omega_{\nu,obs}$. So we derive:

$$\Omega_{\nu,obs} = \Omega_{CMB} \cdot \frac{7}{8} \cdot \left(\frac{4}{11}\right)^{4/3} \cdot N_{eff} \tag{8.22}$$

Using Eqs. (8.15) and (8.20), we derive:

$$\Omega_{\nu,obs} = 3.8742 \cdot 10^{-5}(\pm 9.7\%) \tag{8.23}$$

So the relative difference between theory and observation is:

$$\Delta_{theo-obs}\Omega_\nu = \frac{\Omega_{\nu,theo} - \Omega_{\nu,obs}}{\Omega_{\nu,obs}} = \pm 2.1\% \tag{8.24}$$

Theorem 7 Explanation of Ω_ν

(1) The density parameter Ω_ν of the primordial neutrinos is derived on the basis of the time evolution of the light horizon ranging from the Planck scale to the present-day light horizon and ranging from the Big Bang until today. The result is:

$$\boxed{\Omega_{\nu,theo} = 3.9556 \cdot 10^{-5}} \tag{8.25}$$

So the relative difference between observation and theory is:

$$\Delta_{theo-obs}\Omega_\nu = \frac{\Omega_{\nu,theo} - \Omega_{\nu,obs}}{\Omega_{\nu,obs}} = \pm 2.1\% \tag{8.26}$$

So our theoretical result is within the error of measurement of 9.7 % of the observation. Hence our result is in precise accordance with observation.

(2) Thereby the neutrinos are formed by a linear combination of three quanta of spacetime, QST.

These QST are **excitation modes of the vacuum** *with the following properties:*

(2.1) The excitation modes are simple longitudinal modes.

(2.2) The excitation modes extend in three dimensions by combining three modes.

(2.3) The excitation do not include an operator $\hat{U}_{D=3\to D}$.

(2.4) The excitation modes obey the conditions (2.1), (2.2) and (2.3), and with the remaining possibilities, the excitation modes minimize the energy.

Chapter 9

Formation of the Higgs Boson

In this section we analyze the formation of the Higgs boson by the **excitation of the vacuum** with the following properties:

(1) The excitation modes are simple longitudinal modes.

(2) The excitation modes extend in three dimensions by combining three modes.

(3) The excitation modes possibly include an operator $\hat{U}_{D=3\to D}$.

(4) A ZPO in $D > 3$ dimensions cannot exist in three dimensional space. Remind that the ZPO is the mode of lowest energy.

(5) Otherwise the excitation modes are at minimal energy.

Moreover, we describe how that model explains the formation of the quarks and of the electron, muon and tauon, including the corresponding antiparticles.

9.1 Derivation of the Higgs boson from QST

In this part we construct the formation of the Higgs boson by QST that are obtained as excitation modes of the vacuum with minimal possible energy or mass.

9.1.1 Dimension of QST of the Higgs boson

First we determine a possible operator $\hat{U}_{D=3\to D}$ or the dimension of the QST forming the Higgs boson. For it we apply the basic solution of the hierarchy problem, see theorem (6) and Fig. (7.1).

The observed energy of the Higgs boson is as follows, see e. g. Tanabashi et al. (2018):

$$E_H = 125.18\,\text{GeV} = 2.0054 \cdot 10^{-8}\,\text{J} \tag{9.1}$$

In order to apply property (3), see above, we realize the following: The zero-point energy $ZPE_{\Lambda,D}$, that is directly below that energy $E_H = 125.18\,\text{GeV}$, is $ZPE_{\Lambda,D=5}$, see theorem (6) and Fig. (7.1).

So the three QST of the Higgs boson have dimension five. The ZPO at dimension four with $ZPE_{\Lambda,D=4}$ are hardly stable, see Fig. (3.7), and correspondingly they are not essential in the most stable elementary particles. Accordingly, the $ZPE_{\Lambda,D=3}$ are essential for elementary particles, namely for neutrinos, and the $ZPE_{\Lambda,D=5}$ are essential for elementary particles, namely for the Higgs boson.

Corresponding to the identified dimension five, we also apply the polarization factor $\frac{5-1}{D_{hori}-1}$ or $\frac{4}{300}$. Thus, the basic zero-point energy is as follows, see Eq. (7.15):

$$ZPE_{\Lambda,D=5} = E_{D_{hori}} \cdot \frac{5-1}{Z_{D_{hori}\to D=5} \cdot 300} = \frac{E_P}{2} \cdot \frac{4}{2^{(301-5)/5} \cdot 300} \tag{9.2}$$

Hence the $ZPE_{\Lambda,D}$ underlying the Higgs boson is as follows (see Fig. 9.1):

$$ZPE_{\Lambda,D=5} = 1.9693 \cdot 10^{-11}\,\text{J} \tag{9.3}$$

Hereby we applied the following dimensional horizon:

$$D_{hori} = 301 \tag{9.4}$$

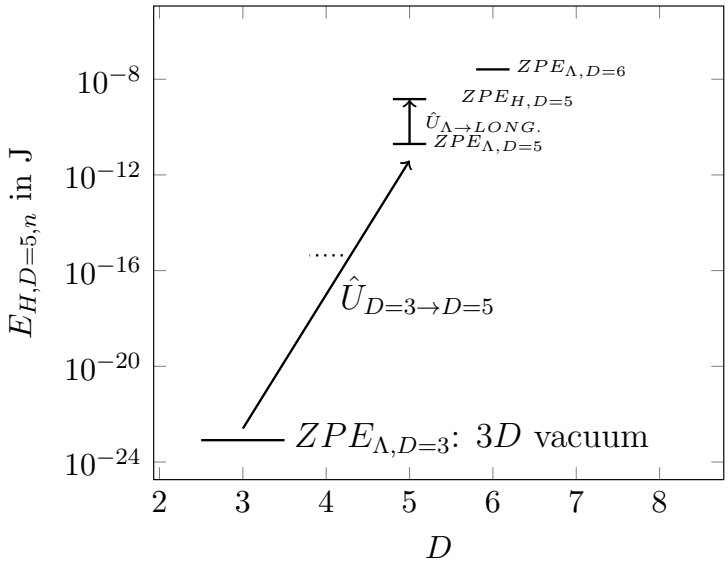

Figure 9.1: Excitation of a QST $ZPE_{\Lambda,D=3}$ of the present-day $3D$ vacuum by a transition $\hat{U}_{D=3\to D=5}$ to a QST $ZPE_{\Lambda,D=5}$, followed by a polarizing excitation $\hat{U}_{\Lambda\to 1D}$.

9.1.2 Polarization of the QST of the Higgs boson

The Higgs boson is formed by three quanta of spacetime, QST, each with longitudinal polarization, see proposition (21) and Fig. (9.1). So the factor $\frac{5-1}{300}$ that reduced the $ZPE_{\Lambda,D=5}$, see Eq. (9.2), is eliminated:

$$ZPE_{H,D=5} = ZPE_{\Lambda,D=5} \cdot \frac{300}{5-1} = 1.477 \cdot 10^{-9}\,\mathrm{J} \tag{9.5}$$

9.1.3 Eigenvalues n of QST of the Higgs boson

In the present-day three dimensional space, the zero-point energy of the five dimensional space cannot exist, see property (4). So the lowest possible eigenvalue is one, $n = 1$. Hence the lowest three possible eigenvalues are one, two and three, $n = 1$, $n = 2$ and $n = 3$, see property (5) and Fig. (9.2). The corresponding energies of the QST are as follows:

$$E_{H,D=5,n} = ZPE_{H,D=5} \cdot (2n + 1) \tag{9.6}$$

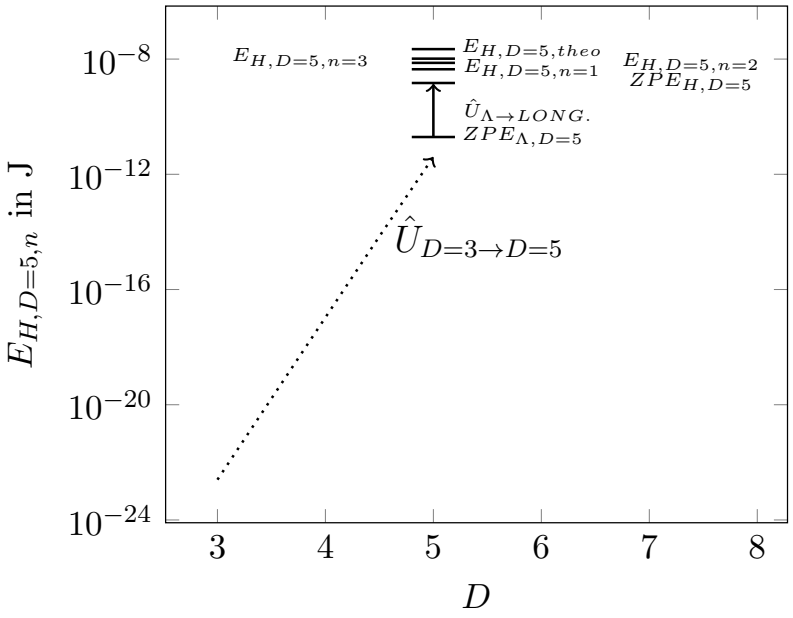

Figure 9.2: Excitation of a QST $ZPE_{\Lambda,D=3}$ of the present-day $3D$ vacuum by a transition $\hat{U}_{D=3\to D=5}$ to a QST $ZPE_{\Lambda,D=5}$, followed by a polarizing excitation $\hat{U}_{\Lambda\to LONG.}$ and by excitation by $\hat{a}^+$.

In particular we derive the energies of the QST that form the Higgs boson, see Fig. :

$$E_{H,D=5,n=1} = ZPE_{H,D=5} \cdot 3 = 4.431 \cdot 10^{-9}\,\text{J} = 27.66\,\text{GeV} \quad (9.7)$$

$$E_{H,D=5,n=2} = ZPE_{H,D=5} \cdot 5 = 7.385 \cdot 10^{-9}\,\text{J} = 46.099\,\text{GeV} \quad (9.8)$$

$$E_{H,D=5,n=3} = ZPE_{H,D=5} \cdot 7 = 10.339 \cdot 10^{-9}\,\text{J} = 64.539\,\text{GeV} \quad (9.9)$$

The energy of the combined particle is the sum:

$$E_{H,D=5,n=1,2,3} = ZPE_{H,D=5} \cdot 15 = 138.298\,\text{GeV} = E_{H,theo} \quad (9.10)$$

9.2 Comparison with observation: m_{Higgs}

The observed energy $E_{Higgs} = m_{Higgs} \cdot c^2$ of the Higgs boson is as follows, see e. g. Tanabashi et al. (2018):

$$E_{H,obs} = 125.18\,\text{GeV} \tag{9.11}$$

So the relative difference between theory and observation is as follows, see Fig. (9.3):

$$\Delta_{theo-obs}\Omega_H = \frac{E_{H,theo} - E_{H,obs}}{E_{H,obs}} = \pm 10.5\% \tag{9.12}$$

Discussion of the binding energy: In general, there is a binding energy that binds the three QST forming the Higgs boson. So the theoretical energy value $E_{H,D=5,theo} = 138.3\,\text{GeV} = m_{H,theo} \cdot c^2$ of the Higgs boson is expected to decrease.

So far, we modeled the gravitational interaction only. The corresponding gravitational binding energy is negligible. However, modeling electromagnetic, weak and strong interactions might decrease the above value appropriately.

9.3 Masses caused by $m_{H,theo}$

In the above section, we derived the mass and energy of the Higgs boson:

$$m_{H,theo} = \frac{E_{H,D=5,theo}}{c^2} = 138.3\,\frac{\text{GeV}}{\text{c}^2} \tag{9.13}$$

That mass causes the masses of the $W^{+,0,-}$ boson, of the quarks, and of the electron, muon and tauon, see e. g. (Tanabashi et al., 2018, p. 181, 182). In this section we elaborate, how the mass $m_{H,D=5,theo}$ causes the above masses. For it we derive the Higgs field that is caused by $m_{H,D=5,theo}$, see e. g. (Tanabashi et al., 2018, p. 181, 182).

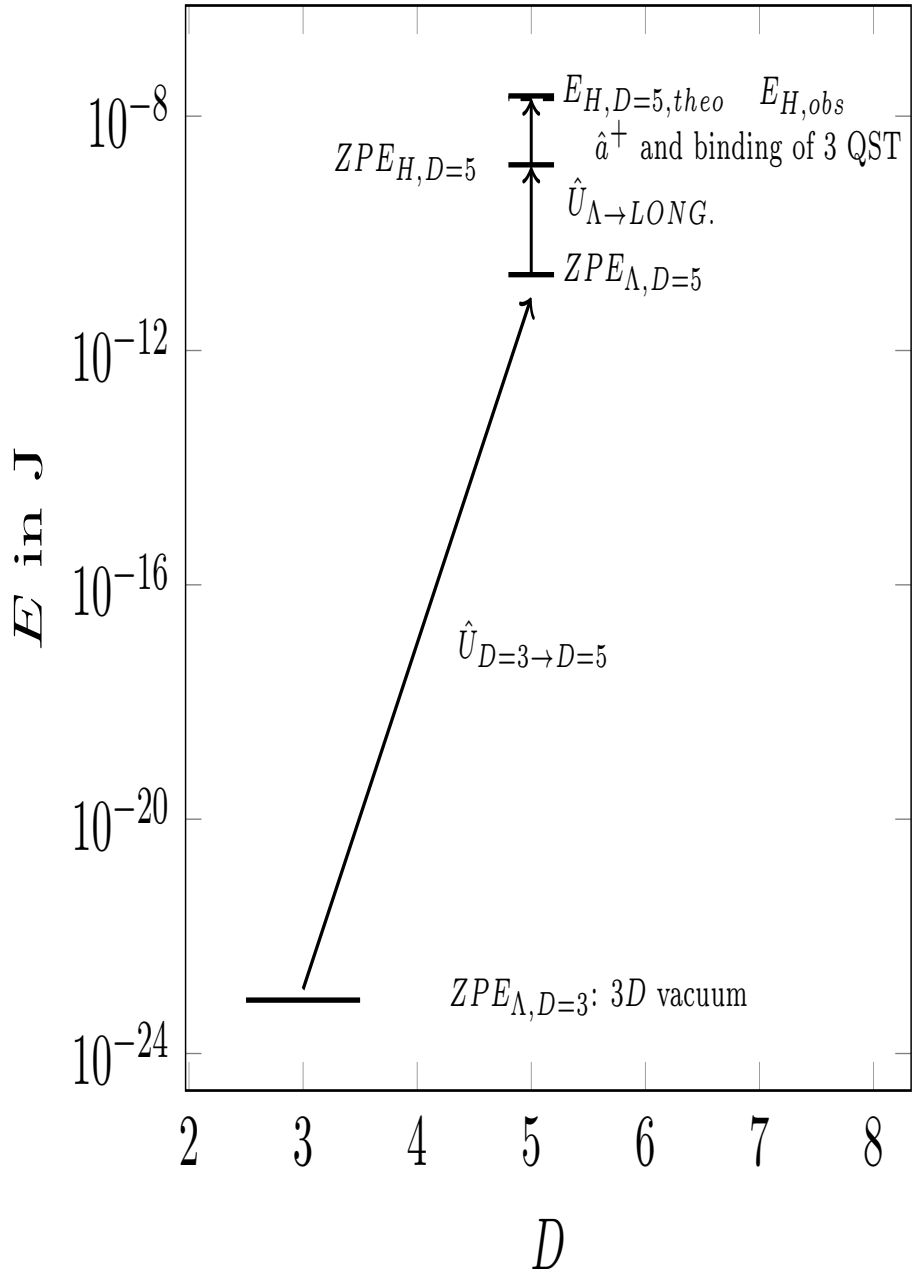

Figure 9.3: Higgs boson: formation by excitation of the vacuum, theoretical energy $E_{H,D=5,theo}$, observed energy $E_{H,D=5,obs}$ (dashed). The remaining small energy difference is interpreted as interaction energy that is set free during the process of binding the three quanta of spacetime, QST, that form the Higgs boson.

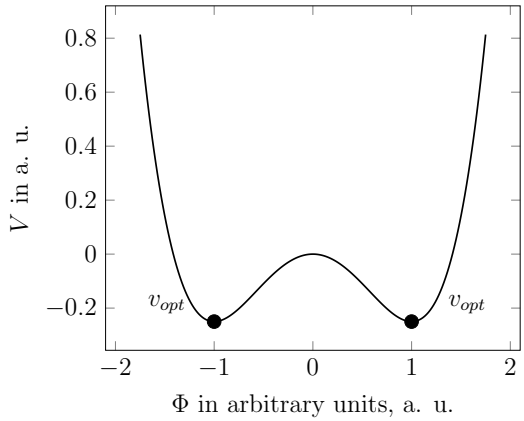

Figure 9.4: Standard model potential V of the Higgs field Φ: At low energy, the optimal expectation value v_{opt} is achieved.

9.3.1 Higgs field

The Higgs boson constitutes the **Higgs field** Φ, a two dimensional complex field, see (Tanabashi et al., 2018, p. 181):

$$\Phi = \frac{1}{\sqrt{2}} \cdot \begin{pmatrix} \sqrt{2}\Phi^+ \\ \Phi^0 + i \cdot a^0 \end{pmatrix} \tag{9.14}$$

In particular, the vacuum expectation value

$$\langle \Phi \rangle = \frac{1}{\sqrt{2}} \cdot \begin{pmatrix} 0 \\ v \end{pmatrix} \tag{9.15}$$

is characterized by the so-called **expectation value** v.

Self-interaction: The Higgs field interacts with itself, and this is modeled by a usual Φ^2-Φ^4 potential, see e. g. Landau and Lifschitz (1979b). That potential is called **standard model potential**, see e. g. (Tanabashi et al., 2018, p. 181):

$$V(\Phi) = m^2 \cdot \Phi^2 + \lambda \cdot \Phi^4 \tag{9.16}$$

Hereby m is named **mass parameter**, and λ is a **limiting interaction parameter** of the Higgs field.

Phase transition: If square m^2 is negative, then there can occur a symmetry breaking phase transition at low energy. In particular, at minimal potential, we derive the following Higgs field:

$$\Phi_{opt} = \frac{1}{\sqrt{2}} \cdot \sqrt{\frac{|m^2|}{\lambda}} \tag{9.17}$$

In the limit of very low energy, that optimal field Φ_{opt} is equal to the expectation value in Eq. (9.15), and so we derive the optimal expectation value, see Fig. (9.4):

$$v_{opt} = \sqrt{\frac{|m^2|}{\lambda}} \tag{9.18}$$

Parameters: Hereby the interaction parameter λ is not determined in the standard model of elementary particles. Whereas the optimal expectation value v_{opt} can be obtained from muon decay measurements:

$$v_{opt,obs} = 246.221\,\text{GeV} \tag{9.19}$$

Mass m_H: In the standard model of elementary particles, the mass m_H of the Higgs boson is determined as follows, see e. g. (Tanabashi et al., 2018, p. 182):

$$m_H = \sqrt{2\lambda} \cdot v_{opt}/c^2 \tag{9.20}$$

So the mass m_H determines the field limiting interaction parameter λ of the Higgs field:

$$\lambda = \frac{m_H^2 \cdot c^4}{2 \cdot v_{opt}^2} = \frac{E_H^2}{2 \cdot v_{opt}^2} \tag{9.21}$$

For the case of our theoretical value $m_{H,theo}$ we derive:

$$\lambda_{theo} = \frac{m_{H,theo}^2 \cdot c^4}{2 \cdot v_{opt}^2} = \frac{E_H^2}{2 \cdot v_{opt}^2} = 0.1577 \tag{9.22}$$

And with that parameter λ_{theo}, the mass $m_{H,theo}$ determines the optimal field:

$$v_{opt} = m_{H,theo} \cdot c^2 / \sqrt{2\lambda_{theo}} \tag{9.23}$$

The Higgs field causes several masses of essential elementary particles via specific interaction parameters. Examples are the $W^{+,0,-}$ bosons, , see e. g. Tanabashi et al. (2018).

9.3.2 Boson masses caused by $m_{H,theo}$

In this section, we derive the boson masses caused by $m_{H,theo}$.

Masses m_W: The mass m_W of the $W^{+,-}$ boson is related to the gauge coupling of the weak interaction g_w as follows, see e. g. (Tanabashi et al., 2018, p. 182), (Kobel et al., 2017, p. 69):

$$m_W \cdot c^2 = \frac{g_w \cdot v_{opt}}{2} \tag{9.24}$$

We insert v_{opt}, see Eq. (9.23):

$$m_W = m_{H,theo} \cdot \frac{g_w}{\sqrt{8\lambda_{theo}}} \tag{9.25}$$

So the measurement of $m_W \cdot c^2 = 80.38\,\mathrm{GeV}$ provides the coupling:

$$g_w = \frac{m_W}{m_{H,theo}} \cdot \sqrt{8\lambda_{theo}} = 0.6528 \tag{9.26}$$

Mass m_Z: Similarly, the mass $m_Z = 91.1876\,\frac{\mathrm{GeV}}{\mathrm{c}^2}$, see (Tanabashi et al., 2018, p. 33), of the Z or W^0 boson is related to the gauge coupling of the weak interaction g'_w as follows, see e. g. (Tanabashi et al., 2018, p. 182), (Kobel et al., 2017, p. 69):

$$\frac{m_W^2}{m_Z^2} = \frac{g_w^2}{g_w^2 + g_w'^2} \tag{9.27}$$

We solve for the coupling g'_w:

$$g'_w = g_w \cdot \sqrt{1 - \frac{m_Z^2}{m_W^2}} = 0.3083 \tag{9.28}$$

9.3.3 Fermion masses caused by $m_{H,theo}$

In this section, we derive the fermion masses caused by $m_{H,theo}$.

The mass of a fermion m_{f_i} is related to the Higgs field v_{opt} via the specific **Higgs-fermion interaction** h_{f_i} as follows, see e. g. (Tanabashi et al., 2018, p. 182):

$$m_{f_i} \cdot c^2 = \frac{h_{f_i} \cdot v_{opt}}{\sqrt{2}} \tag{9.29}$$

We insert v_{opt}, see Eq. (9.23):

$$m_{f_i,theo} = m_{H,theo} \cdot \frac{h_{f_i}}{2\sqrt{\lambda_{theo}}} \tag{9.30}$$

In this manner the mass $m_{H,theo}$ causes the masses of the electron, muon and tauon as well as of the quarks. The additional parameters h_{f_i} have been introduced by the standard model of elementary particles, however, these parameters have not yet been explained by that standard model, see e. g. (Tanabashi et al., 2018, p. 182).

Theorem 8 Formation of the Higgs boson

(1) The mass $m_{H,theo}$ of the Higgs boson is precisely derived on the basis of the time evolution of the light horizon ranging from the Planck scale to the present-day light horizon and ranging from the Big Bang until today. The result is:

$$m_{H,theo} = \frac{E_{H,D=5,theo}}{c^2} = 138.3 \, \frac{\text{GeV}}{\text{c}^2} \tag{9.31}$$

(2) Thereby the Higgs boson is formed by a linear combination of three quanta of spacetime, QST.

These QST are **excitation modes of the vacuum** *with the following properties:*

(2a) The excitation modes are simple longitudinal modes.

(2b) The excitation modes extend in three dimensions by combining three modes.

(2c) The excitation modes include the operator $\hat{U}_{D=3\to D=5}$. So a ZPO in $D = 5$ is formed.

(2d) That ZPO in $D = 5$ cannot exist in three dimensional space, so the excitation modes with $n = 1$, $n = 2$ and $n = 3$ are formed at minimal energy.

(3) The Higgs boson represents the Higgs field, and this field causes the masses of the $W^{+,0,-}$ bosons and of the quarks, electrons, muons and tauons, including the corresponding antiparticles.

Corollary 4 Formation of all non-gluon light particles

The QST explain the formation of all non-gluon light particles as follows:

(1) According to the basic solution of the hierarchy problem, the lightest particles have ZPOs in $3D$.

(1a) Especially light particles are the particles of the dark energy, as these reduced their energy during the era of cosmic unfolding by the redshift and by polarization.

(1b) The neutrinos are slightly heavier according to their polarization.

(2) According to the basic solution of the hierarchy problem, the second lightest and stable particles have ZPOs in $5D$. They form the Higgs boson.

(2a) The Higgs boson causes the masses of the $W^{+,0,-}$ bosons.

(2b) The Higgs boson causes the masses of the remaining leptons, the electron, muon and tauon.

(2c) The Higgs boson causes the masses of the quarks.

(3) Altogether, all elementary non-gluon particles of the standard model of elementary particles are formed by the QST.

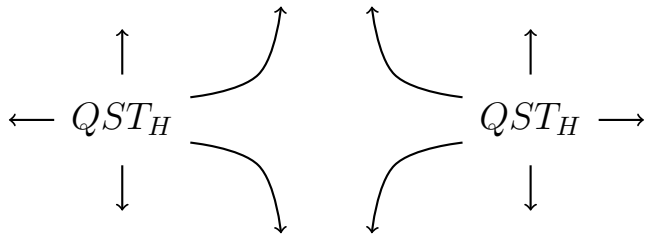

Figure 9.5: If two interacting QST_H are sources of QST_{eff}, then these QST_{eff} flow outwards and thus cause a repulsive interaction.

(4) Additionally, the particles of the dark energy are relatively light and formed by the QST.

(5) The mass of a particle that is based on a black hole amounts to one half of a Planck mass or more.

(5a) Candidates are primordial black holes, see e. g. Carmesin (2020b).

(5b) Candidates are also the particles of cold dark matter, see Carmesin (2018h), Carmesin (2018f) or Carmesin (2019d).

However, these have not yet been observed in a very detailed manner, see e. g. Tanabashi et al. (2018).

9.4 Effective interaction

We propose a model of an effective energy of interaction E_{eff} of the three QST of the Higgs boson, QST_H.

Formation of quanta: The three QST_H emit new quanta of spacetime, according to the DEQ of the QST, see (Carmesin, 2021c, Eq. 2.52):

$$\dot{\varepsilon}^2 = \frac{G^{*2}}{c^2} \tag{9.32}$$

These new QST form an energy of effective interaction, and so we name them QST_{eff}.

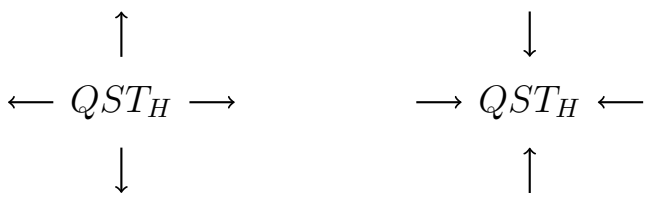

Figure 9.6: If two interacting QST_H are one source and one drain of QST_{eff}, then these QST_{eff} flow from one QST_H to the other QST_H in a dipole manner. So quanta QST_{eff} approach QST_H. Hence an attractive interaction is caused.

Source and drain of quanta: As the rate $\dot{\varepsilon}$ is squared in the above Eq., the quanta can form or vanish, so a QST_H can be a source of QST_{eff}, or a QST_H can be a drain of QST_{eff}. There are three essential cases:

(1) If two interacting QST_H are both sources, then the generated QST_{eff} flow to the sides as shown in Fig. (9.5). Thus, there occurs a repulsive momentum transfer upon the two partial flow systems including the sources.

(2) If two interacting QST_H are drains, then the QST_{eff} flowing inwards can be described by anti-QST, $Q\bar{S}T_{eff}$ flowing outwards, hence there occurs a repulsive interaction as in case (1).

(3) If one interacting QST_H is a drain, while the other is a source, then the QST_{eff} and the drain approach each other, see Fig. (9.6). Similarly the $Q\bar{S}T_{eff}$ and the source approach each other. So an attractive interaction is generated.

Low energy case: As the energy is minimized here, the third case takes place. Additionally, as the Higgs boson exhibits no net interaction except gravity, the energies of QST_{eff} flowing inward and of QST_{eff} flowing outward add up to zero.

ZPE: The energy of the QST_{eff} generated by a QST_H with energy E_H is equal to one forth of the energy E_H, see (Carmesin, 2021c, PROP. 6). In particular, the zero-point energy ZPE_{eff}

of a QST_{eff} is one fourth of the zero-point energy $ZPE_{H,D=5}$ of the QST_H (Eq. 9.5):

$$ZPE_{eff} = \frac{1}{4} \cdot ZPE_{H,D=5} = 9.2197\,\text{GeV} = \frac{1}{4} \cdot \hbar\omega_H \qquad (9.33)$$

Effective energies: In this paragraph we formulate an effective energy term. For it we proceed in two steps:

(A) We use the excitation energies of the QST_H, see Eq. (9.6):

$$\Delta E_{H,D=5,n} = E_{H,D=5,n} - ZPE_{H,D=5} = ZPE_{H,D=5} \cdot 2n \quad (9.34)$$

These generate QST_{eff} that have one fourth of that energy:

$$E_{eff,n} = ZPE_{eff} \cdot 2n \qquad (9.35)$$

(B) The QST_{eff} of two QST_H cause the respective interaction energy, we model a corresponding effective interaction energy by using the geometric average:

$$E_{eff,n_i,n_j} = \sqrt{2n_i \cdot 2n_j} \cdot ZPE_{eff} \qquad (9.36)$$

The minimal energy of interaction is achieved, when the QST_H with $n = 3$ is a drain and the other two are sources or vice versa. So we derive the following effective interaction energies:

$$E_{eff,1,2} = \sqrt{2 \cdot 4} \cdot ZPE_{eff} = 6.5194\,\text{GeV} \qquad (9.37)$$

$$E_{eff,1,3} = -\sqrt{2 \cdot 6} \cdot ZPE_{eff} = -7.9847\,\text{GeV} \qquad (9.38)$$

$$E_{eff,2,3} = -\sqrt{4 \cdot 6} \cdot ZPE_{eff} = -11.292\,\text{GeV} \qquad (9.39)$$

Altogether, the effective energy of interaction is the sum:

$$E_{eff} = E_{eff,1,2} + E_{eff,1,3} + E_{eff,2,3} = -12.757\,\text{GeV} \qquad (9.40)$$

The full theoretical energy $E_{H,full,theo}$ is the sum of the energy $E_{H,without} = 138.296\,\text{GeV}$ of the Higgs boson without interaction and the above effective energy of interaction:

$$\boxed{E_{H,full,theo} = E_{H,without} + E_{eff} = 125.541\,\text{GeV}} \qquad (9.41)$$

Comparison with observation: The Higgs boson has been observed by various methods and the results are in the following interval $I_{H,obs}$, see (Tanabashi et al., 2018, Fig. 11.4):

$$E_{H,obs} \in [124.51 \pm 0.52\,\text{GeV}; 126.02 \pm 0.51\,\text{GeV}] = I_{H,obs} \quad (9.42)$$

Moreover, an average has been obtained for observed values as follows, see (Tanabashi et al., 2018, p. 34):

$$E_{H,obs} = 125.18\,\text{GeV} \pm 0.16\,\text{GeV}\ (0.13\%) \quad (9.43)$$

The full theoretical value is within the observed interval. Using Eqs. (9.43) and (9.42), we express the observed mass as follows:

$$E_{H,obs} = 125.18\,\text{GeV} \pm 1.35\,\text{GeV}\ (1.1\%) \quad (9.44)$$

So our result is in precise accordance with observation.

Theorem 9 Effective interaction

(1) The QST provide an effective interaction that can be attractive as well as repulsive.

(2) That effective interaction provides an appropriate energy so that the theoretical energy of the Higgs boson is within the observed interval:

$$\boxed{E_{H,full,theo} = 125.541\,\text{GeV} \in [124.51; 126.02]\,\text{GeV} = I_{H,obs}} \quad (9.45)$$

(3) The relative difference between theory and observation is below 0.29 %.

Interpretation: This effective interaction shows that the QST are capable of forming interactions with different signs such as electromagnetic, weak and strong interactions. Moreover, that effective interaction is in accordance with the Gaussian theorem. That effective might be generalized to interactions with more kinds of charges or different symmetry, such as weak and strong interactions. However, this is beyond the scope of this book. That theory is expected to be presented in a forthcoming volume of this book series.

Chapter 10

Derivation of Ω_Λ

So far we used models of an ideal universe: Firstly, for the case of a homogeneous universe, we derived $\Omega_\Lambda = \frac{2}{3}$, see (Carmesin, 2021c, THM. 21(3)). Secondly, we analyzed the case of a monochromatic vacuum in chapter (6).

In this chapter, we apply quantum physics and GRT in order to derive the formation of the polychromatic vacuum, and to determine Ω_Λ, in particular.

First we show that the present-day vacuum is polychromatic. Then we analyze that polychromatic vacuum. In particular, we derive an algorithm for the calculation of Ω_Λ. Using that algorithm we calculate Ω_Λ. Thereby we do not execute any fit, of course. Moreover, we critically discuss the used physics and the applied algorithm.

10.1 Polychromatic vacuum: derivation

In this section we derive the fact that the dark energy consists of quanta with different energies.

A quantum of the dark energy that forms at the present time t_0 has an energy that depends on the dimensional horizon of the present time t_0, see theorem (5):

$$E_\Lambda(D = 3, t_0) = \text{function}(D_{hori}(t_0)) \tag{10.1}$$

As the present time is not special in physics, the same holds for any time t_{form} at which a quantum of dark energy forms:

$$E_\Lambda(D=3,t_{form}) = \text{function}(D_{hori}(t_{form})) \tag{10.2}$$

In order to derive that function from Eqs. (6.12) and (6.13), we substitute t_0 by t_{form}:

$$\boxed{E_\Lambda(D=3,t_{form}) = \frac{2\cdot E_{D_{hori}(t_{form})}}{Z_{D_{hori}(t_{form})\to 3}\cdot (D_{hori}(t_{form})-1)}} \tag{10.3}$$

$$\text{with}\quad Z_{D_{hori}(t_{form})\to 3} = 2^{(D_{hori}(t_{form})-3)/3} \tag{10.4}$$

As a consequence, the density ρ_Λ that forms at a time t_{form} is a function of the dimensional horizon $D_{hori}(t_{form})$ of that time t_{form}:

$$\rho_\Lambda(t_{form}) = \text{function}'(D_{hori}(t_{form})) \tag{10.5}$$

In order to derive that function from Eq. (6.14), we substitute t_0 by t_{form}:

$$\boxed{\rho_\Lambda(t_{form}) = \frac{2E_{D_{hori}(t_{form})}}{V_{D=3}\cdot (D_{hori}(t_{form})-1)\cdot c^2\cdot L_P^3\cdot Z^4_{D_{hori}(t_{form})\to 3}}} \tag{10.6}$$

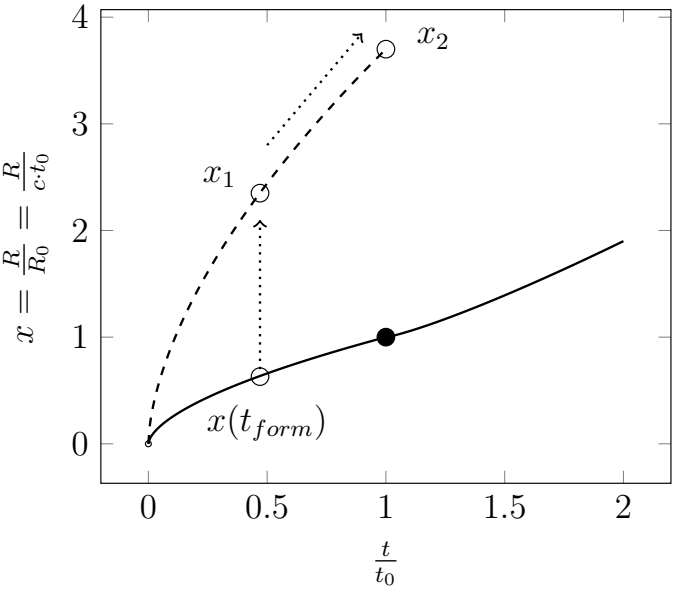

Figure 10.1: Scale factor $x = \frac{R}{R_0}$ as a function of $\frac{t}{t_0}$, calculated backwards from t_0 as usual (solid line).
t_{form}: considered time of formation of an amount of vacuum.
$x(t_{form})$: scale factor corresponding to t_{form}, it is the light horizon present at t_{form}.
x_1: scaled light horizon corresponding to t_{form},
$x_2 = x_1 \cdot k_{t_{form} \to t_0}$: evolved value of x_1,
for details see Eqs. (10.7) until (10.12),
arrows: steps of the calculation.

10.2 Polychromatic vacuum: analysis

In this section we present the method and results of the analysis of the polychromatic vacuum.

10.2.1 Derivation of $D_{hori}(t_{form})$

A key quantity is the dimensional horizon corresponding to a time of the formation of a quantum of dark energy $D_{hori}(t_{form})$, see Eqs. (10.4), (10.3) and (10.6). In this section, we derive that key quantity.

Dimensional distance enlargement factor: First we derive the dimensional distance enlargement factor, from which $D_{hori}(t_{form})$ can be directly derived, see Eq. (10.4). That factor is determined by the following Eq., see (Carmesin, 2019d, Eq. 2.217):

$$\boxed{Z_{D_{hori}(t_{form})\to D=3} = \frac{R_{lh}(t_{form}) \cdot k_{t_{form}\to t_0}}{R_{lh}(t_0)} \cdot Z_{D_{hori}(t_0)\to D=3}} \tag{10.7}$$

Hereby, the present-day light horizon $R_{lh}(t_0)$ and the present-day dimensional distance enlargement factor $Z_{D_{hori}(t_0)\to D=3}$ have been derived in chapter (3).

Scaled version of Eq. (10.7): In order to focus on the key structure of Eq. (10.7), we scale that Eq. For it we expand by $R_0 = c \cdot t_0$. Moreover we abbreviate, see Fig. (10.1):

$$x_0 = \frac{R_{lh}(t_0)}{R_0} \tag{10.8}$$

$$x_1 = \frac{R_{lh}(t_{form})}{R_0} \tag{10.9}$$

$$x_2 = x_1 \cdot k_{t_{form}\to t_0} \tag{10.10}$$

So we get:

$$Z_{D_{hori}(t_{form})\to D=3} = \frac{x_1 \cdot k_{t_{form}\to t_0}}{x_0} \cdot Z_{D_{hori}(t_0)\to D=3} \quad \text{or} \tag{10.11}$$

$$Z_{D_{hori}(t_{form})\to D=3} = \frac{x_2}{x_0} \cdot Z_{D_{hori}(t_0)\to D=3} \tag{10.12}$$

Derivation of x_1: First we derive the light horizon $R_{lh}(t_{form})$ corresponding to the time t_{form}, see e. g. Carmesin (2019d):

$$\begin{aligned} R_{lh}(t_{form}) &= c \cdot t_{form} \cdot \eta(t_{form}) \quad \text{with} \\ \eta(t_{form}) &= \int_0^{x_{t_{form}}} \frac{dx}{\sqrt{\Omega_r + \Omega_M \cdot x + \Omega_\Lambda \cdot x^4}} \end{aligned} \tag{10.13}$$

Thereby $x_{t_{form}}$ can be calculated from the time t_{form}, see e. g. Carmesin (2019d):

$$I(x_{t_{form}}) = \int_0^{x_{t_{form}}} \frac{x \cdot dx}{\sqrt{\Omega_r + \Omega_M \cdot x + \Omega_\Lambda \cdot x^4}} = \frac{t_{form}}{t_{H_0}} \quad (10.14)$$

Hereby the inverse function I^{-1} of the above integral is used:

$$x_{t_{form}} = I^{-1}\left(\frac{t_{form}}{t_{H_0}}\right) \quad (10.15)$$

Derivation of x_2: The time evolution according to the FLE is as follows, see e. g. Carmesin (2019d):

$$J(x_2) = \int_{x_1}^{x_2} \frac{x \cdot dx}{\sqrt{\Omega_r + \Omega_M \cdot x + \Omega_\Lambda \cdot x^4}} = \frac{t_0 - t_{form}}{t_{H_0}} \quad (10.16)$$

Hereby the inverse function J^{-1} of the above integral is used:

$$x_2 = J^{-1}\left(\frac{t_0 - t_{form}}{t_{H_0}}\right) \quad (10.17)$$

10.3 Fixed point procedure

Similarly as for the case of Ω_γ, we apply a fixed point algorithm.

For it we introduce a **fixed point function** that maps a hypothetical value of the density parameter $\Omega_{\Lambda,hypo}$ to a test value $\Omega_{\Lambda,test}$, according to the laws of quantum gravity:

$$\boxed{\Omega_{\Lambda,test} = \Omega_{\Lambda,test}(\Omega_{\Lambda,hypo})} \quad (10.18)$$

That value $\Omega_{\Lambda,test}$ is determined as follows: We use $\Omega_{\Lambda,hypo}$ together with the other density parameters (these are provided in this chapter, see the introduction), in order to solve the above integrals in this chapter. Using these, we derive for each time of formation t_{form} the corresponding dimensional horizon $D_{hori}(t_{form})$. With it we derive the respective density $\rho_\Lambda(t_{form})$, see Eq. (10.6).

For each time of formation t_{form} ranging from the first formation of three dimensional space at a time $t_{D=3}$ to the present-day time, we derive the amount of vacuum $\Delta V(t_{form})$ formed according to the FLE, and we evaluate the average of the densities $\rho_\Lambda(t_{form})$ each weighted by $\Delta V(t_{form})$. So we obtain the averaged density:

$$\langle \rho_\Lambda \rangle = \frac{\int_{t_{D=3}}^{t_0} \Delta V(t_{form}) \rho_\Lambda(t_{form}) dt_{form}}{\int_{t_{D=3}}^{t_0} \Delta V(t_{form}) dt_{form}} \tag{10.19}$$

With it we obtain the density parameter:

$$\Omega_{\Lambda,test} = \frac{\langle \rho_\Lambda \rangle}{\rho_{cr.,t_0}} \tag{10.20}$$

10.4 Fixed point $\Omega_{\Lambda,fixed\,point}$

By using the above fixed point function, we determine the fixed point as a solution of the following fixed point equation:

$$\boxed{\Omega_{\Lambda,test} = \Omega_{\Lambda,test}(\Omega_{\Lambda,hypo}) = \Omega_{\Lambda,hypo} = \Omega_{\Lambda,fixed\,point}} \tag{10.21}$$

The fixed point provides the density parameter according to the laws of quantum gravity:

$$\Omega_{\Lambda,test} = \Omega_{\Lambda,test}(\Omega_{\Lambda,hypo}) = \Omega_{\Lambda,hypo} = \Omega_{\Lambda,fixed\,point} \tag{10.22}$$

The graph of the fixed point function is illustrated in Fig. (10.2). Moreover, that Fig. shows the graph of the function that represents the identity. So the intersection of both graphs represents the solution of the fixed point equation:

$$\Omega_{\Lambda,fixed\,point} = 0.6834 \tag{10.23}$$

So the relative difference of theoretical and observed value, $\Omega_{\Lambda,obs} = 0.6847$, see table (15.2), is as follows:

$$\Delta_{theo-obs}\Omega_\Lambda = \frac{\Omega_{\Lambda,fixed\,point} - \Omega_{\Lambda,obs}}{\Omega_{\Lambda,obs}} = \pm 0.19\% \tag{10.24}$$

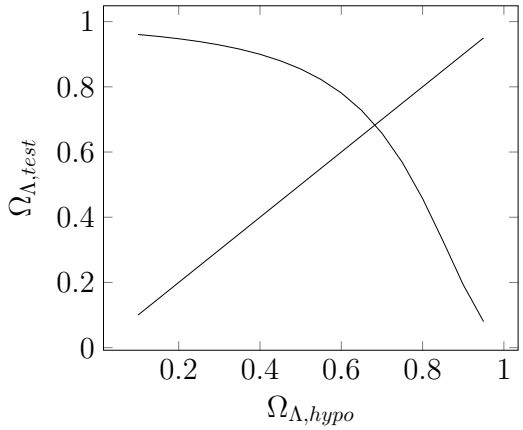

Figure 10.2: Fixed point Ω_Λ (Eq. 4.18). The intersection with the diagonal is the fixed point: $\Omega_\Lambda = 0.6834$, deviating from the observed value by 0.19 % only, see Collaboration (2020a). We obtained that value without executing any fit.

For the case of the fixed point, we illustrate the dimensional distance enlargement factor as a function of the redshift or time, see Fig. (10.3). Since that function varies as a function of z, the energy of the quanta of the dark energy varies as well, see above. So the present-day vacuum is polychromatic.

Theorem 10 Polychromatic vacuum

(1) The present-day vacuum is polychromatic.

(2) The present-day polychromatic vacuum has the following density parameter:

$$\boxed{\Omega_\Lambda = 0.6834} \tag{10.25}$$

The relative difference between theoretical and observed values is as follows:

$$\Delta_{theo-obs}\Omega_\Lambda = \frac{\Omega_{\Lambda,fixed\ point} - \Omega_{\Lambda,obs}}{\Omega_{\Lambda,obs}} = \pm 0.19\% \tag{10.26}$$

The error of observation amounts to 1.1 %, see Tab. 15.2. So our theoretical result is in precise accordance with the observed value, as its deviation from observation is smaller than the error of observation.

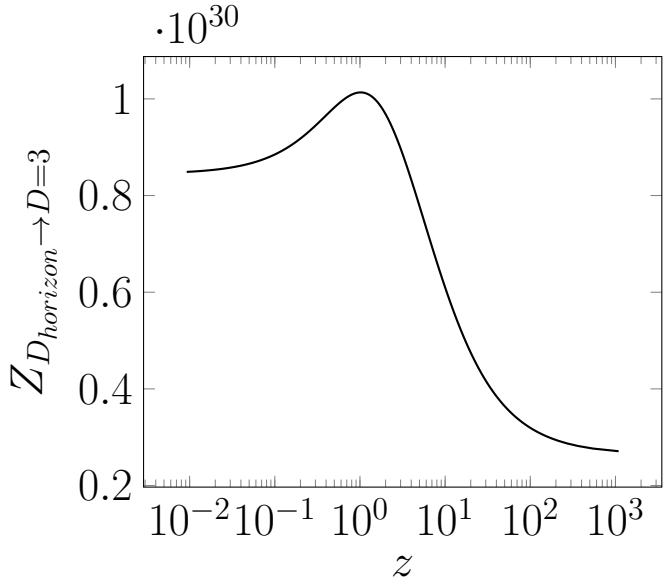

Figure 10.3: Distance enlargement factor $Z_{D_{horizon} \to D=3}$ as a function of the redshift.

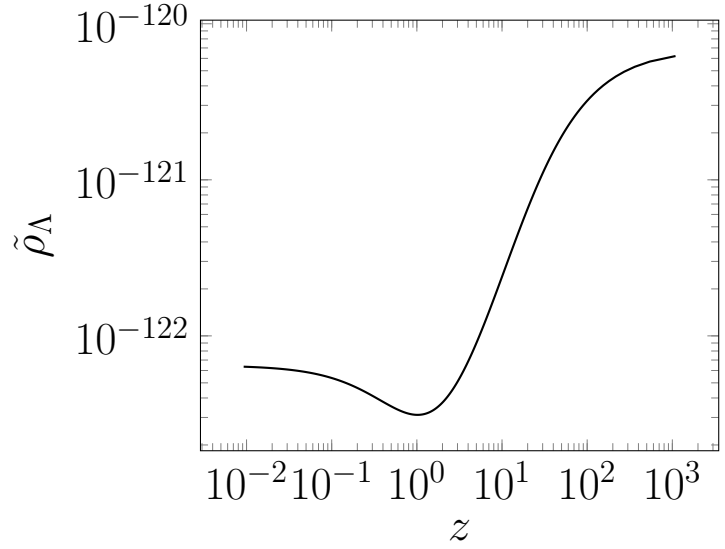

Figure 10.4: Density $\tilde{\rho}_\Lambda$ as a function of the redshift.

Chapter 11

Derivation of σ_8

In this section we derive the amplitude of matter fluctuations σ_8 from the time evolution of the dark energy derived in the chapter (10). That parameter is an essential cosmological parameter, accordingly we derive it in this section. We introduced and analyzed that parameter in detail in (Carmesin, 2021c, chapter 7). Here we derive σ_8 on the basis of results obtained in (Carmesin, 2021c, chapter 7) and in chapter (10).

Results obtained by quantum gravity: In order to derive σ_8, we use the ratio $(1+\kappa)^2$ of the density $\rho_{\Lambda,het}$ of the present-day dark energy in our heterogeneous universe and the density $\rho_{\Lambda,const.}$ of the dark energy in a homogeneous universe, see (Carmesin, 2021c, Eq. 7.141):

$$\boxed{(1+\kappa)^2 = \frac{\rho_{\Lambda,het}(z=0)}{\rho_{\Lambda,const.}}} \tag{11.1}$$

Hereby, κ has been introduced as a parameter that describes the difference between the real heterogeneous universe and a homogeneous universe as a reference. We solve the above Eq. for κ:

$$\kappa = \sqrt{\frac{\rho_{\Lambda,het}(z=0)}{\rho_{\Lambda,const.}}} - 1 \tag{11.2}$$

At a redshift z, that parameter κ obeys the following relation derived by quantum gravity, see (Carmesin, 2021c, Eq. 7.131):

$$\boxed{\kappa = \frac{\Omega_M}{\Omega_\Lambda} \cdot \frac{9}{20} \cdot \frac{1}{(1+z)^2} \cdot \sigma_8} \tag{11.3}$$

We solve the above Eq. for σ_8. Moreover, we apply the above Eq. for κ, as that Eq. holds at zero redshift, we insert $z = 0$:

$$\sigma_8 = \frac{\Omega_\Lambda}{\Omega_M} \cdot \frac{20}{9} \cdot \left(\frac{\rho_{\Lambda,het}(z=0)}{\rho_{\Lambda,const.}} - 1 \right) \tag{11.4}$$

In order to determine σ_8, we use the following results:

Results obtained by the polychromatic vacuum: The time evolution of the dark energy provides the present-day value of the density of the dark energy, see chapter (10):

$$\tilde{\rho}_{\Lambda,het}(z=0) = 6.5993 \cdot 10^{-123} \tag{11.5}$$

The corresponding value averaged from $z = 1090$ until $z = 0$ is as follows:

$$\tilde{\rho}_{\Lambda,aver.}(z=0) = 4.7301 \cdot 10^{-123} \tag{11.6}$$

Results obtained for the homogeneous universe: In the homogeneous universe, the density parameter of the dark energy is as follows, see (Carmesin, 2021c, theorem 21(3)):

$$\Omega_{\Lambda,const.} = 2/3 \tag{11.7}$$

Consequently, the scaled density of the dark energy is as follows:

$$\tilde{\rho}_{\Lambda,const.} = \Omega_{\Lambda,const.} \cdot \tilde{\rho}_{\Lambda,t_0} \tag{11.8}$$

Hereby, $\tilde{\rho}_{\Lambda,t_0}$ is obtained from the Hubble constant, see table (15.2):

$$\tilde{\rho}_{cr.,t_0} = 7.037 \cdot 10^{-123} \tag{11.9}$$

With it we derive:

$$\tilde{\rho}_{\Lambda,const.} = 2/3 \cdot 7.037 \cdot 10^{-123} = 4.6913 \cdot 10^{-123} \tag{11.10}$$

Calculation of σ_8: We apply Eq. (11.4), and we insert the ideal values $\Omega_\Lambda \approx \Omega_{\Lambda,const.} = 2/3$, $\Omega_M \approx 1 - \Omega_{\Lambda,const.} = 1/3$. Moreover, we use Eqs. (11.10) and (11.5). So we derive:

$$\sigma_{8,theo,ideal} = 2 \cdot \frac{20}{9} \cdot \left(\sqrt{\frac{6.5993 \cdot 10^{-123}}{4.6913 \cdot 10^{-123}}} - 1 \right) = 0.82688 \quad (11.11)$$

In order to compare with the value of σ_8 observed by observation of the CMB emitted at $z = 1090$, see Collaboration (2020a), we replace $\tilde{\rho}_{\Lambda,const.} = 4.6913 \cdot 10^{-123}$ by $\tilde{\rho}_{\Lambda,aver.}(z = 0) = 4.7301 \cdot 10^{-123}$, obtained with the polychromatic vacuum. Correspondingly, we derive:

$$\sigma_{8,theo} = 2 \cdot \frac{20}{9} \cdot \left(\sqrt{\frac{6.5993 \cdot 10^{-123}}{4.7301 \cdot 10^{-123}}} - 1 \right) = 0.806 \quad (11.12)$$

11.1 Comparison with observation: σ_8

The observation of the CMB provides values for σ_8 ranging from 0.793 to 0.812, see (Collaboration, 2020a, Tab. 8). We calculate the average of these observed values:

$$\sigma_{8,obs} = 0.8057 \quad (11.13)$$

Moreover, we determine the corresponding empirical standard deviation:

$$\Delta\sigma_{8,obs} = 0.008 \quad (11.14)$$

Accordingly, we derive the relative error of measurement:

$$\Delta_{obs}\sigma_8 = \frac{\Delta\sigma_{8,obs}}{\sigma_{8,obs}} = \pm 1\% \quad (11.15)$$

So the relative difference between $\sigma_{8,theo}$ and $\sigma_{8,obs}$ is as follows:

$$\Delta_{theo-obs}\sigma_8 = \frac{\sigma_{8,theo} - \sigma_{8,obs}}{\sigma_{8,obs}} = \pm 0.04\% \quad (11.16)$$

That relative difference $\Delta_{theo-obs}\sigma_8$ is within the error of measurement $\Delta_{obs}\sigma_8$.

Theorem 11 Amplitude of matter fluctuations σ_8

(1) We derived the present-day amplitude of matter fluctuations σ_8 by using quantum gravity.

(2) Thereby, we used the following numerical input only: We used the Hubble constant H_0, see table (15.2) as a time reference, and we used the universal constants G, c, k_B and h, see table (15.1).

(3) In this manner we obtained the following result

$$\boxed{\sigma_{8,theo} = 0.806} \tag{11.17}$$

(4) Our obtained result is in precise accordance with observation, since the difference $\Delta_{theo-obs}\sigma_8$ between theory and observation is smaller than the error of measurement $\Delta_{obs}\sigma_8$.

$$\Delta_{theo-obs}\sigma_8 = 0.04\% < 1\% = \Delta_{obs}\sigma_8 \tag{11.18}$$

Chapter 12

Simultaneous Derivation of Ω_j

In this section we develop a simultaneous derivation of the density parameters. There are the following four essential density parameters, see COR. (2):

$$\vec{\Omega}_{ess.} = \begin{pmatrix} \Omega_K \\ \Omega_r \\ \Omega_\Lambda \\ \Omega_M \end{pmatrix} = \begin{pmatrix} 0 \\ ? \\ ? \\ \Omega_M = 1 - \Omega_\Lambda - \Omega_r \end{pmatrix} \tag{12.1}$$

Thereby, $\Omega_K = 0$ is known, at least as an average. Moreover, $\Omega_M = 1 - \Omega_\Lambda - \Omega_r$ depends on two other density parameters. Furthermore, the density parameter of radiation Ω_r is a sum of three density parameters:

$$\Omega_r = \Omega_\nu + \Omega_\gamma + \Omega_{ERS} \tag{12.2}$$

Hereby Ω_{ERS} is customarily included in Ω_ν, see (Hinshaw et al., 2013, S. 4.3). very small and roughly known from observation. This it does not occur explicitly in our calculation. Hence there remain the following three essential and independent density parameters:

$$\vec{\Omega}_{ess.\ indep.} = \begin{pmatrix} \Omega_\gamma \\ \Omega_\nu \\ \Omega_\Lambda \end{pmatrix} \tag{12.3}$$

So far we developed one procedure of calculation for each of these three density parameters Ω_γ, Ω_ν and Ω_Λ. Hence we de-

velop a procedure for a simultaneous derivation of these three density parameters.

As a matter of fact, these three density parameters establish a triple with mutual dependence. However, that mutual dependence might be very small and negligible, indeed an appropriate separation is possible here. In fact, we derive such a separation that holds as a very good approximation. For it we show that the dimensional horizon is equal to 301 for all physical systems, for which the dimensional transitions have been analyzed.

12.1 Dimensional horizon

In order to derive the dimensional horizon D_{hori}, we express the density of radiation by a first function of D_{hori} as follows[1], see (Carmesin, 2019d, Eq. 2.163):

$$\tilde{\rho}_{r,D,1}(D_{hori}) = 2^{\frac{4\cdot(D_{hori}-3)}{3}} \cdot \frac{1}{4 \cdot \tilde{r}_{lh}^4 \cdot \tilde{\rho}_{r,t_0}} \tag{12.4}$$

In order to derive the dimensional horizon D_{hori}, we express the density of radiation by a second function of that dimensional horizon, $\tilde{\rho}_{r,D,2}(D_{hori})$:

The critical density $\tilde{\rho}_{c,D}$ represents the density of radiation, since the energy has the form of radiation at all critical densities, in an extremely good approximation.

Moreover, at each high dimension[2], the density is almost precisely determined by the dimension, as the density is almost constant in each high dimension, and that density is determined by the critical density, see Figs. (3.8), (3.9) and (3.11):

$$\tilde{\rho}_{c,D} = \tilde{\rho}_{r,D,2}(D) \tag{12.5}$$

[1]That function has been derived by using the following idea: The dimensional horizon D_{hori} can be determined from the dimensional distance enlargement factor $Z_{D_{hori}\to D=3}$. That factor is equal to the ratio $q_{D_{hori}\to t_0}$ / $k_{D_{hori}\to t_0}$. The denominator $k_{D_{hori}\to t_0}$ depends on the density $\tilde{\rho}_{r,t_0}$, while the numerator depends on the light horizon $\tilde{r}_{lh}$. So the density $\tilde{\rho}_{r,t_0}$ can be expressed as a function of the dimensional horizon D_{hori} and of the light horizon $\tilde{r}_{lh}$.

[2]Such dimensions occur for a short time after the Big Bang, see chapter (3).

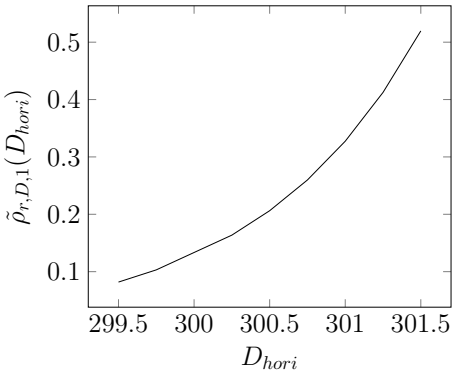

Figure 12.1: First function $\tilde{\rho}_{r,D,1}(D_{hori})$ as a function of D_{hori}.

In particular, that function can be applied to D_{hori}:

$$\tilde{\rho}_{c,D_{hori}} = \tilde{\rho}_{r,D,2}(D_{hori}) \tag{12.6}$$

The critical densities have been evaluated for three very different physical systems, and thereby the following intervals occur at all dimensions above 100:

$$0.5 > \tilde{\rho}_{c,D_{hori}} > \begin{cases} 0.4 & \text{for binary fluid and } D_{hori} > 100 \\ 0.44 & \text{for bose gas and } D_{hori} > 100 \\ 0.4 & \text{for connections and } D_{hori} > 100 \end{cases} \tag{12.7}$$

At D_{hori}, the two functions in Eq. (12.6) are equal:

$$\tilde{\rho}_{r,D,1}(D_{hori}) = \tilde{\rho}_{r,D,2}(D_{hori}) \tag{12.8}$$

We solve that equation graphically. For it we represent the function $\tilde{\rho}_{r,D,1}(D_{hori})$ in Fig. (12.1). The possible critical densities $\tilde{\rho}_{c,D}$ are between 0.4 and 0.5 (Eq. 12.7). So the dimensional horizon rounded to a natural number is equal to 301:

$$\boxed{D_{hori} = 301, \text{ if rounded to a natural number}} \tag{12.9}$$

12.2 Derivation of Ω_ν

The derivation of the density parameter of neutrinos Ω_ν in chapter (8) applies the dimensional horizon D_{hori}, whereas it does

neither use Ω_Λ nor Ω_γ. Thus, the derivations and calculations in that C. are separated from those in C. (4) and (10). As a result we obtained in C. (8), see Eq. (8.25):

$$\boxed{\Omega_{\nu,theo} = 3.9556 \cdot 10^{-5} \text{ and } \Delta_{theo-obs}\Omega_\nu = \pm 2.1\%} \quad (12.10)$$

12.3 Derivation of Ω_r

The derivation of the density parameter of photons Ω_γ in C. (4) applies the dimensional horizon D_{hori}, the density parameter of neutrinos Ω_ν and the idealized constant density parameter of dark energy $\Omega_{\Lambda,const.} = \frac{2}{3}$. We showed in C. (4) that a constant density parameter $\Omega_{\Lambda,const.} = \frac{2}{3}$ is adequate, this fact corresponds to the observational finding that more than 95 % of the present-day photon energy is found in the CMB, and that CMB is almost homogeneous even today, though the present-day universe exhibits a large heterogeneity characterized by $\sigma_8 = 0.806$. As a consequence, it is not necessary to use the general density parameter Ω_Λ for a heterogeneous universe, if the aim is to derive Ω_γ.

Thus, the derivations and calculations in C. (4) can be used here as well. The only difference is that we now apply the result $\Omega_{\nu,theo} = 3.9556 \cdot 10^{-5}$ in Eq. (12.10). In that manner we derive the following density parameter:

$$\boxed{\Omega_{r,theo} = 9.306 \cdot 10^{-5}} \quad (12.11)$$

Thus the relative difference to the observed value $\Omega_{r,obs} = 9.265 \cdot 10^{-5}$ is:

$$\boxed{\Delta_{theo-obs}\Omega_r = \frac{\Omega_{r,theo} - \Omega_{r,obs}}{\Omega_{r,obs}} = \pm 0.44\%} \quad (12.12)$$

12.4 Derivation of Ω_Λ

Since the density parameter of neutrinos $\Omega_{\nu,theo}$ and the density parameter of radiation $\Omega_{r,theo}$ have been calculated indepen-

dently of the density parameter of dark energy Ω_Λ, the latter density parameter Ω_Λ can be derived and calculated by using the results of the chapters (8) and (4). In addition to that algorithmic reason, we note a corresponding physical reason: The density parameter of neutrinos Ω_ν does not depend on the dark energy at all, and the density parameter of photons Ω_γ can be determined for the particular case of a homogeneous universe, and the result can be transferred to the realistic case of the present-day heterogeneous universe.

In that manner we derive the following density parameter:

$$\boxed{\Omega_{\Lambda,theo} = 0.68265} \tag{12.13}$$

Thus the relative difference to the observed value $\Omega_{\Lambda,obs} = 0.6847$ is:

$$\boxed{\Delta_{theo-obs}\Omega_\Lambda = \frac{\Omega_{\Lambda,theo} - \Omega_{\Lambda,obs}}{\Omega_{r,obs}} = \pm 0.3\%} \tag{12.14}$$

With it, σ_8 takes the following value:

$$\boxed{\sigma_{8,theo} = 0.8044} \tag{12.15}$$

Thus the relative difference to the observed value $\sigma_{8,obs} = 0.8057$ is, see C. (11):

$$\boxed{\Delta_{theo-obs}\sigma_8 = \frac{\sigma_{8,theo} - \sigma_{8,obs}}{\sigma_{8,obs}} = \pm 0.16\%} \tag{12.16}$$

Theorem 12 Derived cosmological constants

(1) Using quantum gravity, the corresponding universal constants G, c, k_B as well as h and H_0 as a time reference, we derived all other essential cosmological constants.

(2) In particular, these cosmological constants are Ω_K, Ω_r, Ω_Λ, Ω_M and σ_8

(3) Moreover, we derived the density parameters of neutrinos Ω_ν and radiation Ω_γ, also based on part (1).

(4) Additionally, we derived the mass m_H of the Higgs boson, also based on part (1).

(5) For all derived constants and quantities in parts (2) to (4), the difference between theory and observation is smaller than the error of observation. So all these derived constants and quantities are in precise accordance with observation.

(6) Hence all derived constants and quantities in parts (2) to (4), are results of the physics of quantum gravity including the constants G, c, k_B, h and H_0. In particular, they are not independent constants of nature.

(6a) As all masses of elementary particles are represented or caused by the neutrinos and m_H, also these masses do not represent independent constants of nature.

Chapter 13

Solution of H_0 and σ_8 tensions

In this C. we solve the H_0 and σ_8 tensions by using our theory.

13.1 Explanation of the H_0 tension

In this section we model observations of the Hubble constant H_0, that is the present-day value of the Hubble parameter $H(z)$. Each observation of H_0 uses radiation that is emitted at a distance with a corresponding redshift z.

In the standard model of cosmology, the Hubble constant H_0 is a fixed parameter. However, observation shows that the observed values of H_0 depend on that redshift of the emission of the used radiation, see Fig. (13.1).

13.1.1 H_0 in the standard model

According to the observation in Fig. (13.1), the standard model of cosmology, SMC, must be generalized. For it we start with the definition of H_0 in the SMC:

$$H_0^2 = \frac{8\pi \cdot G}{3} \cdot \rho_{cr.,t_0} \quad \text{with} \quad \rho_{cr.,t_0} = \rho_{r,t_0} + \rho_{m,t_0} + \rho_\Lambda \qquad (13.1)$$

13.1.2 H_0 described as an average

In order to generalize H_0 in the SMC, we describe it in terms of a time averaged density $\langle \rho_\Lambda \rangle$, as ρ_Λ is a function of the redshift

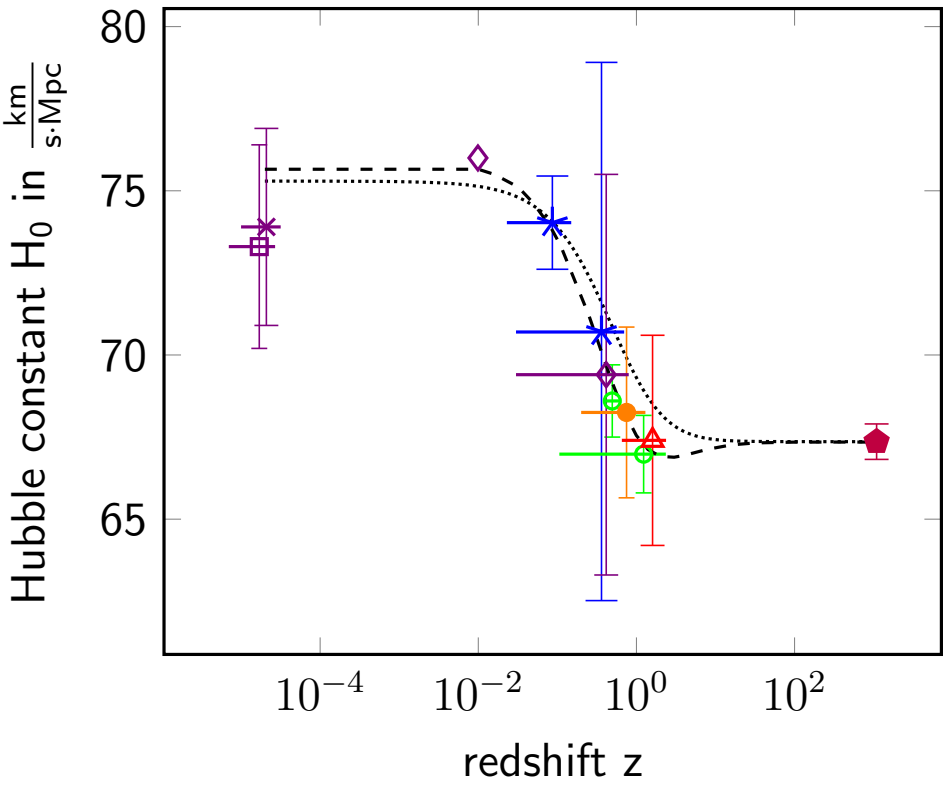

Figure 13.1: H_0 as a function of the redshift z of the probe.
Probes:
×, megamaser, Pesce et al. (2020).
⋆, distance ladder, Riess et al. (2019) (left), Suzuki et al. (2011).
o, baryonic acoustic oscillations, BAO , Zaldarriaga et al. (2020). Weiland et al. (2018)),
•, weak gravitational lensing, Lu and Haiman (2020)).
Δ, strong gravitational lensing, Birrer et al. (2020).
◇, gravitational wave, Escamilla-Rivera and Najera (2021), Fishbach et al. (2019).
□, surface brightness, Blakeslee et al. (2021),
pentagon, CMB, Collaboration (2020b).
Theories:
both without any fit
· · · · · · · · · Semiclassical dark energy theory, Carmesin (2021c).
– – – – – quantum theory of dark energy,

z or the time t, see Fig. (13.1). Thereby the average ranges from a time t_e at which the radiation of a probe is emitted until the present-day time t_0.

Naturally, the density is weighted by the volume $\delta V(t_{form})$ that is formed according to the FLE at a time t:

$$\langle \rho_\Lambda \rangle(t_e) = \frac{\int_{t_e}^{t_0} \delta V(t) \rho_\Lambda(t) dt}{\int_{t_e}^{t_0} \delta V(t) dt} \tag{13.2}$$

The density ρ_Λ in Eq. (13.1) is naturally replaced by its average:

$$H_0^2(t_e) = \frac{8\pi \cdot G}{3} \cdot \rho_{cr.,t_0} \quad \text{with} \quad \rho_{cr.,t_0} = \rho_{r,t_0} + \rho_{m,t_0} + \langle \rho_\Lambda \rangle(t_e) \tag{13.3}$$

So this Eq. holds in the SMC. Moreover, this Eq. describes an appropriate value of $H_0(t_e)$ for a probe based on radiation emitted at a time t_e.

13.1.3 Reference value for H_0

In this section we introduce a reference value for H_0. That value should combine two advantages: It should present a relatively long period of averaging, and there should be an observation with a relatively small error of measurement, so that a possible comparison is relatively meaningful. Accordingly, we choose the value for H_0 of the CMB, $H_0(z = 1090) = H_{0,CMB}$, see Fig. (13.1):

$$H_0^2(t_{CMB}) = \frac{8\pi G}{3} \cdot \rho_{cr.,t_0} \quad \text{with} \quad \rho_{cr.,t_0} = \rho_{r,t_0} + \rho_{m,t_0} + \langle \rho_\Lambda \rangle(t_{CMB}) \tag{13.4}$$

We apply that reference value. For it we derive the ratio with $H_0^2(t_e)$ for another time of emission t_e:

$$\frac{H_0^2(t_e)}{H_0^2(t_{CMB})} = \frac{\rho_{r,t_0} + \rho_{m,t_0} + \langle \rho_\Lambda \rangle(t_e)}{\rho_{cr.,t_0}} \tag{13.5}$$

Here we identify the density parameters:

$$\frac{H_0^2(t_e)}{H_0^2(t_{CMB})} = \Omega_r + \Omega_M + \frac{\langle\rho_\Lambda\rangle(t_e)}{\rho_{cr.,t_0}} \tag{13.6}$$

Next we analyze the last summand.

13.1.4 Reference value for Ω_Λ

In order to apply the density parameter Ω_Λ of the reference value, we expand the last summand in the above Eq.:

$$\frac{H_0^2(t_e)}{H_0^2(t_{CMB})} = \Omega_r + \Omega_M + \frac{\langle\rho_\Lambda\rangle(t_e)}{\langle\rho_\Lambda\rangle(t_{CMB})} \cdot \frac{\langle\rho_\Lambda\rangle(t_{CMB})}{\rho_{cr.,t_0}} \tag{13.7}$$

The last fraction is the density parameter of the reference value:

$$\Omega_{\Lambda,CMB} = \frac{\langle\rho_\Lambda\rangle(t_{CMB})}{\rho_{cr.,t_0}} \tag{13.8}$$

So we derive:

$$\frac{H_0^2(t_e)}{H_0^2(t_{CMB})} = \Omega_r + \Omega_M + \frac{\langle\rho_\Lambda\rangle(t_e)}{\langle\rho_\Lambda\rangle(t_{CMB})} \cdot \Omega_{\Lambda,CMB} \tag{13.9}$$

Similarly as in chapter (11), we describe the ratio in the above Eq. by a factor $(1+\kappa(t_e))^2$:

$$\frac{\langle\rho_\Lambda\rangle(t_e)}{\langle\rho_\Lambda\rangle(t_{CMB})} = (1+\kappa(t_e))^2 \tag{13.10}$$

Thus, we derive:

$$\frac{H_0^2(t_e)}{H_0^2(t_{CMB})} = \Omega_r + \Omega_M + \Omega_{\Lambda,CMB} \cdot (1+\kappa(t_e))^2 \tag{13.11}$$

We solve the above Eq. for $H_0(t_e)$:

$$\boxed{H_0(t_e) = H_0(t_{CMB}) \cdot \sqrt{\Omega_r + \Omega_M + \Omega_{\Lambda,CMB} \cdot (1+\kappa(t_e))^2}} \tag{13.12}$$

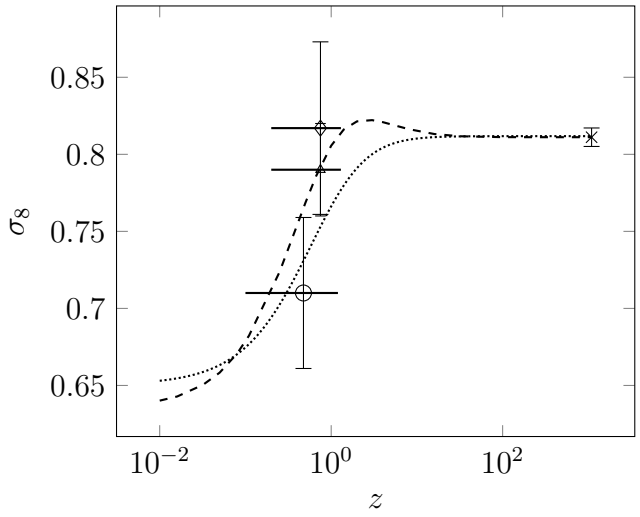

Figure 13.2: σ_8 as a function of the redshift z of the probe: galaxy clustering and lensing ($\diamond$, (Abbott et al., 2019, p. 6, 15)), weak gravitational lenses ((Lu and Haiman, 2020, p. 1, 2)), baryonic acoustic oscillations (o, (Tröster et al., 2020, p. 1, 2)), CMB ($\times$, (Collaboration, 2020b, p. 16)). *Dark energy theory II* (dotted). *Dark energy theory IV* (dashed).

13.1.5 Calculation of $H_0(t_e)$

The theory provides the time evolution of the density ρ_Λ, see Fig. (10.4). With it the time averages and the factor $(1+\kappa(t_e))^2$ are determined, see Eq. (13.10). Therefrom the time evolution of the Hubble parameter $H_0(t_e)$ is calculated and presented as a function of the redshift z by the dashed line in Fig. (13.1).

That Fig. shows that the theory is in precise accordance with observation. Hence the theory solves the H_0 tension. Thus, the H_0 tension is explained by the fact that the density ρ_Λ varies as a function of time, see Fig. (10.4).

13.2 Explanation of the σ_8 tension

The observed values of the Hubble constant H_0 present a function of the redshift of the respective probes, see Fig. (13.1). Similarly the observed values of the amplitude of matter fluc-

tuations σ_8 is function of the redshift of the respective probes, see Fig. (13.2).

Again this can be explained by the present theory. For it we apply the theory derived in (Carmesin, 2021c, C. 7): We use the linear growth factor, see (Carmesin, 2021c, Eq. 7.94)):

$$D(z) = H(z) \int_0^z d\zeta \, \frac{1+\zeta}{H^3(\zeta)} \tag{13.13}$$

If the probe has been emitted at t_{CMB}, then we derive:

$$D_{CMB}(z) = H_{0,CMB} E(z) \int_0^z d\zeta \, \frac{1+\zeta}{H^3_{0,CMB} E^3(\zeta)} \tag{13.14}$$

Hereby $E(z)$ denotes the dimensionless Hubble parameter, see Eq. (1.23). If the probe has been emitted at t_e, then we obtain:

$$D_{t_e}(z) = H_{0,t_e} E(z) \int_0^z d\zeta \, \frac{1+\zeta}{H^3_{0,t_e} E^3(\zeta)} \tag{13.15}$$

We derive the ratio:

$$\frac{D_{t_e}(z)}{D_{CMB}(z)} = \frac{H^2_{0,t_e}}{H^2_{0,CMB}} \tag{13.16}$$

The value of σ_8 can be derived from the overdensity δ_{R_8} (δ_{R_8} is the overdensity $\delta(\vec{r}) = \frac{\rho(\vec{r})-\langle\rho\rangle}{\langle\rho\rangle}$ at a scale of 8 Mega parsec) as follows, (Carmesin, 2021c, Eq. 7.157)):

$$\sigma_8 = \frac{\delta_{R_8}}{D(z)} \tag{13.17}$$

Thus, the observed value based on a probe emitted at t_{CMB} is as follows:

$$\sigma_{8,CMB} = \frac{\delta_{R_8}}{D_{CMB}(z)} \tag{13.18}$$

Similarly, the observed value based on a probe emitted at t_e is as follows:

$$\sigma_{8,t_e} = \frac{\delta_{R_8}}{D_{t_e}(z)} \tag{13.19}$$

We derive the ratio:

$$\frac{\sigma_{8,t_e}}{\sigma_{8,CMB}} = \frac{D_{CMB}(z)}{D_{t_e}(z)} = \frac{H^2_{0,CMB}}{H^2_{0,t_e}} \tag{13.20}$$

We solve for σ_{8,t_e}:

$$\sigma_{8,t_e} = \sigma_{8,CMB} \cdot \frac{H^2_{0,CMB}}{H^2_{0,t_e}} \tag{13.21}$$

Therefrom the time evolution of the amplitude of matter fluctuations σ_8 is calculated and presented as a function of the redshift z by the dashed line in Fig. (13.2).

That Fig. shows that the theory is in precise accordance with observation. Hence the theory solves the σ_8 tension. Thus, the σ_8 tension is explained by the fact that the density ρ_Λ varies as a function of time, see Fig. (10.4).

Chapter 14

Discussion

In this C. we systematically discuss our theory and results. For it we apply the **five categories of explanatory power**, (Ylikoski and Kourikoski, 2010, S. 4.1 - 4.5).

(1) Non-sensitivity: The theory should not be very sensitive to changes in the background condition, (Ylikoski and Kourikoski, 2010, section 4.1). We achieve this by exactly explicating the conditions we use and by restricting these conditions to a small and very intensively tested set, see section (14.1.1). In other words, the present theory is robust.

(2) Precision: Our results are in precise accordance with observation, as the difference to observation is smaller than the error of observation, see sections (14.1.2) and (14.1.3).

(3) Factual accuracy: The theory at a given level of abstraction should exhibit a relatively small number of idealizations or falsehoods, (Ylikoski and Kourikoski, 2010, section 4.3). In our theory we overcome several idealizations that are still common today:

(3a) Instead of presuming three dimensional space, we derive gravitational instabilities that cause higher dimensional space, see e. g. chapter 3 or Carmesin (2017b).

(3b) Instead of presuming that the increase of the universe is based on an increase of volume only, we derive the dimensional phase transitions and their contribution to the increase of space, see e. g. chapter 3 or Carmesin (2017b).

(3c) Instead of presuming that general relativity theory, GRT, could be a local theory, we derived the nonlocality of GRT and the solution of the EPR paradox as a consequence, see e. g. (Carmesin, 2021c, THM. 5 and COR. 2).

(4) Integration: In our theory we basically integrate various fields of physics:

(4a) We integrate GRT and quantum physics.

(4b) We integrate the microscopic dynamics described by the Schwarzschild metric and the global dynamics of space, see e. g. (Carmesin, 2021c, CHAP. 1).

(4c) We integrate the standard model of cosmology, SMC, and the standard model of elementary particles, SMEP, by using the dimensional phase transitions.

(4d) Using these basic integrations, we solve a variety of fundamental problems of physics, see section (14.3).

(4e) Using the above basic integrations, we derive several predictions, see section (14.3).

(5) Cognitive salience: It should be relatively easy to understand a theory, and in particular a theory should apply concepts that are already known, see (Ylikoski and Kourikoski, 2010, section 4.5). Accordingly, the cognitive salience of our theory is especially large for the following reasons:

(5a) Our theory essentially applies the well known concepts of GRT, quantum physics, elementary particles and dimension of space.

(5b) Moreover, our theory reveals how to unify these concepts, and so our theory makes aware connections among these concepts. Thus, the understanding of these concepts becomes easier, without using any simplification and with providing novel results.

14.1 Comparison with observation

In this section we present theoretical values x_{theo}, corresponding observed values x_{obs} and respective relative errors

$$\Delta_{theo-obs}x = \frac{x_{theo} - x_{obs}}{x_{obs}} \cdot 100\% \tag{14.1}$$

Hereby, we analyze absolute values only.

14.1.1 Condition of derivation

Thereby we derived all theoretical values by using quantum gravity, the corresponding universal constants G, c, k_B and h, as well as the Hubble parameter H_0 at $z = 1090$ as a reference for the present-day time after the Big Bang. In particular, we do not apply any other numerical input, such as fit parameters or boundary values, for instance.

14.1.2 Cosmological and density parameters

We derived all essential cosmological parameters, see corollary (2). Here we compare the values that have been derived simultaneously in C. (12).

quantity	x_{theo}	x_{obs}	$\lvert\Delta_{theo-obs}x\rvert$	reference
Ω_Λ	0.68265	$0.6847 \pm 1.1\%$	0.3%	THM. (10)
$\Omega_{K,av.}$	0	$0.0007 \pm 171\%$	100%	COR. (2(3))
Ω_M	0.31726	$0.3153 \pm 1.1\%$	0.6%	THM. (10)
$10^5 \cdot \Omega_\gamma$	5.35	$5.335 \pm 5.68\%$	0.26%	THM. (4)
$10^5 \cdot \Omega_\nu$	3.9556	$3.8742 \pm 9.7\%$	2.1%	THM. (7)
$10^5 \cdot \Omega_r$	9.306	$9.265 \pm 3.1\%$	0.44%	THM. (4)
σ_8	0.8044	$0.8057 \pm 1\%$	0.16%	THM. (11)

Table 14.1: Using H_0, we derived all cosmological parameters. Here we applied $\Omega_\Lambda + \Omega_M + \Omega_r = 1$.

Our comparison in Table (14.1) shows: The relative difference of our theoretical values and the corresponding observed values is smaller than the error of measurement. So our results are in precise accordance with observation.

14.1.3 Masses

The masses of the elementary particles of the SMEP can be divided into two groups:

(1) masses of neutrinos

(2) masses of the Higgs boson and masses caused by the Higgs boson, including masses of quarks, $W^{+,0,-}$ bosons, electrons, muons and tauons.

(3) the remaining elementary particles of the SMEP are the photons and gluons, these have zero mass.

Accordingly, we derived the masses of neutrinos in terms of the density parameter Ω_ν and the mass of the Higgs boson, $m_{H,full,theo} = E_{H,full,theo}/c^2$.

quantity	x_{theo}	x_{obs}	$\Delta_{theo-obs}x$	reference
$10^5 \cdot \Omega_\nu$	3.9556	$3.8742 \pm 9.7\%$	$\pm 2.1\%$	THM. (7)
m_H in $\frac{\text{GeV}}{\text{c}^2}$	125.541	$125.18 \pm 1.1\%$	$\pm 0.29\%$	PROP. (9)

Table 14.2: Using H_0, we derived the masses that represent or cause all masses of the SMEP.

Our comparison in Table (14.2) shows: The relative difference of our theoretical values and the respective observed values is smaller than the error of measurement. Thus our theory is in precise accordance with observation. This holds for all masses that represent or cause all masses of the SMEP.

14.2 Predictions

In this section we apply the basic solution of the hierarchy problem in order to predict novel elementary particles. In a dimension D the ZPE of the longitudinal mode is as follows:

$$ZPE_{LONG,D} = \frac{E_P}{2}/2^{\frac{D_{hori}-D}{D}} = 6.1049 \cdot 10^{18}\,\text{GeV}/2^{\frac{D_{hori}-D}{D}} \tag{14.2}$$

Here we used $D_{hori} = 301$. The corresponding object consists of the three lowest excitation modes with $n = 1$, $n = 2$ and $n = 3$:

$$E_{object,D} = \Sigma_{n=1}^{n=3}(2n+1)ZPE_{LONG,D} = 15 \cdot ZPE_{LONG,D} \tag{14.3}$$

Four dimensional QST: In $D = 4$ the predicted object has the energy $E_{object,D=4} = 4.077\,\text{MeV}$ and is very unstable, see Fig. (3.7).

14.2.1 Observation of dimensional phase transition?

A stochastic gravitational wave background, GWB, has been observed, and it is interpreted as a relic of phase transitions in

the early universe. Thereby a transition temperature with the corresponding energy in the following interval has been found, see e. g. (Ratzinger and Schwaller, 2021, p. 5) or (Arzoumanian et al., 2021, Fig. 1):

$$E_{GWB,obs} \in [1; 10]\,\text{MeV} \tag{14.4}$$

This observation can be interpreted as follows: At the last dimensional phase transition of the cosmic unfolding, the above four dimensional elementary particles or QST with $E_{object,D=4} = 4.077\,\text{MeV}$ unfolded to an object with energies below one eV, see theorem (6), and thereby the object emitted its energy in the form of gravitational waves.

Six dimensional QST: In $D = 6$ the predicted object has the energy $E_{object,D=6} = 145\,\text{TeV}$. Using Pb-Pb collisions, the LHC could in principle achieve collision energies of 1150 TeV, see (Naumann, 2009, p. 21) or Tanabashi et al. (2018). So that predicted particle could possibly be observed with the current LHC in appropriate experiments.

Seven dimensional QST: In $D = 7$ the predicted object has the energy $E_{object,D=7} = 20\,821\,\text{TeV}$. So that predicted particle cannot be observed by using the current LHC and Pb-Pb collisions. Possibly, that particle could be formed by novel experimental setups or by an accelerator built in the future.

Eight dimensional QST: In $D = 8$ the predicted object has the energy $E_{object,D=8} = 864\,060\,\text{TeV}$. Similarly as for $D = 7$, that predicted particle could possibly be formed by novel experimental setups or by an accelerator built in the future.

Higher dimensional QST: Moreover, objects or elementary particles are predicted for all dimensions ranging from $D \geq 9$ towards $D = D_{hori} \approx 301$. The corresponding energies are de-

termined by Eq. (14.3). Thereby the Planck scale is reached at $D = D_{hori}$. These elementary particles can presumably be observed directly by novel or innovative experiments Additionally, these can be observed indirectly, similarly the particles of the dark energy have been 'observe indirectly' by measuring the dark energy, H_0, the H_0 tension and the σ_8 tension, for instance.

14.3 Solved problems

We summarize solved problems in order to make transparent how our theory integrates various fields and can be used to solve problems:

problem of rapid enlargement of distances (Guth (1981), solved since 2017, see e. g. Carmesin (2017b), Carmesin (2021a))

horizon problem (Guth (1981), solved since 2017, see e. g. Carmesin (2017b), Schöneberg and Carmesin (2021))

'inflaton' hypothesis and reheating problem (see Guth (1981) and Nanopoulos et al. (1983), Broy (2016), solved since 2017, see e. g. Carmesin (2017b), Carmesin (2020a))

dark matter problem (Zwicky (1933), Sanders (2010), see e. g. solved since 2018, Carmesin (2018h), Carmesin (2019d))

dark energy problem (Josset et al. (2017), solved since 2018, see e. g. Carmesin (2018g), Carmesin (2021c))

H_0 tension (Riess et al. (2019), solved since 2018, Carmesin (2018g), Carmesin (2021c))

fine-tuning problem (Landsman (2016), solved since 2019, see Carmesin (2019d), and for the case of all cosmological constants, see section (14.1.2).

flatness problem (Guth (1981), solved since 2020, Carmesin (2020b), Carmesin (2021c))

zero energy hypothesis (Tryon (1973), solved 2020, Carmesin

(2020b))

graviton hypothesis (Blokhintsev and Galperin (1934), solved in Carmesin (2021c))

EPR paradox and nonlocality (Einstein et al. (1935), solved in Carmesin (2021c))

σ_8 tension (Tröster et al. (2020), solved in Carmesin (2021c))

hierarchy problem of particle physics, (Shaposhnikov and Shkerin (2018), solved here)

mass problem of the Higgs boson and the neutrinos (Aad et al. (2012), Chatrchyan et al. (2012) Peskin (2015), Tanabashi et al. (2018), solved here)

interaction problem of the nature of an interaction that can be repulsive as well as attractive, solved here in the framework of an effective interaction energy, see section PROP. 9)

14.4 Discussion

Here we apply a theory[1] that is based on quantum gravity and that explains many phenomena in a robust, precise, factually accurate, integrative and cognitive salient manner. These five properties are the elements of a systematic analysis of our theory, see Ylikoski and Kourikoski (2010), and they provide a clear evidence of our theory. We emphasize that we do not use any fit parameter, instead we use quantum gravity and the universal constants G, c, k_B and h only.

Several fundamental problems are solved for the first time here. For it we use our theory. These problems include the hierarchy problem of elementary particle physics and the problem

[1] I derived the present theory progressively. The publication started in 2017 in books, papers and my book series. See e. g. Carmesin (2017b), Carmesin (2018h), Carmesin (2018g), Carmesin (2018f), Carmesin (2018a), Carmesin (2019d), Carmesin (2017b), Carmesin (2019a), Carmesin (2019f), Carmesin (2020b), Carmesin (2020a), Carmesin (2021c), Carmesin (2021a), Carmesin (2021d).

of explaining the masses in elementary particle physics, see e. g. Peskin (2015). These problems are solved by a completely novel unification of cosmology and elementary particle physics: Here we show that the dimensional phase transitions that took place in the early universe additionally provide the states that can be excited in order to form elementary particles such as the neutrinos, the Higgs boson and the particles caused by it such as quarks, electrons or W bosons.

14.5 Outlook

There are many interesting questions that could be analyzed on the basis of that theory in the future, examples are as follows: Is it possible to derive the interactions and symmetries in elementary particle physics, see e. g. Tanabashi et al. (2018), on the basis on quantum gravity? Is it possible to explain open questions of structure formation by using quantum gravity? How can the dimensional phase transitions in the early universe be observed directly and used technically, see Sect. (14.2.1)? How can the elementary particles predicted here be observed directly and applied technologically, see Sect. (14.2.1)?

For instance, a device could use the stimulated emission of QST and provide QST - particles at high precision and luminosity. Hereby radiation and particles could be combined such as in the XFEL. Such a device could be applied in order to provide communication and transport process using higher dimension. Such a process would be at a velocity $v \leq c$ at the higher dimension and appear to be at higher velocity than c in three dimensions, see Carmesin (2021a). Moreover, such processes could treat an encapsulated area without destruction. E. g., caries in a tooth could be treated without drilling a hole. In particular, this could be achieved at energies that are already very common in medical devices, since a four dimensional particle is available at an energy of few MeV, see 14.2.1.

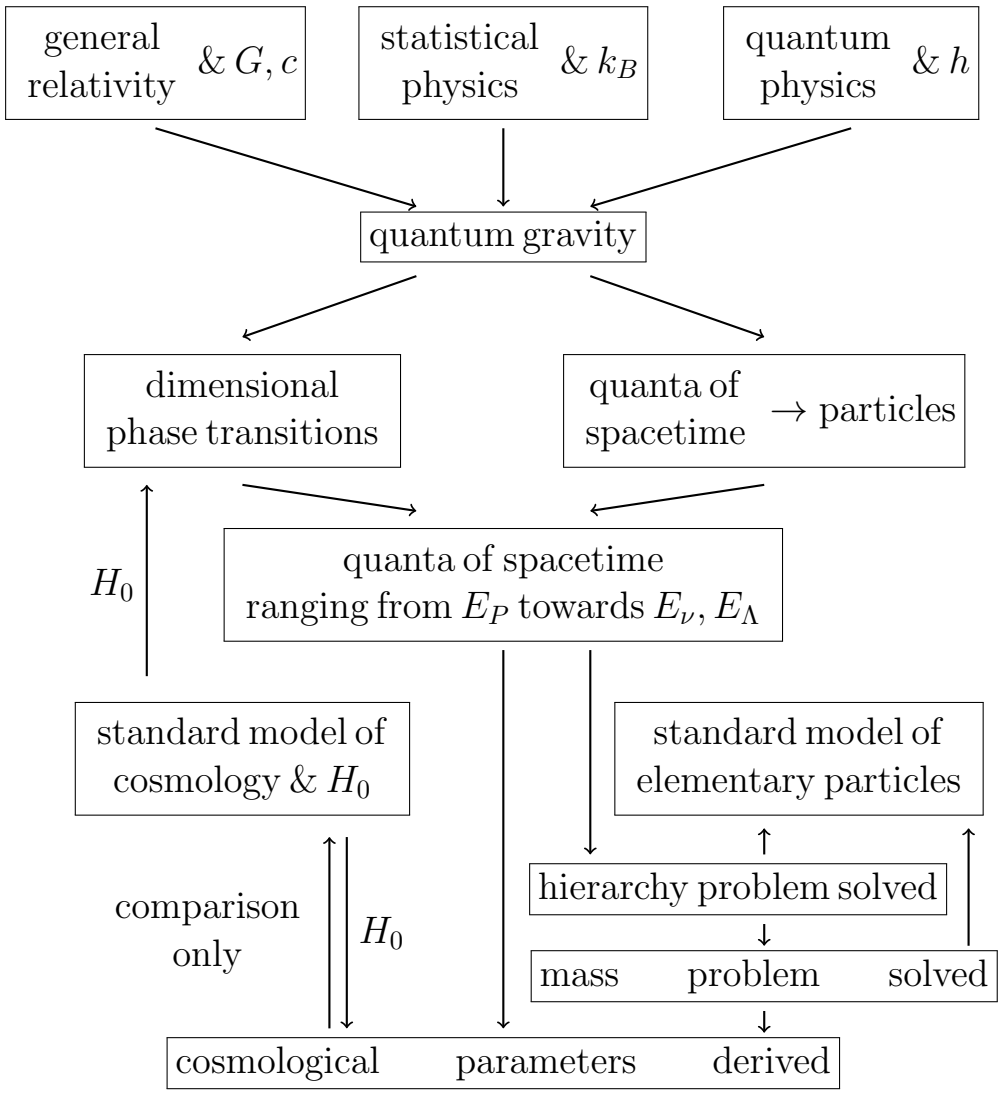

Figure 14.1: Paths from basic theories to derivations, explanations and calculations: These derivations reflect the structure of physics and have been published since Carmesin (2017b).

14.6 Unification of SMC and SMEP

The standard models of cosmology, SMC, and of elementary particles, SMEP, have been unified as follows, see Fig. (14.1): Based on the three basic concepts, GRT, SP and QP, QG has been developed. Therefrom, QST and dimensional phase transitions including cosmic unfolding have been derived, see e. g. Carmesin (2017b), Carmesin (2019d), Carmesin (2021c).

Using these results, we derived the basic solution of the hierarchy problem of elementary particles. Thereby, cosmic unfolding provides the QST that solve the hierarchy problem.

Based on that solution of the hierarchy problem, we derived the basic masses. Using these, we derived all essential cosmological parameters. Altogether, we derived our results from the basic theories only, and we used corresponding universal constants including the time reference H_0 only, and we achieved precise accordance with observation.

14.6.1 Public documentation and discussion

The theory in Fig. (14.1) has been published since Carmesin (2017b), and it has been discussed at many conferences. This process is described as follows:

Reviewed papers: Several results have been published in peer reviewed papers, see[2].

Conferences: Many results have been presented at conferences, see[3].

[2]Peer reviewed papers: Carmesin (2016), Carmesin (2018a), Carmesin (2018d),Carmesin (2018e),Carmesin (2018c), Helmcke et al. (2018), Sprenger and Carmesin (2018), Carmesin (2019b), Carmesin (2020a), Carmesin and Carmesin (2020), Heeren et al. (2020), Schöneberg and Carmesin (2020), Carmesin (2021b), Carmesin (2021d), Schöneberg and Carmesin (2021), Lieber and Carmesin (2021), Sawitzki and Carmesin (2021)

[3]Presentations at conferences: Carmesin (2017a), Carmesin and Carmesin (2018a),Carmesin and Carmesin (2018b), Helmcke et al. (2018), Sprenger and Carmesin

Books: Four books have been published, see[4]. Additionally, a book series has been started, and therein, four books have already been published, see[5].

Internet: Many results are available at my page at Research gate:
http://www.researchgate.net/profile/ Hans_Otto_Carmesin
Some results are available at my homepage:
hans-otto.carmesin.org

14.6.2 An essential insight by quantum gravity

Quantum gravity reveals that there occurred an enormous sequence of phase transitions in the early universe: a cosmic unfolding of space, ranging from the Planck scale to the millimeter scale. The corresponding quantum states cause all masses of elementary particles, and they form neutrinos, Higgs bosons, the quanta of dark energy as well as many novel elementary particles, ranging from the Planck mass to the neutrino mass scale.

(2018), Carmesin and Brüning (2018), Carmesin (2019e), Carmesin (2019a), Brüning et al. (2019), Rademacker et al. (2019), Carmesin (2019g), Brüning and Carmesin (2019), Carmesin (2020a), Carmesin and Carmesin (2020), Heeren et al. (2020), Schöneberg and Carmesin (2020), Carmesin (2021b), Carmesin (2021d), Schöneberg and Carmesin (2021), Lieber and Carmesin (2021), Sawitzki and Carmesin (2021)

[4]Books: Carmesin (2017b), Carmesin (2018h), Carmesin (2018g), Carmesin (2018f)

[5]Book series: Carmesin (2019d), Carmesin (2020c), Carmesin (2020b), Carmesin (2021c)

Chapter 15

Appendix

15.1 Universal constants

In this section we present universal constant.

quantity	observed value	reference
G	$6.674\,08(31) \cdot 10^{-11}\ \frac{\mathrm{m}^3}{\mathrm{kg}\cdot\mathrm{s}^2}$	Tanabashi et al. (2018)
c	$299\,792\,458\ \frac{\mathrm{m}}{\mathrm{s}}$, exact	Tanabashi et al. (2018)
h	$6.626\,070\,15\ \cdot 10^{-34}$ Js, exact	Newell et al. (2018)
k_B	$1.380\,649\ \cdot 10^{-23}\ \frac{\mathrm{J}}{\mathrm{K}}$, exact	Newell et al. (2018)
ϵ_0	$8.854\,187\,817\ \cdot 10^{-12}\ \frac{\mathrm{F}}{\mathrm{m}}$	Tanabashi et al. (2018)

Table 15.1: Universal constants ((Newell et al., 2018, table 3), (Tanabashi et al., 2018, table 1.1)).

15.2 Observed values

quantity	observed value	reference
H_0 in $\frac{\text{km}}{\text{s·Mpc}}$	67.36 ± 0.54 (0.8 %)	[PC]
Ω_Λ	0.6847 ± 0.0073 (1.1 %)	[PC]
Ω_K	0.0007 ± 0.0019	[PC]
z_{eq}	$3402 \pm 26(0.76\%)$	[PC]
Ω_M	$0.3153 \pm 0.0073(2.3\%)$	[PC]
Ω_r	$9.265^{+0.288}_{-0.283} \cdot 10^{-5}$ (3.1 %)	[PC]
σ_8	$0.8057 \pm 0.008(1\%)$	[PC]
ρ_{cr,t_0} in $\frac{kg}{m^3}$	$8.660^{+0.137}_{-0.137} \cdot 10^{-27}$ (1.6 %)	[PC]
$\tilde{\rho}_{cr,t_0}$	$7.037 \cdot 10^{-123}$	[PC]
$\tilde{\rho}_{v,t_0}$	$4.8181 \cdot 10^{-123}$	[PC]
Ω_b	0.0493 ± 0.00032	[PC]
Ω_c	0.2645 ± 0.0048	[PC]
R_{lh}	$4.1412 \cdot 10^{26}$ m	[C2019]
T_{CMB}	2.7255(6)(0.02%) K	[T2018]
Ω_{CMB}	5.4501	Eqs. (4.30, 4.31)
Ω_ν	$3.8742 \cdot 10^{-5}(9.7\%)$	S. (8.3)

Table 15.2: Observations: [PC] marks data based on the CMB ((Collaboration, 2020a, table 2)), in particular based on the modes TT, TE, EE, the low energy and lensing. Quantities with a tilde are presented in natural units alias Planck units (see subsection 15.3). Hereby 1 Mpc = $3.0856776 \cdot 10^{19}$ km. [C2019] is based on an evaluation in Carmesin (2019d). [T2018] is based on (Tanabashi et al., 2018, section 28.3.1).

15.3 Natural units

Planck (1899) introduced Planck units. We mark quantities in natural units by a tilde, see Tab. 15.3 or Carmesin (2019d).

physical entity	Symbol	Term	in SI-Units
Planck length	L_P	$\sqrt{\frac{\hbar G}{c^3}}$	$1.616 \cdot 10^{-35}$ m
Planck time	t_P	$\frac{L_P}{c}$	$5.391 \cdot 10^{-44}$ s
Planck energy	E_P	$\sqrt{\frac{\hbar \cdot c^5}{G}}$	$1.956 \cdot 10^{9}$ J
Planck mass	M_P	$\sqrt{\frac{\hbar \cdot c}{G}}$	$2.176 \cdot 10^{-8}$ kg
Planck volume	$V_{D,P}$	L_P^D	
Planck volume, ball	$\bar{V}_{D,P}$	$V_D \cdot L_P^D$	
Planck density	ρ_P	$\frac{c^5}{G^2\hbar}$	$5.155 \cdot 10^{96}$ $\frac{\text{kg}}{\text{m}^3}$
Planck density, ball	$\bar{\rho}_P$	$\frac{3c^5}{4\pi G^2\hbar}$	$1.2307 \cdot 10^{96}$ $\frac{\text{kg}}{\text{m}^3}$
Planck density, ball	$\bar{\rho}_{D,P}$	$\frac{M_P}{\bar{V}_{D,P}}$	
Planck temperature	T_P	$T_P = \frac{E_P}{k_B}$	
scaled volume	$\tilde{V}_D$	$\frac{V_D}{\bar{V}_{D,P}}$	
scaled energy	$\tilde{E}$	E_P	$E = \tilde{E} \cdot E_P$
scaled density	$\tilde{\rho}_D$	$\frac{\tilde{M}}{\tilde{r}^D} = \frac{\tilde{E}}{\tilde{r}^D}$	$\rho_D = \tilde{\rho}_D \cdot \bar{\rho}_{D,P}$
scaled length	$\tilde{x}$	L_P	$x = \tilde{x} \cdot L_P$
Planck charge	q_P	$M_P\sqrt{G4\pi\varepsilon_0}$	$11{,}71\, e$

Table 15.3: Planck - units.

15.4 Glossary

Words marked bold face can usually be found in the glossary.

Abbreviation: S. (section), C. (chapter), DEF. (definition), PROP. (proposition), THM. (theorem).

amplitude of matter fluctuations, σ_8: (C. 1)

Bose gas: Quantum gas consisting of quanta with integer spin (S. 3.6)

Big Bang: Start of time evolution of visible space

cdm, cold dark matter: See Fig. (1.1), Carmesin (2018f) or Carmesin (2019d).

CMB, Cosmic Microwave Background: Radiation emitted at $z \approx 1090$. (Tab. 15.2)

complete time evolution of spacetime: Evolution of the light horizon $R_{lh}(t)$ ranging from the Planck - length L_P to the actual light horizon $R_{lh}(t_0)$ (Fig. 2.4)

cosmic unfolding: It causes the **extremely rapid distance enlargement in the early universe** (S. 3.7).

cosmological constant: Λ corresponds to the dark energy with its density ρ_Λ (Tab. 15.2).

curvature parameter: $k = \frac{-2\bar{E}}{m_0 \cdot c^2}$ (S. 1.3.2)

dark energy: Energy of the cosmological density of the vacuum ρ_Λ (Tab. 15.2).

density, critical: ρ_{cr,t_0} or ρ_{cr} (Tab. 15.2)

density, critical, at a dimensional transition: $\tilde{\rho}_{D,c}$ (S. 1.3.2)

density, critical, shortcuts: $\rho_{cr.conn.}$ (T. 1)

density, overdensity: $\delta(\vec{x}, t) = \rho_1(\vec{x}, t)/\rho_h$ (S. 4.2)

density parameter: $\Omega_j = \rho_j/\rho_{cr,t_0}$ (Tab. 15.2)

density, vacuum: $\rho_\Lambda = \Omega_\Lambda \cdot \rho_{cr,t_0}$ (Tab. 15.2)

dimensional distance enlargement factor: A factor $Z_{D+s\to D}$ occurs at a dimensional phase transition from a dimension $D+s$ to a dimension D and describes the corresponding increase of distances (C. 3).

dimension of the space: (C. 3)

dimensional horizon D_{max} or $D_{horizon}$: It is the maximal dimension that the space within the actual light horizon can have achieved in the past. Thereby the following transformations of space are essential: the isotropic scale and the enlargement of distance caused by a $\rightarrow$ dimensional transition. (C. 3).

dimensional phase transition: Change of spatial dimension D (C. 3).

dimensional unfolding: Change of spatial dimension D (C. 3).

dimensionless Hubble parameter $E = H/H_0$: (C. 1)

distance measures: The basic measure is the **light travel distance** $c \cdot dt$. The **complete distance** or **comoving distance** or **present-day proper distance** includes the enlargement of space, while the **luminosity distance** also includes the **luminosity** of a source and the redshift (S. 1.3.6).

dynamical mass: $M = \frac{E}{c^2}$ (PROP. 4)

expansion of space: Expansion since the Big Bang at constant dimension D

extended FLE, EFLE: FLE extended by quantum effects (S. 3.4.1)

extra radiation species, ERS: (C. 1)

extremely rapid distance enlargement in the early universe: Guth (1981) conjectured that factor, the factor has been explained by dimensional transitions in this book and by Carmesin (2017b), Carmesin (2019d)

event horizon: (S. 2.1)

flat, flatness, flatness problem: Space without curvature is flat (S. 14.3).

frame: Each observation apparatus is localized in spacetime. That localization establishes a frame. An examples is the HUF (C. 1).

Friedmann - Lemaître equation, FLE: (C. 1)

gravitational field: G^* (C. 1)

GRT: General relativity theory (C. 1)

horizon: Global limit of visibility (C. 1)

Hubble - parameter: $H = \frac{\dot{a}}{a}$ (C. 1)

Hubble - constant: $H_0 = H(t_0)$ Hubble parameter at t_0

incomplete: A theory that does not describe the physically known objects or properties is incomplete (S. 2.2)

light horizon, actual: $R_{lh} = 4.142 \cdot 10^{26}\,\mathrm{m}$ (Tab. 15.2)

light horizon, at a time t: $R_{lh,t}$ (Carmesin (2019d))

light-travel distance: $d_{light-travel} = t_{light-travel} \cdot c$

linear growth factor: $D(t)$ (C. 13)

natural units: Planck - units (Tab. 15.3)

pbh, primordial black holes: See Fig. (1.1) and Carmesin (2020b).

Planck scale: At that scale there occurs the **length limit** and the **density limit** in nature. Accordingly, natural units or Planck units have been introduced (Tab. 15.3).

polychromatic vacuum: It includes several wavelengths of the quanta of space (C. 10)

QG, quantum gravity: Combination of gravitation and quantum physics (C. 2 or Carmesin (2019d))

QP, quantum physics: Quantum physics, see C. 1

QST, quantum of spacetime, or quantum of vacuum: Representations are quantized RGWs, quantized spacetime scalar, quantized spacetime tensor (C. 5)

rapid enlargement of distances: (Fig. 2.4)

RGW, rate gravity wave: Carmesin (2021c) or S. (5.3)

rate of the formation of vacuum: (C. 3)

redshift: Relative increase of the wavelength $z = \frac{\Delta\lambda}{\lambda}$ (C. 1)

reduced normalized energy E_D: (C. 3)

scale factor: $k_{t_1 \to t_2}$ (C. 3), it is sometimes described by a **scale radius** a, $a(t) = k_{t_{ref} \to t} a(t_{ref}$ (C. 1).

shortcut: (C. 3)

SP, statistical physics: (C. 1)

SOU, shortest observable uncertainty: (C. 2)

Schwarzschild radius R_S: At this radius the escape velocity is equal to c (S. 2.1)

SMC, Standard Model of Cosmology: (C. 1)

SMEP, Standard Model of Elementary Particles: (C. 1)

spacetime: Combination of space and time (C. 1 or 5).

SRT, special relativity theory: (C. 1)

standard deviation at a sphere with radius R: σ_R (C. 13)

standard deviation at a sphere with radius R_8: $\sigma_8 = \sigma_{R_8}$ It is also called amplitude of matter fluctuations or amplitude of matter fluctuations (C. 13).

unfolding, dimensional: Space unfolds when the dimension decreases (C. 3)

universal constants: (Tab. 15.1)

vacuum: The vacuum has a volume, a density and the velocity c. (C. 1, 3, 10 or Carmesin (2021c))

ZPE: Zero-point energy of omnipresent zero-point oscillations (C. 1, 2, 3)

ZPO: Zero-point oscillations are omnipresent quantum states corresponding to a ground state (C. 1, 2, 3)

Acknowledgement

I thank Matthias Carmesin for helpful discussions. I thank Paul Sawitzki, Philipp Schöneberg, Jörn Kankelfitz, Dennis Feldmann and Jonas Lieber for interesting discussions. I am especially grateful to I. Carmesin for many helpful discussions.

Bibliography

Aad, G. et al. (2012). Observation of a new particle in the search for the standard model higgs boson with the atlas detector at the lhc. *Phys. Lett. B*, 716:1.

Abbott, B. P. e. a. (2016). Observation of gravitational waves from a binary black hole merger. *Phys. Rev. Lett.*, 116:1–16.

Abbott, T. M. C. et al. (2019). Dark energy survey year 1 results: Cosmological contraints from galaxy clustering and weak lensing. *Phys. Rev. D*, 98:1–31.

Akiyama, K. et al. (2019). First m87 event horizon telescope results. iv. imaging the central supermassive black hole. *The Astrophysical Journal*, 875:1–17.

Amendola, L. (2021). Lecture notes: Cosmology. University Heidelberg server.

Arzoumanian, Z. et al. (2021). Searching For Gravitational Waves From Cosmological Phase Transitions With The NANOGrav 12.5-year dataset. *arXiv*, 2104.13930v1:1–13.

Balabin, R. M. (2009). Enthalpy difference between conformations of normal alkanes: Raman spectroscopy study of n-pentane and n-butane. *J. Phys. Chem. A*, 113:1012–1019.

Ballentine, L. E. (1998). *Quantum Mechanics*. World Scientific Publishing, London and Singapore.

Bennett, C. L. et al. (2013). Nine-year Wilkinson microwave anisotropy probe (WMAP) Observations: final maps and results. *The Astrophysical Journal Supplement Series*, 208:1–54.

Bethge, K. and Schröder, Ulrich, E. (1991). *Elementarteilchen und ihre Wechselwirkungen.* Wissenschaftliche Buchgesellschaft, Darmstadt, 2 edition.

Birrer, S. et al. (2020). TDCOSMO: IV. Hierarchical time-delay cosmography - joint inference of the Hubble constant and galaxy density profiles. *A. and A.*, 643:1–40.

Blakeslee, J. P. et al. (2021). The hubble constant from infrared surface brightness fluctuation distances. *arxiv*, page 2021.02221v1.

Blokhintsev, D. I. and Galperin, F. M. (1934). Neutrino hypothesis and conservation of energy. *Pod Znamenem Marxisma*, 6:147–157.

Boltzmann, L. (1877). Über die Beziehung zwischen dem zweiten Hauptsatz der mechanischen Wärmetheorie und der Wahrscheinlichkeitsrechnung respektive den Sätzen über das Wärmegleichgewicht. *Sitzungsberichte der königlichen Akademie der Wissenschften zu Wien*, 76:428.

Brahe, T. (1588). *De mundi aetherei recentioribus phaenomenis.* Brahe, Uraniborg.

Broy, B. J. (2016). *Inflation and effective Shift Symmetries.* PhD thesis, University Hamburg, Hamburg.

Brüning, P. and Carmesin, H.-O. (2019). The Elementary Oscillation of Dark Energy. *Verhandl. DPG (VI)*, 54(3):30.

Brüning, P., Carmesin, H.-O., and Helmcke, B. J. (2019). Numerical Investigation of the Emergence of Dark Energy and the Time Evolution of the Hubble Constant. *Verhandl. DPG (VI)*, 54(3):30.

Carmesin, H.-O. (1996). *Grundideen der Relativitätstheorie*. Verlag Dr. Köster, Berlin.

Carmesin, H.-O. (2016). Mit dem Zwillingsparadoxon zur speziellen und allgemeinen Relativitï¿½tstheorie. *PhyDid B Internetzeitschrift*.

Carmesin, H.-O. (2017a). Quantum Gravity: Discoveries about the early Universe including big bang, big bounce and a critical discussion of these. German Astronomical Society Conference at University Göttingen.

Carmesin, H.-O. (2017b). *Vom Big Bang bis heute mit Gravitation: Model for the Dynamics of Space*. Verlag Dr. Köster, Berlin.

Carmesin, H.-O. (2018a). A Model for the Dynamics of Space - Expedition to the Early Universe. *PhyDid B, FU Berlin, hal-02077596*, pages 1–9.

Carmesin, H.-O. (2018b). A Model for the Dynamics of Space - Expedition to the Early Universe. *PhyDid B*, pages 1–9.

Carmesin, H.-O. (2018c). Eine Theorie des Gravitationswellensignals ausschließlich mit Schulmitteln - verallgemeinerbar auf elektromagnetische Sender, Wellenlehre und Schwarzschild - Metrik. In Friege, G. and Scholz, R., editors, *Blubb - Gravitationswellen - schwarze Löcher*, pages 21–38. Westermann, Braunschweig.

Carmesin, H.-O. (2018d). Einstein in der Schule (Teil 1) Unterrichtskonzepte zur allgemeinen Relativitätstheorie. *Astronomie und Raumfahrt im Unterricht*, 55(3/4):55–59.

Carmesin, H.-O. (2018e). Einstein in der Schule (Teil 2) Unterrichtskonzepte zur allgemeinen Relativitätstheorie. *Astronomie und Raumfahrt im Unterricht*, 55(6):33–36.

Carmesin, H.-O. (2018f). *Entstehung der Raumzeit durch Quantengravitation - Theory for the Emergence of Space, Dark Matter, Dark Energy and Space-Time.* Verlag Dr. Köster, Berlin.

Carmesin, H.-O. (2018g). *Entstehung dunkler Energie durch Quantengravitation - Universal model for the Dynamics of Space, Dark Matter and Dark Energy.* Verlag Dr. Köster, Berlin.

Carmesin, H.-O. (2018h). *Entstehung dunkler Materie durch Gravitation - Model for the Dynamics of Space and the Emergence of Dark Matter.* Verlag Dr. Köster, Berlin.

Carmesin, H.-O. (2019a). A novel Equivalence Principle for Quantum Gravity. *Verhandl. DPG (VI)*, 54(3):42.

Carmesin, H.-O. (2019b). A Novel Equivalence Principle for Quantum Gravity. *PhyDid B - Didaktik der Physik - Beiträge zur DPG - Frühjahrstagung - Aachen - Germany - hal-02511998*, pages 1–9.

Carmesin, H.-O. (2019c). A Novel Equivalence Principle for Quantum Gravity. *PhyDid B Internet Journal*, pages 1–9.

Carmesin, H.-O. (2019d). Die Grundschwingungen des Universums - The Cosmic Unification - With 8 Fundamental Solutions based on G, c and h. In Carmesin, H.-O., editor, *Universe: Unified from Microcosm to Macrocosm - Volume 1.* Verlag Dr. Köster, Berlin.

Carmesin, H.-O. (2019e). Equivalence Principle of Quantum Gravity. *Verhandl. DPG (VI)*, 54(2):74.

Carmesin, H.-O. (2019f). Kontroverse Konstante. *Physik Journal*, 18(7):14.

Carmesin, H.-O. (2019g). The Elementary Particle of Dark Matter. *Verhandl. DPG (VI)*, 54(3):42.

Carmesin, H.-O. (2020a). Explanation of the Rapid Enlargement of Distances in the Early Universe. *PhyDid B*, pages 9–17.

Carmesin, H.-O. (2020b). The Universe Developing from Zero-Point Energy: Discovered by Making Photos, Experiments and Calculations. In Carmesin, H.-O., editor, *Universe: Unified from Microcosm to Macrocosm - Volume 3*. Verlag Dr. Köster, Berlin.

Carmesin, H.-O. (2020c). Wir entdecken die Geschichte des Universums mit eigenen Fotos und Experimenten. In Carmesin, H.-O., editor, *Universe: Unified from Microcosm to Macrocosm - Volume 2*. Verlag Dr. Köster, Berlin.

Carmesin, H.-O. (2021a). Lernende erkunden die Raumzeit. *Der Mathematik Unterricht*, 2:1–10.

Carmesin, H.-O. (2021b). Lernende erkunden die Raumzeit. *Der Mathematik Unterricht*, 2:47–56.

Carmesin, H.-O. (2021c). Quanta of Spacetime Explain Observations, Dark Energy, Graviton and Nonlocality. In Carmesin, H.-O., editor, *Universe: Unified from Microcosm to Macrocosm - Volume 4*. Verlag Dr. Köster, Berlin.

Carmesin, H.-O. (2021d). The Origin of the Energy. *PhyDid B, FU Berlin*, pages 1–6.

Carmesin, H.-O. and Brüning, P. (2018). A Monte Carlo Simulation of Cosmic Inflation. *Verhandl. DPG*, page DD27(3).

Carmesin, H.-O. and Carmesin, M. (2018a). Explanation of Cosmic Inflation by Gravitation. *Verhandl. DPG*, page GR16(7).

Carmesin, H.-O. and Carmesin, M. (2018b). Explanation of Cosmic Inflation by Quantumgravitation. *Verhandl. DPG*, page EP14(5).

Carmesin, H.-O., Emse, A., Piehler, M., Pröhl, I. K., Salzmann, W., and Witte, L. (2020). *Universum Physik Sekundarstufe II Niedersachsen Qualifikationsphase*. Cornelsen Verlag, Berlin.

Carmesin, H.-O., Emse, A., Piehler, M., Pröhl, I. K., Salzmann, W., and Witte, L. (2021). *Universum Physik Sekundarstufe II Nordrhein-Westfalen Einführungsphase*. Cornelsen Verlag, Berlin.

Carmesin, M. and Carmesin, H.-O. (2020). Quantenmechanische Analyse von Massen in ihrem eigenen Gravitationspotenzial. *PhyDid B, FU Berlin*, pages 19–27.

Cavendish, H. (1798). Experiments to determine the density of the earth. *Phil. Trans. R. Soc. Lond.*, 88:469–516.

Chatrchyan, S. et al. (2012). Observation of a new boson at a mass of 125 gev with the cms experiment at the lh. *Phys. Lett. B*, 716:30.

Collaboration, P. (2014). Planck 2013 Results: XVI. Cosmological Parameters. *Astronomy and Astrophysics*, 571:1–66.

Collaboration, P. (2020a). Planck 2018 results. VI. Cosmological parameters. *Astronomy and Astrophysics*, pages 1–73.

Collaboration, P. (2020b). Planck 2018 results. VI. Cosmological parameters. *Astronomy and Astrophysics*, pages 1–73.

Cooray, A. (2016). Extragalactic background light measurements and applications. *R. Soc. open sci.*, 3:1–14.

Dalton, J. (1808). *A New System of Chemical Philosophy Part I*. Bickerstaff, London.

Einstein, A. (1905). Zur Elektrodynamik bewegter Körper. *Annalen der Physik*, 17:891–921.

Einstein, A. (1915). Die Feldgleichungen der Gravitation. *Sitzungsberichte der Königlich Preußischen Akademie der Wissenschaften*, pages 844–847.

Einstein, A. (1916). Näherungsweise Integration der Feldgleichungen der Gravitation. *Sitzungsberichte der Königlich Preußischen Akademie der Wissenschaften*, pages 688–696.

Einstein, A. and de Sitter, W. (1932). On the relation between the expansion and the mean density of the universe. *Proc. Nat. Acad. Sci.*, 18:213–214.

Einstein, A., Podolski, B., and Rosen, N. (1935). Can quantum-mechanical description of physical reality be considered complete? *Phys. Rev.*, 47:777–780.

Escamilla-Rivera, C. and Najera, A. (2021). Dynamical dark energy models in the light of Gravitational-Wave Transient Catalogues. *arXiv*, 2103.02097v1:1–25.

Falvo, C., Gamboa-Suarez, A., Cazayus-Claverie, S., Parneix, P., and Calvo, F. (2018). Isomerization kinetics of flexible molecules in the gas phase: Atomisitc versus coarse-grained sampling. *The Journal of Chemical Physics*, 149:1–14.

Fishbach, M. et al. (2019). A Standard Siren Measurement of the Hubble Constant from GW170817 without the Electromagnetic Counterpart. *Astrophysical J. Letters*, 871:1–10.

Friedmann, A. (1922). Über die Krümmung des Raumes. *Z. f. Physik*, 10:377–386.

Gauss, C. F. (1840). Recursion der Untersuchungen über die Eigenschaften der positiven ternären quadratischen Formen von Ludwig August Seeber. *J. reine angew. Math.*, 20:312–320.

Guth, A. H. (1981). Inflationary universe: A possible solution to the horizon and flatness problems. *Physical Review D*, 23:347–356.

Heeren, L., Sawitzki, P., and Carmesin, H.-O. (2020). Comprehensive Derivation of a Density Limit of the Evolution of Space. *PhyDid B, FU Berlin*, pages 39–42.

Heisenberg, W. (1927). Über den anschaulichen Inhalt der quantentheoretischen Kinematik und Mechanik. *Z. f. Phys.*, 43:172–198.

Helmcke, B. J., Carmesin, H.-O., Sprenger, L., and Brüning, P. (2018). Three methods for the observation of the Big Bang with our school telescope. *PhyDid B*, pages 55–60.

Hinshaw, G. et al. (2013). Nine-year wilkinson microwave anisotropy probe (wmap) observations: Cosmological parameter results. *ApJ supplements series*, 208:1–25.

Hubble, E. (1929). A relation between distance and radial velocity among extra-galactic nebulae. *Proc. of National Acad. of Sciences*, 15:168–173.

Josset, T., Perez, A., and Sudarsky, D. (2017). Dark energy as the weight of violating energy conservation. *PRL*, 118:021102233–243.

Kepler, J. (1627). *Tabulae Rudolphinae*. Jonae Saurii, Ulm.

Kerr, R. (1963). Gravitational field of a spinning mass as an example of algebraically special metrics. *Physical Review Letters*, 11:237–238.

Kiefer, C. (2003). Quantum gravity - a general introduction. In Giulini, D., Lämmerzahl, C., and Kiefer, C., editors, *Quantum Gravity*, pages 3–13. Springer, Berlin, 1 edition.

Klaers, J., Schmitt, J., Vewinger, F., and Weitz, M. (2010). Bose-einstein condensation of photons in an optical microcavity. *arxiv*, 1007p4088:1–16.

Kobel, M., Bilow, U., Lindenau, P., and Schorn, B. (2017). *Teilchenphysik*. Joachim Herz Stiftung, Hamburg.

Landau, L. and Lifschitz, J. (1979a). *Lehrbuch der theoretischen Physik - Quantenmechanik*. Akademie-Verlag, Berlin.

Landau, L. and Lifschitz, J. (1979b). *Lehrbuch der theoretischen Physik - Statistische Physik*. Akademie-Verlag, Berlin.

Landsman, K. (2016). The fine-tuning argument: Exploring the improbability of our existence. In Landsman, K. and van Wolde, E., editors, *The Challenge of Chance*. Springer, Berlin.

Lemaitre, G. (1927). Un univers homogene de masse constante et de rayon croissant rendant compte de la vitesse radiale des nebuleuses extra-galactiques. *Annales de la Societe Scientifique de Bruxelles*, A47:49–59.

Lieber, J. and Carmesin, H.-O. (2021). Dynamics in the early universe. *PhyDid B, FU Berlin*, pages 1–10.

Lohse, M. et al. (2018). Exploring 4D Quantum Hall Physics with a 2D Topological Charge Pump. *Nature*, 553:55–58.

Lu, T. and Haiman, Z. (2020). The matter fluctuation amplitude inferred from weak lensing power spectrum and correlation function in CFHT lens data. *MNRAS*, pages 1–11.

Mayo, A. E. and Bekenstein, J. D. (1996). No hair for spherical black holes: Charged and nonminimally coupled scalar field with self-interaction. *Phys. Rev. D*, 54:5059–5069.

Michell, J. (1784a). On the means of discovering the distance... *Phil. Trans. R. Soc. Lond.*, 74:35–57.

Michell, J. (1784b). On the means of discovering the distance, magnitude, etc. of the fixed stars in consequence of the diminution of the velocity of their light, in case such a diminution should be found to take place in any of them, and such other data should be procured from observations, as would be farther necessary for that purpose. *Phil. Trans. R. Soc. Lond.*, 74:35–57.

Michelson, A. A. and Morley, E. (1887). On the relative motion of the earth and the luminiferous ether. *American Journal of Science*, 34:333–345.

Moore, T. A. (2013). *A General Relativity Workbook*. University Science Books, Mill Valley, CA.

Nanopoulos, D., Olive, K. A., and Srednicki, M. (1983). After primordial inflation. *Physics Letters B*, 127:30–34.

Naumann, T. (2009). Cern faq. *CERN-Brochure*, 2009-003-GER:1–61.

Newell, D. B. et al. (2018). The CODATA 2017 values of h, e, k, and N_A for the revision of the SI. *Metrologia*, 55:L13–L16.

Newman, A. I. and Janis, J. (1965). *J. Math. Phys.*, 6:915.

Newton, I. (1686). *Newton's Principia - first American Edition - English 1729*. Daniel Adee, New York.

Oldershaw, Robert, L. (1998). Democritus - scientific wizard of the 5th century bc. *Speculations in Science and Technology*, 21:37–44.

Overbye, D. (2018). All light there is to see: 4 x 10^{84} photons. *The New York Times*.

Penzias, A. and Wilson, R. W. (1965). A measurement of excess antenna temperature at 4080 mc/s. *Astrophysical Journal Letters*, 142:419–421.

Pesce, D. W. et al. (2020). The megamaser cosmology project: Xiii. combined hubble constant constraints. *Astrophysical Journal Letters*, 891:L1.

Peskin, Michael, E. (2015). On the trail of the higgs boson. *Annalen der Physik*, 528:20–34.

Planck, M. (1899). Über irreversible Strahlungsvorgänge. *Verlag der Königlich Preußischen Akademie der Wissenschaften*, pages 440–480.

Planck, M. (1900). On the theory of the energy distribution law of the normal spectrum. *Verhandl. Dtsch. Phys. G.*, 2:237.

Planck, M. (1911). Eine neue Strahlungshypothese. *Verh. d. DPG*, 13:138–148.

Popper, K. (1974). *Objektive Erkenntnis*. Hoffmann und Campe, Hamburg, 2 edition.

Rademacker, O., Brüning, P., and Carmesin, H.-O. (2019). Formation of Gosset Lattices of Dark Matter. *Verhandl. DPG (VI)*, 54(3):30.

Ramirez, J. and Laso, M. (2001). Conformational kinetics in liquid n-butane by transition path sampling. *Journal of Chemical Physics*, 115:7285–7292.

Ratzinger, W. and Schwaller, P. (2021). Whispers from the dark side: Confronting light new physics with nanograv data. *SciPost Phys.*, 10:1–11.

Riess, A. G., Casertano, S., Yuan, W., Macri, L., and Scolnic, D. (2019). Large Magellanic Cloud Cepheid Standards Provide a 1 % Foundation for the Determination of the Hubble Constant and Stronger Evidence for Physics beyond Lambda-CDM. *The Astrophysical Journal ApJ*, 876:1–13.

Riess, A. G. et al. (2018). Type Ia Supernova Distances at Redshift ¿ 1.5 form the Hubble Space Telescope Multi-Cycle Treasury Programs: The Earla Expansion Rate. *ApJ*, 853:126.

Rodrigo, C. A. and Freitas, M. P. (2009). A theoretical view on the conformer stabilization of butane. *J. Org. Chem.*, 74:8384–8387.

Ruben, D.-H. (1990). *Explaining Explanation*. Routledge, London.

Sanders, Robert, H. (2010). *The Dark Matter Problem*. Cambridge University Press, Cambridge.

Sawitzki, P. and Carmesin, H.-O. (2021). Dimensional transitions in a Bose gas. *PhyDid B, FU Berlin*, pages 1–10.

Schöneberg, P. and Carmesin, H.-O. (2020). Solution of a Density Problem in the Early Universe. *PhyDid B, FU Berlin*, pages 43–46.

Schöneberg, P. and Carmesin, H.-O. (2021). Solution of the horizon problem. *PhyDid B, FU Berlin*, pages 1–6.

Schwarzschild, K. (1916). Über das Gravitationsfeld eines Massenpunktes nach der Einstein'schen Theorie. *Sitzungsberichte der Deutschen Akad. d. Wiss.*, pages 186–196.

Scolnic, D. M. et al. (2018). The complete light-curve sample of spectroscopically confirmed type ia supernovae from pan-starrs1 and cosmological constraints from the combined pantheon sample. *ApJ*, 859:101.

Shaposhnikov, M. and Shkerin, A. (2018). Gravity, scale invariance and the hierarchy problem. *J. HEP*, 10:1–42.

Sommerfeld, A. (1978). *Mechanik der deformierbaren Medien*. Verlag Harri Deutsch, Frankfurt, 6 edition.

Sprenger, L. and Carmesin, H.-O. (2018). A Computer Simulation of Cosmic Inflation. *PhyDid B*, pages 61–64.

Straumann, N. (2013). *General Relativity* . Springer, Dordrecht - Heidelberg - New York - London, 2 edition.

Suzuki, N. et al. (2011). The hubble space telescope cluster supernova survey: V. improving the dark energy constraints above z $>$ 1 and building an early-type-hosted supernova sample. *ApJ*, 746:85.

Tanabashi, M., particle data group, et al. (2018). Review of particle physics. *Phys. Rev. D*, 98:1–1898.

Tröster, T. et al. (2020). Cosmology from large-scale structure. *Astronomy and Astrophysics*, 633:1–9.

Tryon, Edward, P. (1973). Is the universe a vacuum fluctuation? *Nature*, 246:396–397.

Tsoucalas, G., Laios, K., Karamanou, M., and Androutsos, G. (2013). The atomic theory of leucippus and its impact on medicine before hippocrates. *Hellenic Journal of Nuclear Medicine*, 16:68–69.

van der Waals, J. D. (1873). *Over de Continuiteit van den gasen vloeistoftoestand*. Sijthoff, Leiden.

Weiland, J. L. et al. (2018). Elucidating ΛCDM: Impact of Baryon Acoustic Oscillation Measurements on the Hubble Constant Discrepancy. *ApJ*, 853:119.

Wußing, H. and Brentjes, S. (1987). *Geschichte der Naturwissenschaften*. Aulis-Deubner, Köln, 2 edition.

Ylikoski, P. and Kourikoski, J. (2010). Dissecting explanatory power. *Philosophical Studies*, 148:201–219.

Zaldarriaga, M. et al. (2020). Combining Full-Shape and BAO Analyses of Galaxy Power Spectra: A 1.6% CMB-independent constraint on H_0. *JCAP*, 5:32.

Zilberberg, O. et al. (2018). Photonic topological pumping through the edges of a dynamical four-dimensional quantum Hall system. *Nature*, 553:59–63.

Zwicky, F. (1933). Die Rotverschiebung von extragalaktischen Nebeln. *Helvetica Physica Acta*, 6:110–127.